

# HIERARCHICAL CONTROL OF HYBRID POWER SYSTEMS

By

*María Elena Torres Hernández*

A thesis submitted in partial fulfillment of the requirements for the degree of  
MASTER OF SCIENCE  
in  
ELECTRICAL ENGINEERING  
UNIVERSITY OF PUERTO RICO  
MAYAGÜEZ CAMPUS  
2007

Approved by:

---

Efrain O'Neill, Ph.D.  
Member, Graduate Committee

---

Date

---

Eduardo Ortiz, Ph.D.  
Member, Graduate Committee

---

Date

---

Carlos Cuadros, Ph.D.  
Member, Graduate Committee

---

Date

---

Miguel Vélez Reyes, Ph.D.  
President, Graduate Committee

---

Date

---

Jose Colucci, Ph.D.  
Representative of Graduate Studies

---

Date

---

Isidoro Couvertier  
Chairperson of the department

---

Date

# Abstract

In this thesis, we present a Hierarchical control of Hybrid Power Systems (HPS) that consist of a Wind Turbine, Photovoltaic Panels, connection to the AC utility, a Battery Bank, and a zonal model of a load. The hierarchical control system consists of lower level controllers for each generation and storage component developed using Sliding Mode Control (SMC), and Model Predictive Control (MPC). The supervisory controller objective is to supply the energy demand while maximizing usage of renewable sources, minimizing connection to the grid, and effective use of the available battery storage. The performance of the system is studied by means of simulations. The thesis presents HPS model development, control design and simulation results under different operating scenarios. The simulation results of the proposed hierarchical control shows a good performance of the system.

# Resumen

En esta tesis, se presenta un control jerárquico para un Sistema Híbrido de Potencia (SHP) que consiste en una turbina de viento, un panel solar, conexión a la utilidad AC, un banco de baterías y un modelo zonal de la carga. El nivel inferior del sistema de control jerárquico está constituido por controladores con el objetivo de controlar cada sistema de generación de energía y de los componentes de almacenamiento; las técnicas que se utilizaron en este nivel de la jerarquía son control por deslizamiento y control predictivo basado en modelos. En el nivel superior se encuentra el control supervisor cuyo objetivo es suplir la energía demandada por la carga mientras maximiza el uso de las fuentes renovables, minimiza el uso de la utilidad AC y maneja de una forma efectiva el almacenamiento de la energía de la batería. El comportamiento de todo el sistema es estudiado a través de simulaciones. La tesis presenta el modelo del SHP, el diseño del control y los resultados de simulación bajo diferentes escenarios de operación. Los resultados obtenidos del sistema propuesto muestran un buen comportamiento del sistema.

# Acknowledgements

I would like to thank my Advisor, Professor Miguel Vélez Reyes for all his support, direction, and patience. Thanks for letting me work under your supervision. I will always admire you as a professor, as a professional and as an excellent person.

I would like to thank Dr. Efrain O'Neill, Dr. Eduardo Ortiz, and Dr. Carlos Cuadros for serving as members of my graduate committee.

Thanks to my family, Luis and my friends for believe in me and giving support when I needed, especially in difficult situations. Thanks to the Center for Power Electronics Systems (CPES); to the Electrical and Computer Engineering Department faculty and staff; and to all of the people who directly or indirectly have helped through my graduate period because the little things that somebody does one had influenced my life; so to all of you thanks.

Thanks to other authors who permit me to publish their figures on my thesis.

And the most important, I want to thank God for giving me the motivation and strength to finish this dream.

This work was primarily supported by the ERC Program of the National Science Foundation under grant EEC-9731677.

# Table of Contents

Abstract .....	II
Resumen.....	III
Acknowledgements.....	IV
List of tables .....	IX
List of figures .....	X
1. Introduction .....	1
1.1 Justification.....	1
1.2 Research Objectives .....	2
1.3 Summary of Contributions .....	2
1.4 Thesis Structure .....	3
2. Literature Review.....	4
2.1 Overview.....	4
2.2 Hybrid Power Systems (HPS) .....	4
2.2.1 Hybrid Power Systems Classification .....	5
2.2.2 Elements of Hybrid Power Systems .....	7
2.2.2.1 Wind Energy Conversion System (WECS) .....	7
2.2.2.2 Photovoltaic Panel .....	9
2.2.2.3 Battery Bank .....	10
2.3 Hierarchical Control.....	11
2.3.1 Control levels.....	11
2.3.1.1 The Strategic Level .....	12
2.3.1.2 The Tactical Level.....	13

2.3.1.3	The Operational Level.....	13
2.4	Sliding Mode Control (SMC) .....	13
2.4.1	Basics Concepts of SMC .....	14
2.4.2	SMC in Power Systems.....	15
2.4.2.1	DC/DC Converters of a Variable Structure system .....	15
2.4.2.2	SMC in DC/DC converters .....	16
2.5	Model Predictive Control (MPC) .....	17
2.5.1	MPC technologies .....	18
2.5.2	MPC in Power Systems.....	23
2.6	Energy Management (EM) in Power Systems.....	24
2.6.1	Energy Management in Hybrid Power Systems.....	27
3.	HPS Simulation Model .....	29
3.1	Hybrid Power System .....	29
3.2	Wind Turbine.....	32
3.3	Photovoltaic Panel.....	35
3.4	Battery Bank .....	38
4.	Hierarchical Controller for a HPS.....	41
4.1	Individual Control Units.....	41
4.1.1	SMC for a Wind Turbine.....	42
4.1.1.1	Sliding Mode controller Design .....	42
4.1.1.2	Modes of Operation.....	43
4.1.1.3	Simulation Results .....	46
4.1.2	Power Control of a Photovoltaic Array using SMC .....	52
4.1.2.1	Sliding Mode Controller Design .....	52

4.1.2.2	Modes of Operation.....	52
4.1.2.3	The control Law .....	55
4.1.2.4	Simulation Results .....	55
4.1.3	Control Strategy for the Battery Bank and the Grid .....	57
4.1.3.1	Controller Design .....	59
4.1.3.2	Modes of Operation.....	59
4.1.3.3	Simulation Results .....	62
4.1.4	On- Off Control for the Load .....	64
4.1.4.1	The control law .....	64
4.1.4.2	Simulation Results .....	65
4.2	Supervisor Control Strategy .....	66
4.2.1	Modes of Generation .....	69
4.2.1.1	Supervisory controller: Mode 1 .....	69
4.2.1.2	Supervisory Controller: Mode 2 .....	70
4.2.1.3	Supervisory Controller: Mode 3 .....	70
4.2.1.4	Supervisory Controller: Mode 4 .....	71
4.2.1.5	Supervisory Controller: Mode 5 .....	71
4.2.2	Operation Strategy.....	72
4.2.3	Simulation Results.....	74
4.2.3.1	Battery Bank Fully Charged.....	75
4.2.3.2	Battery Bank Totally Discharged.....	80
4.2.3.3	Sufficient power generation .....	85
4.2.3.4	Zonal EPDS .....	89
4.2.3.5	Changing source priority on supervisory controller .....	95

4.2.3.6	Changing source priority on supervisory controller (4 PV panels) .....	99
4.3	Conclusions.....	103
5.	Control for a HPS using Model Predictive Control .....	104
5.1	Dynamic Matrix Control (DMC).....	104
5.2	PV Controller Design using DMC .....	106
5.2.1	Simulation Results.....	108
5.2.2	MPC-PV against SMC-PV .....	110
5.3	Wind Controller using DMC.....	111
5.4	Supervisory Controller.....	111
5.4.1	Supervisor Control with battery bank fully charged .....	112
5.4.2	Supervisor Control with Battery Bank Totally Discharged.....	115
5.5	Conclusions.....	118
6.	Conclusions and Future Work.....	119
6.1	Summary of the work .....	119
6.2	Conclusions.....	119
6.3	Future Work .....	121
	References.....	123
	Appendices.....	128

# List of tables

Table 1 Basics Configuration on Hybrid Power Systems.....	6
Table 2 Wind turbine and PMSG parameters. ....	35
Table 3 Photovoltaic Module Specifications.....	37
Table 4 Parameters of the Battery Bank.....	40

# List of figures

Figure 1 structure of a typical Wind Energy System.....	8
Figure 2 Structure of a typical solar energy system connected to a DC bus [50] .....	9
Figure 3 Electric characteristic for a PV cell. ....	10
Figure 4 Multilevel control of a system. ....	12
Figure 5 Sliding Mode Idea [23] .....	15
Figure 6 DC/DC Converter.....	17
Figure 7 Basic structure of MPC [10].....	20
Figure 8 Controller state at the $k_{th}$ sampling instant adapted from [39].....	21
Figure 9 Two area power network.....	24
Figure 10 Generic Power/Energy management and distribution system adapted from [45].	26
Figure 11 Principles of Energy Management. ....	26
Figure 12 Electric Vehicle Power Flow. ....	28
Figure 13 Hybrid generation System.....	30
Figure 14 Matlab/Simulink Simulation model of the HPS. ....	31
Figure 15 Simulink model of the wind subsystem. ....	32
Figure 16 Simulink model of Wind Turbine. ....	33
Figure 17 Simulink model of Permanent Magnet Synchronous Generator.....	34
Figure 18 Simulink model of the solar panel. ....	36
Figure 19 Current-Voltage curve of PV array .....	37
Figure 20 Battery Model adapted from [53].....	38
Figure 21 Simulink model of Li-Ion Battery.....	39

Figure 22 Operation Points of both sliding surfaces [54].	44
Figure 23 Block diagram of controlled wind subsystem	45
Figure 24 Wind Speed	47
Figure 25 Power Coefficient of wind turbine	47
Figure 26 Power Reference of wind subsystem. a) Mode 1 b) Mode 2	48
Figure 27 Angular Shaft Speed	48
Figure 28 Sliding surfaces of wind turbine. a) 1 <sup>st</sup> mode b) 2 <sup>nd</sup> mode of generation.	49
Figure 29 Control signals of wind subsystem	50
Figure 30 DC bus Currents (Wind subsystem)	51
Figure 31 Zones of operation for control modes under sufficient power generation conditions [15].	54
Figure 32 Power signals to decide mode of operation of solar subsystem.	55
Figure 33 Sliding surfaces of solar subsystem	56
Figure 34 Control signals of solar subsystem	57
Figure 35 DC bus currents	58
Figure 36 Implementation of slope-on strategy adapted from [2].	61
Figure 37 Battery Bank and Grid currents when the battery is discharged.	63
Figure 38 Battery Bank and Grid currents when the battery bank is fully charged.	64
Figure 39 Control signal for load zones	66
Figure 40 Grid and Load currents	67
Figure 41 Supervisory controller interaction model.	68
Figure 42 Scheme for inputs and outputs in the supervisor control.	69
Figure 43 Mode transition criteria for the supervisor control	72
Figure 44 Load shedding scheme	73

Figure 45 Matlab/Simulink Model of supervisory controller.....	73
Figure 46 a) Wind speed and b) Cell temperature variations.....	74
Figure 47 Battery Voltage and SOC (Battery Bank Fully Charged).....	75
Figure 48 Load current divided by zones (Battery Bank Fully Charged). ....	76
Figure 49 Control signals of Wind Turbine and PV array (Battery Bank Fully Charged) .....	76
Figure 50 Control signals and sliding surfaces of PV array .....	77
Figure 51 Control signals and sliding surfaces of Wind Turbine .....	77
Figure 52 DC bus currents and operation modes (Battery Bank Fully Charged). ....	79
Figure 53 Battery voltage and SOC (Battery Bank discharged).....	80
Figure 54 Load current divided by zones (Battery Bank Discharged). ....	81
Figure 55 Control signals of Wind Turbine and PV array (Battery Bank Discharged) .....	81
Figure 56 Control signal and sliding surfaces of solar subsystem.....	82
Figure 57 Control signal and sliding surfaces of wind subsystem.....	82
Figure 58 DC bus currents and operation modes (Battery Bank Discharged). ....	84
Figure 59 SOC of Battery Bank (Sufficient power regime).....	85
Figure 60 DC bus current of HPS (sufficient power generation).....	86
Figure 61 Power reference and fictitious power of PV array (sufficient generation power) ..	87
Figure 62 Wind subsystem decision criteria (sufficient power regime) .....	87
Figure 63 PV array control signals (sufficient power generation) .....	88
Figure 64 PV array sliding surfaces (sufficient power regime) .....	88
Figure 65 Renewable energy control signals (sufficient power regime) .....	89
Figure 66 Voltage and SOC of Battery Bank (a) totally discharged, (b) fully charged .....	90
Figure 67 Control signals of wind and solar subsystems with the battery bank (a) totally discharged, (b) fully charged.....	90

Figure 68 Sliding surfaces and angular speed of wind subsystem with battery bank (a) totally discharged, (b) fully charged.....	91
Figure 69 Control signals of wind subsystem with battery bank (a) totally discharged, (b) fully charged.....	92
Figure 70 Sliding surfaces solar subsystem with battery bank (a) totally discharged, (b) fully charged.....	92
Figure 71 Control signals of solar subsystem with battery bank (a) totally discharged, (b) fully charged.....	93
Figure 72 DC bus current of HPS. The Battery Bank is (a) totally discharged, (b) fully charged. ....	94
Figure 73 Battery bank signals a) Voltage b) State of Charge.....	95
Figure 74 PV array control signals.....	96
Figure 75 Wind turbine control signals.....	96
Figure 76 Renewable sources control signals.....	97
Figure 77 DC bus current.....	98
Figure 78 Battery bank signals a) Voltage b) State of Charge.....	99
Figure 79 PV array control signals.....	100
Figure 80 Wind turbine control signals.....	100
Figure 81 Renewable sources control signals.....	101
Figure 82 DC bus current.....	102
Figure 83 Multi-objective controller.....	106
Figure 84 DMC flow diagram including constraints on control signal.....	107
Figure 85 DMC Control signal of PV array.....	108
Figure 86 DC bus currents (PV array with DMC).....	109
Figure 87 Wind Turbine Step Response.....	111

Figure 88 Voltage and SOC of Battery Bank.....	112
Figure 89 Control signals PV (DMC) and WT (SMC). .....	113
Figure 90 DC Bus current of HPS (PV controlled by DMC) .....	114
Figure 91 Voltage and SOC of the Battery Bank .....	115
Figure 92 Control signals of HPS .....	116
Figure 93 DC bus currents of HPS .....	117

# Chapter 1

---

## 1. Introduction

### 1.1 Justification

Hybrid Power Systems (HPS) are power systems that combine different electric power energy sources. One of the main problems of the HPS is related to the control and supervision of the power distribution system. The dynamic interaction between the grid and/or the loads and the power electronic interface of renewable source can lead, to new system, critical problems stability and power quality that are not common in conventional power systems.

Electronic Power Distribution Systems (EPDS) are power distribution systems where the electric power flow is controlled using power electronic converters. EPDS are present in many applications such as ship power systems, electric hybrid vehicles, hybrid power systems among others. Advanced control techniques can improve the performance of such systems by improving energy management capability and its capability to adapt to faults and other significant changes in operating conditions.

The purpose of this research is to develop control strategies for a hybrid EPDS using Sliding Mode Control (SMC), and Model Predictive Control (MPC); SMC is very robust with

respect to system parameters variations and external disturbances; MPC has shown to be a very good control methodology for process control and other applications. MPC has been applied in conventional power systems and to hybrid vehicles but no applications to HPS EPDS is known.

## **1.2 Research Objectives**

The main objective is to design and implement a Hybrid Power System Controller for energy management.

Additional objectives of this work were:

- To implement the model of a Hybrid Power System using Matlab.
- To compare the performance of Hybrid Power System with Sliding Mode Control against other control methodologies.
- To validate the proposed scheme using simulations.

## **1.3 Summary of Contributions**

Here, we expanded the works of [1] and [2] in control of Hybrid Power Systems. In [1] the supervisor control developed had three modes of operation and did not result in an acceptable performance of the battery bank. The latter [2] proposes a control for the battery bank but the developments of other control strategies are not evident. Here, we include other subsystems as traditional generators and add local shedding schemes when there is insufficient generation.

The main contribution of this work is the development and validation of a hierarchical control with two levels. The highest level is an on-line Supervisor control for a modular Hybrid Power System with five modes of operation. This controller determines the mode of operation of the all subsystems of the HPS. It is also easy to implement.

Other contribution is the MPC control of the PV array in the lowest level of the hierarchical structure.

## **1.4 Thesis Structure**

Chapter 2 provides a literary review and it is arranged in five subtopics: Hybrid Power Systems (HPS), Sliding Mode Control, Model Predictive Control, Energy Management in Power Systems, and Hierarchical Control. Chapter 3 depicts the information related to the model of the HPS describing the general construction of each subsystem. Chapter 4 shows the control design of the HPS using Sliding Mode techniques, the modes in which the system operates, and simulation results. Chapter 5 provides the control design of the Photovoltaic Subsystem using Model Predictive Control techniques, and simulation results. Finally, Chapter 6 presents the conclusions of the study and some recommendations for future work.

# Chapter 2

---

## **2.Literature Review**

### **2.1 Overview**

This section is divided in five sub-sections; the first part, gives a brief overview about hybrid power systems – that includes their configurations, operation strategy, limitations, and control requirements. The second part shows an examination of Hierarchical Control and the different levels of control. The third part explains Sliding Mode Control Technique and its applications in Power Systems, and Power electronics devices. In the fourth part a review of model predictive control and its applications in power systems is presented. Finally, the fifth part discusses Energy Management theory applied to Power Systems.

### **2.2 Hybrid Power Systems (HPS)**

Hybrid power systems are a combination of traditional generators, like diesel generator, with renewable source energy such as wind turbine and photovoltaic panels. The main objective of these systems is to extract maximum power at low costs with good power quality, low pollution, and reliable supply [3].

### **2.2.1 Hybrid Power Systems Classification**

HPS are classified in two categories: (i) grid-connected HPS, which are connected in parallel with the utility grid and can be used at any location; and (ii) stand alone (or off-grid), HPS, which are used to attend loads at remote places because they are independent of the utility grid [4,5].

The Grid Connected HPS generally use renewable generation power units as photovoltaic panels and wind turbines, a battery bank (rarely used) as a backup source, and the ac source is the utility grid. The basic configurations are Plant-oriented or central converter concept, module-oriented or string converter concept, and module-integrated converter concept [6].

Stand Alone HPS are designed and sized to attend specific loads. The power units commonly used are photovoltaic panels (DC source), wind turbines, and Diesel Generators (AC sources), batteries are often used for backup power. Other power electronics components like rectifiers, converters, and inverters are used to match the ac and dc generation source with the voltage and frequency requirements of the load [5]. The basic bus configurations of stand-alone systems are presented on Table 1.

The control system for HPS configurations should minimize fuel consumption by maximizing power from the renewable sources. However, there are power fluctuations by the variability of the renewable energy, which cause disturbances that can affect the quality of the power delivered to the load [3].

Table 1 Basics Configuration on Hybrid Power Systems

	AC	DC	AC/DC
Bus Configurations			
Connection	<p>All generating source and the load are connected to an AC bus. DC sources need to have inverters to match the voltage and frequency requirements of the AC bus [5].</p>	<p>All generating source and the load are connected to a DC Bus. AC sources need rectifiers to change the AC source to DC source [5].</p>	<p>The sources and loads AC are connected directly to the AC bus, and the DC sources and loads are connected to a DC bus [5].</p>
Benefits	<ul style="list-style-type: none"> <li>It is a more modular configuration, which facilitates the growth to manage with increasing energy and power needs [8].</li> </ul>	<ul style="list-style-type: none"> <li>DC loads can be connected directly to the DC bus, which reduces harmonic pollution from power electronic equipment in the load [5].</li> <li>The DC bus eliminates the need for frequency and voltage controls of the generation source connected to the bus and enable the application of variable speed generators in the system [5].</li> <li>The fuel consumption is 10% to 14% lower [8].</li> </ul>	<ul style="list-style-type: none"> <li>Both buses are connected through a bidirectional inverter that permits power flow between the two buses, increase the system power reliability and supply continuity [5].</li> <li>Fuel consumption falls by 30% when equalization is turned off [5].</li> </ul>
Drawbacks	<ul style="list-style-type: none"> <li>The synchronization of the inverters and AC sources to maintain the voltage and frequency of the system and the undesired harmonics introduced into the system by the use of inverters, which increase the level of power quality problems.</li> <li>Need 10% to 18% more electrical energy from the genset than AC/DC configuration [8].</li> </ul>	<ul style="list-style-type: none"> <li>The passes through two-power conversion stage, of the ac generators power, which affects its efficiency.</li> </ul>	<ul style="list-style-type: none"> <li></li> </ul>

The control system should take control actions to maintain the power quality conditions and power balance – with the generators in combination with their energy converters, the solar and wind generators could be controlled to supply maximum power or provide the power necessary to preserve the power balance at the load. The solar and wind generation are controlled in two ways – Maximum power conversion and Power regulation, according to the generation conditions and the load [1].

## **2.2.2 Elements of Hybrid Power Systems**

Next we will describe the different elements in a HPS. It is divided into Wind Energy Conversion System, Photovoltaic Panels, and the Battery Bank.

### ***2.2.2.1 Wind Energy Conversion System (WECS)***

The purpose of WECS is to extract the power from the wind and convert it to electric power. The principal elements of typical WECS are the wind turbine, a generator like a synchronous generators, permanent magnet synchronous generators, induction generators (including the squirrel-cage type and wound rotor type), or an interconnection apparatus as power electronics converters, to interconnect the system to the bus [7].

Wind turbines are classified into the horizontal axis type (with two or three blades, operating either up-wind or down -wind), and the vertical axis type [7].

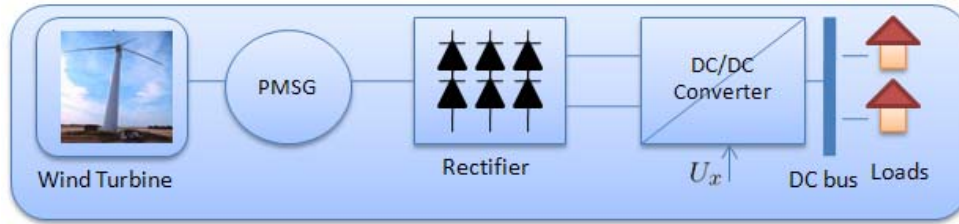


**Figure 1** structure of a typical Wind Energy System.

The wind turbine could be designed for a variable speed or fixed speed operation. Constant speed wind turbines can produce 8% to 15% less energy output as compared to their variable speed counterparts. Nevertheless, they require power electronic converters to give a fixed voltage power and fixed frequency to their loads [7]. Controls are included to hold or regulate rotational speed, and one of the principal objectives is to maximize power.

On other hand, winds turbines typically have at least three different control actuators: blade pitch, generator torque, and machine yaw. Blade pitch is the most effective method of controlling aerodynamics loads [9].

The nonlinear behavior of a wind turbine can make control design difficult. In pitch control, the control inputs gains are typically the partial derivative of the rotor aerodynamic torque with respect to blade pitch angle. These input gains vary with rotor speed, wind speed, and pitch angle. If the control of a wind turbine is designed at one operating point, may give poor results at other operating points. In fact, the controller possibly will result in unstable closed-loop behavior for several operating conditions. To avoid this, for each turbine operating points, regional controllers could be designed, and switched from one region to another. This generally uses as switching parameter wind speed or pitch [9].

The study of switching between controllers for wind turbines was done by Kraan in [10]. Several problems such as undesirable switching transients were reported. However,

Bongers in [11] describes the use of controller conditioning, in which the switching transients are minimized because the next controller to be activated is arranged for this task.

The adaptive control, investigated by Freeman and Balas in [12] and Bossanyi in [13], is another method to control the wind turbine, in which are adapted to changing conditions; the authors reported acceptable simulations results.

### 2.2.2.2 Photovoltaic Panel

The photovoltaic panels are the principal component to convert solar energy into electrical energy. The expression *photovoltaic* denotes the operating mode of a photodiode in which current through the device is totally due to the transduced light energy [14]. The solar cells produce direct current, so when they are used for grid connected power generation, they must be linked by an inverter to convert the DC to AC.

Cells could be electrically connected together to form a photovoltaic module, and several modules could be put together to form arrays. Figure 2 shows the basic structure of a typical solar energy conversion system [14].

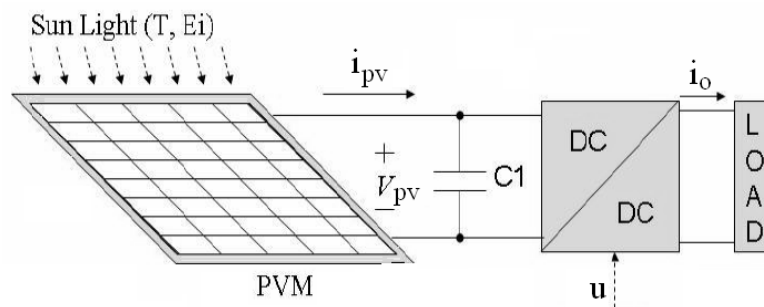


**Figure 2** Structure of a typical solar energy system connected to a DC bus [50]

The electric characteristic for a PV cell is presented on Figure 3, Points A and B correspond to operation under sufficient power generation conditions for a given reference power; on this mode, is desirable to operate on the right hand side of the PV array characteristic (point B) because it allows a wider range of power regulation. Point C represents the Maximum Power Operation Point (MPOP), so the system keeps the stored energy as much as possible; the PV work on this point when the isolation regimes are insufficient [15].

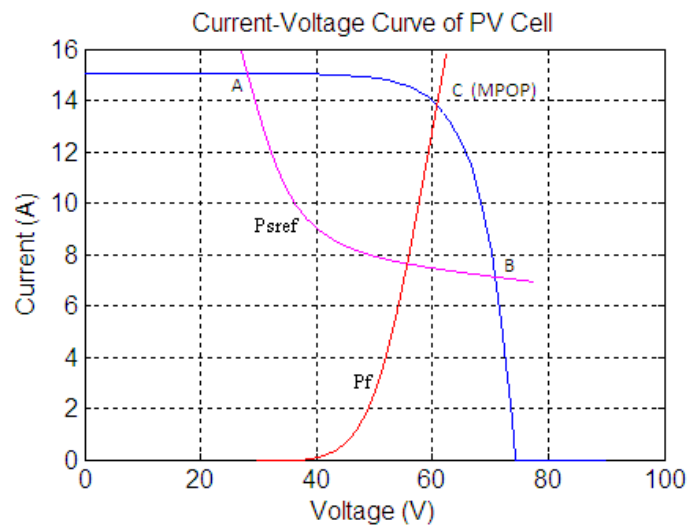


**Figure 3** Electric characteristic for a PV cell.

### 2.2.2.3 Battery Bank

Batteries convert the chemical energy stored inside into electrical energy. Battery applications are huge, that's the reason that they are available in different sizes, voltage, amp-hour ratings, liquid or gel, vented or non-vented, etc [16].

The battery bank is supposed to be designed so the batteries do not discharge more than 50% of their capacity on a regular basis. Discharging up to 80% is acceptable on a

restricted basis, such as an extended utility outage. Completely discharging a battery can reduce its effective life or damage it [16].

The charged period of the battery bank could differ depending upon the availability of other charging sources, the nature of the load and other factors. If renewable energy (wind, solar, etc) powered the system, the charged period of the battery depends on the weather or seasonal variations among others. However, the batteries are not just used for storage; they are too a buffer for all the charging energy which is brought into them [16].

## **2.3 Hierarchical Control**

The hierarchical system theory goes back to 1970s by Mesarovic, Macko, and Takahara's in which the main characteristic is the fact that the *decision-making process* has been divided. There are a number of *decision-maker units* in the structure, but only some of them in a straight line access the control system. The *decision-maker units* that define the tasks and coordinate are at a higher level on the hierarchy; the lower levels have direct contact with the process [17].

The designed control for HPS developed in this thesis is a kind of hierarchical control with four decision maker units.

### **2.3.1 Control levels**

The control problem of a complex system can be divided into different levels; each level has different control objectives that are handled by different controllers. When a

disturbance occurs, the objective is typically to bring the entire system safely back into normal operation as quickly as possible [17].

Figure 4 shows a hierarchical control structure with three different levels of functions.

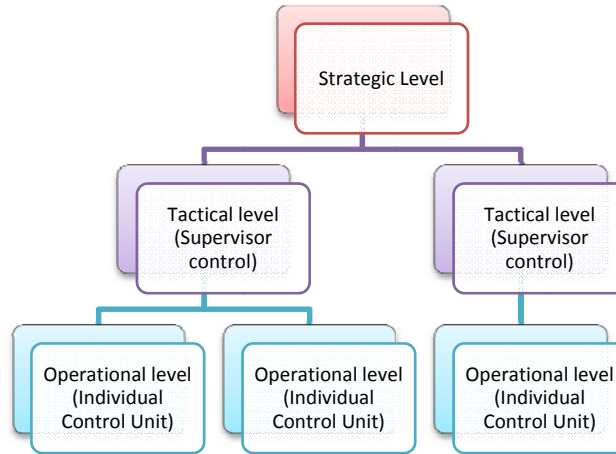


**Figure 4** Multilevel control of a system.

The control strategy developed in this work, is over two lower level; the make decision units to decide the operational mode of the HPS are over tactical level, and the control units to each power generation subsystem is over operational level.

### ***2.3.1.1 The Strategic Level***

This is the highest level of the structure; this level made the decisions concerning overall operation. The operating condition of the system can be characterized as 'start-up', 'production' or 'shutdown' [17], and the time constants are typically in the range of hours to days [18].

### ***2.3.1.2 The Tactical Level***

This level takes the local decisions concerning the local operation. This level acts like a supervisor control which switches between different operations modes or could shut down the controlled subsystem. Typically, the time constants at this level are in the range of minutes or seconds [18].

The operation of a supervisor in hierarchical control has two steps. First, an *observation* step which collects information concerning the controlled system and its environment. Second the *decision* step which uses this information and prior information with the purpose of select desirable control [17].

### ***2.3.1.3 The Operational Level***

On this level the actual control of the plant is being performed; the control objectives for each operation mode have to be defined. Typically the time constants are in the range of milliseconds [18]. Over this level, we developed the individual control units for each subsystem in the EPDS using Sliding Mode Control or Model Predictive Control.

## **2.4 Sliding Mode Control (SMC)**

The basics concepts and definitions presented in this section come from Sliding Mode Control theory developed 30 years ago in Russia by [19] , and to applied to on power electronics converters 20 years ago by [20,21].

Before discussing SMC techniques it is necessary to understand Variable Structure Systems (VSS), as implied by the name, are systems whose structures are changed deliberately through the transient, according to a predetermined structure control law, to accomplish the control objectives [22].

#### **2.4.1 Basics Concepts of SMC**

Sliding Mode Control is a type of Variable Structure Control characterized by a set of feedback control laws and a decision rule, and could be seen as an arrangement of subsystems, where each subsystem has a predetermined control structure and is applicable for specified regions of system behavior, on this control scheme, the feedback is not a continuous function of time [23].

The sliding mode control operates in a basic method as follows: a *sliding surface* is defined with the equilibrium point, and the system is forced to be held into the sliding surface (existence condition), and then the system must reach the equilibrium point (stability) [24]. This control scheme implies a selection of a surface such that the system trajectory exhibits desirable behavior when confined to this surface and the selection of feedback gains so that the system trajectory intersects and stays on the surface [25]. The existence condition and stability must be verified to guarantee the correctly operation of the controlled system.

The main idea of the SMC is illustrated in Figure 5. First, drive system to stable surface (reaching phase), then slide to equilibrium (sliding phase).

Sliding mode control has two advantages: the dynamic behavior of the system may be tailored by the particular choice of switching function, and the closed-loop response becomes insensitive to an external disturbance and parameters variations [23].

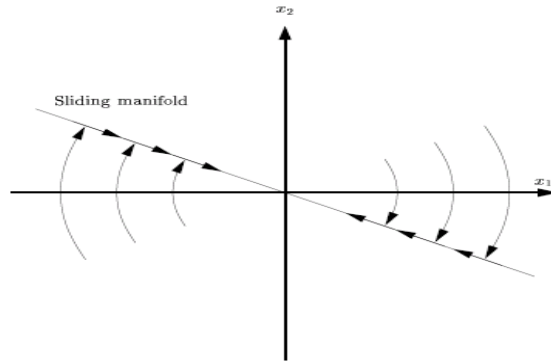


Figure 5 Sliding Mode Idea [23]

## 2.4.2 SMC in Power Systems

The application of the sliding mode control technique in Power Electronics devices such a DC-DC converters shows that this control approach could give good results in terms of robustness toward load and input voltage variations, while maintaining a dynamic response.

SMC was used in Hybrid Power Systems to control a photovoltaic array in [15], and a wind turbine in [26] by Valenciaga *et al.* The objective was to control the operation of the wind subsystem to complement the photovoltaic generation, so the power demand is satisfied.

### 2.4.2.1 DC/DC Converters of a Variable Structure system

DC/DC converters are affine nonlinear systems described by [27]:

$$\dot{x} = f(x) + g(x)u \quad (2.1)$$

$$x \in \mathfrak{R}^n \quad u \in \mathfrak{R}$$

The control signal  $u$  is discontinuous, and could take two values (0 or 1). Its discontinuous points correspond to changes on converter structure, for this reason, DC/DC converters are a variable structure system [27].

The principle of the switching control law is to force the nonlinear plant's state trajectory against a pre-specified surface  $S$  in the state space and to preserve the plant's state trajectory on this surface for following time [28]. The control switching law is defined as follow:

$$u = \begin{cases} 1 & \text{if } s(x) \geq 0 \\ 0 & \text{if } s(x) < 0 \end{cases} \quad (2.2)$$

Where  $s(x)$  is called the switching boundary and it's determined by a surface of  $n-1$  dimension, and  $n$  is the state dimension.

$$S = \{x \in \mathfrak{R}^n: s(x) = 0\} \quad (2.3)$$

$S$  is the *switching surface*, which is also called a sliding surface [22].

The most important task is to design a switched control that will drive the plant state to the switching surface and maintain it on the surface upon interception.

#### **2.4.2.2 SMC in DC/DC converters**

On this section, we are going to explain how to control with SM technique the output current of a DC/DC converter (Figure 6).

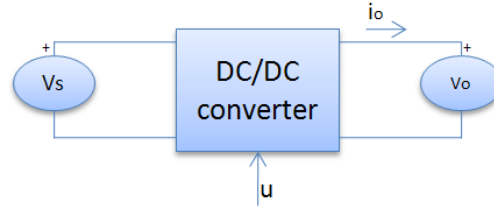


**Figure 6** DC/DC Converter.

To create a sliding surface, in order to achieve the control objective, we choose the switching function as [27]:

$$S(x) = i_o - i_{oref} \quad (2.4)$$

where  $i_{oref}$  is the desired output current.

We suppose that the system has an equilibrium state  $X_e$  with  $i_o = i_{oref}$  for a  $u$  value between one and zero.

To create a sliding mode regime the conditions to be satisfied are [27]:

$$\frac{ds}{dt} = \frac{di_o}{dt} - \frac{di_{oref}}{dt} < 0 \text{ if } u = 1 \quad (2.5)$$

$$\frac{ds}{dt} = \frac{di_o}{dt} - \frac{di_{oref}}{dt} > 0 \text{ if } u = 0$$

## 2.5 Model Predictive Control (MPC)

The MPC method is based on a prediction model of the system response to obtain the control action optimizing the future behavior of a plant by minimizing an objective function in an on-line mode [29].

There are many applications areas where MPC is successfully in use at the present time such as the process industry like chemicals, automotive, food processing, metallurgy, aerospace, pulp and paper, and power systems [30,31] among others. The good

performance of these applications shows the capability of the MPC to accomplish highly efficient control systems able to operate during long periods of time [32].

MPC can be used to integrate issues of optimal control, control of processes with time delays, stochastic control and multivariable control. The advantages over other methods are [29,32]:

- The concepts are very intuitive and the tuning is relatively easy.
- It introduces feed forward control to compensate measurable disturbances.
- MPC permits constraints, and these can be included during the design process.
- On-line computation with lower computational requirements.

Drawbacks are [32]

- The need for an accurate model of the process.
- All the computations have to be carried out at every sampling time.

### **2.5.1 MPC technologies**

This section shows the model predictive control technologies that are commercially available and that have large impact on the industrial world, the various MPC algorithms differ among themselves in the model used to represent the process and the noise model and cost function to be minimized.

The history of industrial MPC began with the *Linear Quadratic Gaussian* (LQG) Controller, in which, the process can be described by a linear state-space model driven by Gaussian noise, and the initial state is assumed to be Gaussian with non-zero mean.

$$\begin{aligned}\dot{x}_{k+1} &= \mathbf{A}x_k + \mathbf{B}u_k + \mathbf{G}w_k \\ y_k &= \mathbf{C}x_k + \xi_k\end{aligned}\tag{2.6}$$

The objective function includes separate state and input weight matrices Q and R to allow for tuning trade-offs and penalizes expected values of squared input and state deviations from the origin.

$$J = \sum_{j=1}^{\infty} x_{k+j}^T \mathbf{Q} x_{k+j} + u_{k+j}^T \mathbf{R} u_{k+j}\tag{2.7}$$

The optimal input  $u_k$ , is computed using an optimal state feedback law  $u_k = k_c x$  where  $K_c$  is calculated by solving a matrix Riccati equation [33].

The LQG controller has stabilizing properties. In LQG theory, it is not simple to include constraints on the process inputs, states and outputs [33,34].

Grieder *et al.* in [35] presented an algorithm to calculate the solution to the constrained infinite-time, linear quadratic regulator (CLQR) combining reachability analysis with multi-parametric quadratic programming to get the optimal piecewise affine (PWA) feedback law. The algorithm reduces the time necessary to compute the PWA solution for the CLQR when compared to other approaches making CLQR an attractive solution even for fast processes. This situation leads to the expansion, in industry, of a general model based control methodology, called now MPC, in which the dynamic optimization problem is solved online at each control interval [36].

Process inputs are calculated so as to optimize the outputs over a time interval known as the *prediction horizon* [37]. The *process model*, that describes the plant dynamic, could take any mathematical form, and is used to predict the future plant outputs, based on current and past values and on the optimal proposed future control actions. The optimizer calculates these actions taking account the constraints and the cost function, that's the reason because the future constraints violations could be predictable and prevented. This structure is show in Figure 7, [33].

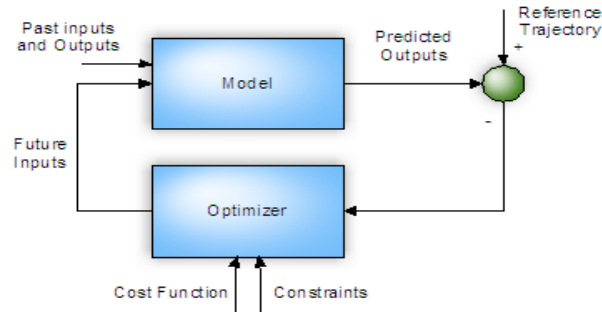


**Figure 7** Basic structure of MPC [10].

The MPC control action at time  $k$  is obtained by solving the optimization problem given by

$$\min_{x(k), u(k)} J(x(k), u(k)) = \sum_{j=1}^{N_p} [\hat{y}(k+j|k) - w(k+j)]^2 + \sum_{j=1}^{N_c} \lambda(j) [\Delta u(k+j-1)]^2 \quad (2.8)$$

Subject to

$$u_{min} \leq u_k \leq u_{max}$$

$$-\Delta u \leq \Delta u_k \leq \Delta u$$

$$y_{min} \leq Cx_k \leq y_{max}$$

$$x(k+1|k) = Ax(k+j|k) + Bu(k+j|k)$$

where  $w$  is the reference trajectory,  $\lambda$  is the control weighting factor, the predicted outputs  $\hat{y}$  depend on the future control signals  $u$ , and on the known values up to instant  $k$  (past inputs and outputs), which are those to be sent to the system and to be calculated. The first input of the optimal control sequence is sent to the process at the same time as the control signals<sup>1</sup> calculated are rejected, and the problem is solved again at the next time interval using updated process measurements [32,33].

Figure 8 shows the state of a SISO MPC system that has been operating for many sampling instants. The current instant is represented by the integer  $k$ ,  $y$  represents the measured output and  $u$  shows the control effort [32,37,38].

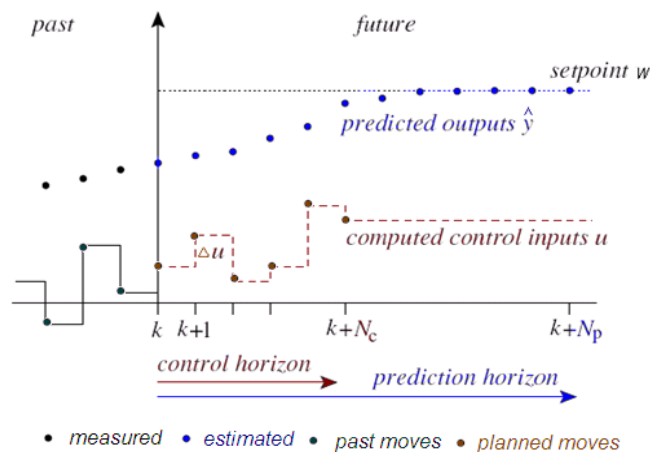


**Figure 8** Controller state at the  $k_{th}$  sampling instant adapted from [39].

In the late seventies, various articles appeared showing an interest in MPC by industry. Richalet *et al.* presented the first description of MPC control applications in 1976 [33]. His publications presenting Model predictive Heuristic Control (MPHC) and the

<sup>1</sup> The number of control intervals over which the manipulated variables are to be optimized is called the *control horizon* [37].

software that developed was named IDCOM (Identification and Command), which permit input and output constraints, impulse response model for the plant, quadratic performance objective over a finite prediction horizon [32].

In 1979, Cutler and Ramarker presented the Dynamic Matrix Control (DMC) as an unconstrained multivariable control. This algorithm uses the linear step response of the plant. Optimal inputs are calculated as the solution to a least squares problem using a quadratic performance objective over a finite prediction horizon [32,33]. In 1982, Garcia and Morari showed that the DMC algorithm was closed-loop stable when the prediction horizon was set long enough to include the steady state effect of all computed input moves [34].

In 1983, Cutler et al. described the Quadratic Program DMC (QDMC) in which input and output constraints appear explicitly, and the solution can be accomplished readily via standard commercial optimization codes. This algorithm represents a second generation of MPC [33].

The second generation did not permit the combination of multiple objectives into one objective (function), and did not allow the designer to reproduce the correct performance requirements. These are the reasons why third generation of MPC appeared with IDCOM algorithms. The third generation MPC used two separate objective functions, one for the outputs and one for the inputs [40]. Hard and soft constraints were incorporated, and the quadratic output objective function was minimized subject to constraint degree [37].

The Shell Multivariable Optimizing Controller (SMOC) proposed by (Marquis & Broustail, 1998; Yousfi & Tournier, 1991) combines state-space methods with the constraint handling features of MPC. This algorithm is equivalent to solving the LQR problem with input and output constraints, except that it is still formulated on a finite horizon, but it does not have the stabilizing properties of the LQR algorithm [33].

The fourth generation is represented by DMC-plus and Robust Model Predictive Control (RMPCT), which present an automatic way for tuning. The user could enter directly the estimates of model uncertainty, and compute the tuning parameters to optimize the performance for the worst-case model mismatch. This generation provides some mechanism to recover from an infeasible solution, distinguishes between several levels of constraints (hard, soft, ranked), allows for a wider range of process dynamics and controller specifications, and addresses the issues resulting from a control structure that changes in real time [33].

### **2.5.2 MPC in Power Systems**

There are several studies of model predictive control in power applications such as area power networks, and vehicular electric power systems.

Camponogara *et al.* in [30] presented a power system application of SC-DMPC in two or more autonomously controlled areas (see Figure 9), each area usually consist of various generators and loads, for studying Load Frequency Control (LFC). They assign MPC controllers to control the generator power output. The purpose of LFC is to keep the

frequency deviation of the system at zero and to preserve the variation of the power flow through the tie-line at zero.

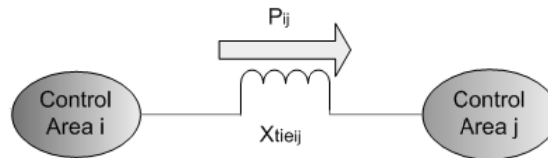


**Figure 9** Two area power network

Venkat *et al.* in [41] use the same example to compare the performance of centralized MPC, communication based MPC, and Standard Automatic Generation Control (AGC). They show that the performance benefits obtained with centralized MPC can be realized throughout distributed MPC strategies.

Hines P, *et al.* in [42] and [43] show a new application of DMPC methods, using agents, to the problem of arresting cascading failures in power systems. On this strategy, one agent is at each node of a power network to control a single variable using MPC and cooperate with its adjacent subsystems in making its decisions. Their results imply that the strategy is successful as long as the time among MPC iterations is sufficiently large that the neighbor network arrives at a steady state before the next control action occurs. The experiments also revealed the value of even simple collaboration schemes in agent networks.

## **2.6 Energy Management (EM) in Power Systems**

The main goal of Energy Management is to minimize costs or maximize benefits; others secondary objectives are to improve energy efficiency and to reduce energy use,

develop and keep efficient monitoring, report, and management strategies for intelligent energy usage, and reduce the impact interruption in energy supplies [44].

The function of Energy Management is to prioritize real time power demand from the loads and distribute power resources available from the generation and storage devices in an optimized approach for maximum efficiency and performance [45].

The power management system could be divided into the following subsystems: power generation, energy storage, power bus, electrical load, power electronics, and Power Management Controller (PMC). Figure 10 shows a generic power/energy management and distribution system. For a particular configuration, not all components or subsystems are required, and some small changes in the system topology might be necessary [45].

Figure 11 presents the principles of the energy management. The major task for the power an energy management system is to prioritize the load-power request and to allocate limited power resources. It is not practical to offer a permanent power capacity higher than the average power demand. Supply and storage must meet brief peaks in power needs [45], which are the reason why in each time interval of optimization, the management determines the operation mode of all components of the power system. It is best if the objective function becomes minimal [46].

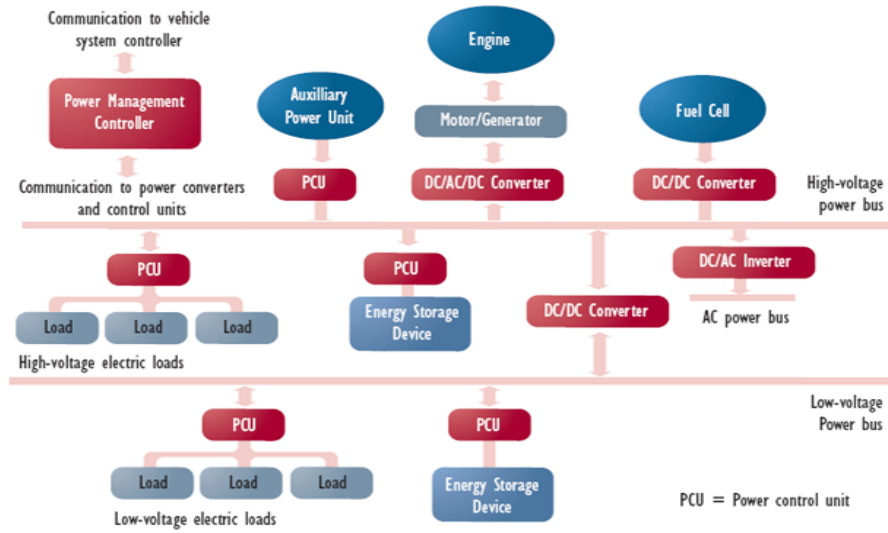


**Figure 10** Generic Power/Energy management and distribution system adapted from [45].

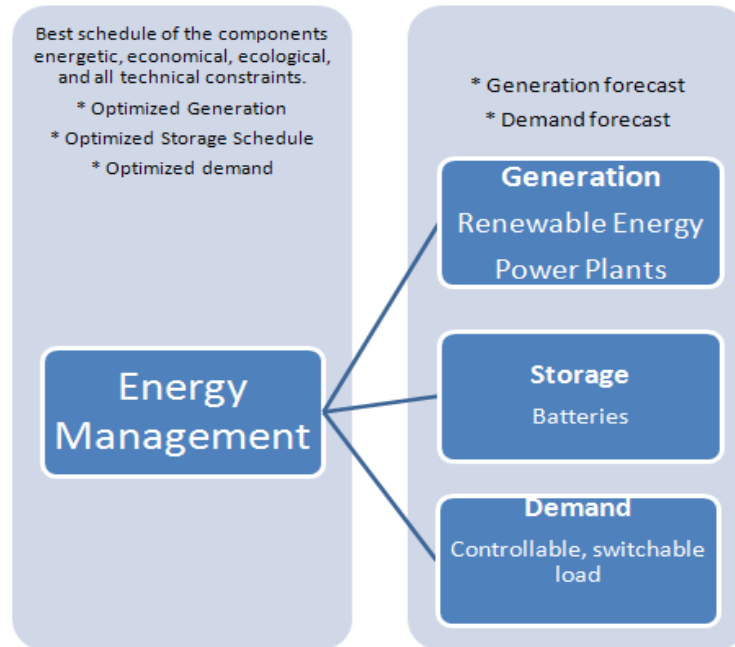


**Figure 11** Principles of Energy Management.

### 2.6.1 Energy Management in Hybrid Power Systems

Energy management is performed in HPS determining online the operation mode of generation subsystems, switching from power regulation to maximum power conversion; the energy balance depends of total demand, and generation [1].

Valenciaga and Puleston in [1] designed a supervisor control, using robust sliding-mode control, with three modes of operation: in mode 1 the wind subsystem is in power regulation against the solar subsystem is off, and the battery bank is in recharge cycle; in mode 2 the wind subsystem is in maximum power conversion at the same time as the solar subsystem is in power regulation, and the battery bank is in recharge cycle; in mode 3, both wind and solar subsystems are in maximum power conversion, and the battery bank supply power to the load. On this scheme, the objective is to control the operation of the wind subsystem to complement the photovoltaic generation, so the power demand is satisfied. In this work, the State of Charge of the battery bank and load shedding are not considered.

The control of wind turbine and the photovoltaic array was developed before in [26] and [15] respectively using sliding mode techniques. However, MPC has not been applied to control of HPS, but West M. *et al.* in [47] applied MPC techniques for EM in hybrid-electric vehicle (HEVs) drive-train incorporating numerous energy/power sources. This strategy is used to control the power drawn from a battery pack and a super-capacitor peak power buffer, to provide an all-electric drive-train. The scheme used is shown in Figure 12. Similar studies to control the electric power system with energy management for HEVs have been

proposed by Koot *et al.* in [48] to reduce the fuel consumption and emissions over a driving cycle.

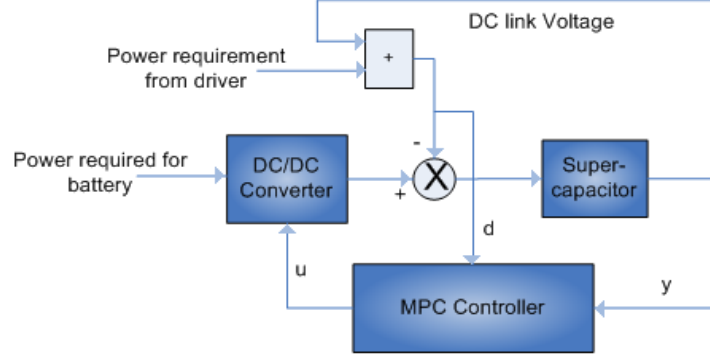


**Figure 12** Electric Vehicle Power Flow.

On this technique, the design procedure starts defining the cost function, such as minimizing the fuel consumption and emissions over a driving cycle. To find the optimal control, they used a variant of MPC employing zone control, and adding an additional slack variable  $\delta$  into the cost function of general predictive control given by

$$J(u, k) = \sum_{j=N_c}^{N_p} [\hat{y}(k+j|k) - w(k+j) + \delta(k+j)]^2 + \sum_{j=1}^{N_c} \lambda(j) [\Delta u(k+j-1)]^2 \quad (2.9)$$

Subject to

$$\tilde{\psi}(k) \leq \tilde{\Psi}(k)$$

$$|\delta(k)| \leq \delta_{max}$$

where  $\tilde{\psi}(k) \leq \tilde{\Psi}(k)$  include all the inputs, outputs and the states constraints, and  $|\delta(k)| \leq \delta_{max}$  is an additional constraint on the slack variable [47].

# Chapter 3

---

## 3.HPS Simulation Model

The first step is the implementation of a simulation model of Hybrid Power System using Simulink; this software was selected because it is a special package for modeling, simulating, and analyzing dynamic systems, supports linear and nonlinear systems, modeled in either continuous time, sampled time, or both [49].

All models were selected from different sources: the wind turbine model is presented in [26], the photovoltaic panels model was developed by Ortiz-Rivera in [50], the battery Bank was presented in [51], and the load model is the DC Zonal Electrical Distribution System (DCZEDS), which is the DC part of the an Integrated Power System (IPS) in [52], all subsystems of the load have a local controller.

### 3.1 Hybrid Power System

The Electric Generation Hybrid System (EGHS) that will be used on this work combines wind energy, solar sources and traditional sources. Each unit constitutes one subsystem to control; the overall system is show in Figure 13. The hybrid power system to be studied here can be divided in six components; power generation (Wind turbine, PV

Panels, and the Grid), energy storage (Battery Bank), power bus, electric load (three zone EPDS), power electronics (DC/DC converters), and the Power Management Controller (PMC).

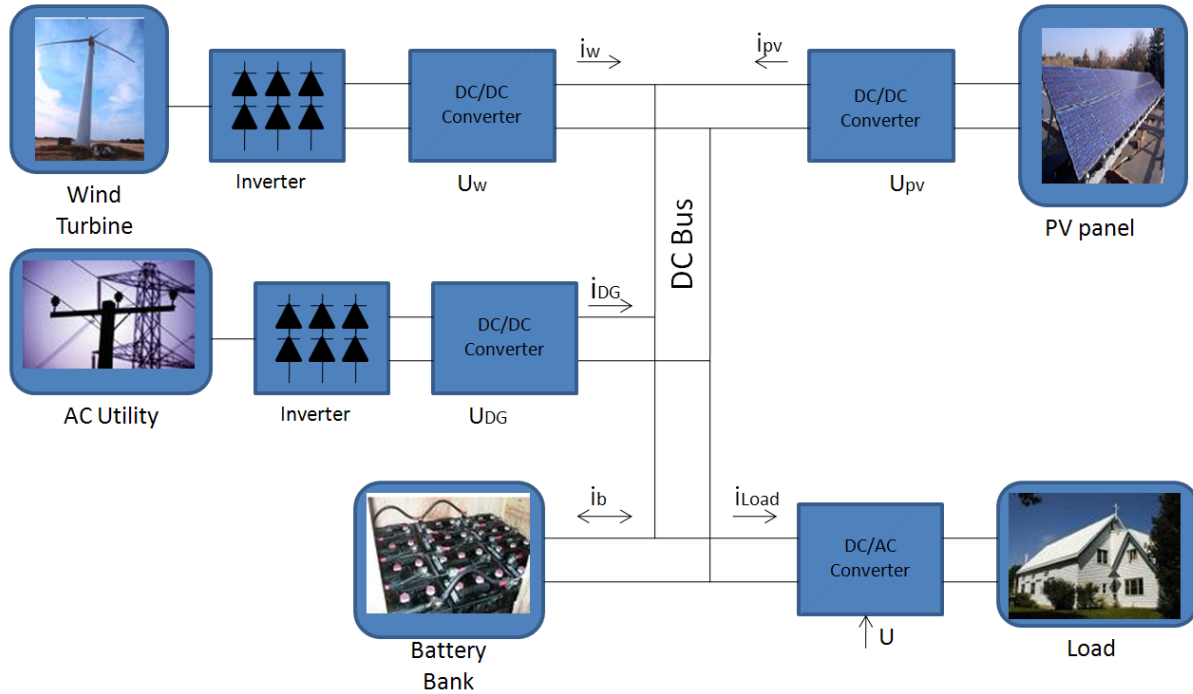


**Figure 13** Hybrid generation System

The wind generation unit comprises a windmill, a multipolar permanent-magnet synchronous generator (PMSG), a rectifier, and a dc/dc converter to interface the generator with the dc bus. The solar unit comprises several panels coupled to the dc bus through a DC/DC converter. The dc bus collects the energy generated by both units and delivers it to the load and, if necessary, to the battery bank.

The voltage of the dc bus is set by the battery bank, which comprises lead-acid batteries coupled in a serial/parallel array; the converters control the operation point of the wind turbine and PV Panels.

The loads served consist of three similar zones. Each zone is connected to the bus by a DC/DC converter.

The PMC is a central control unit for the power/energy management and distribution system to control and coordinate the system. This controller sends to the power converters the control signals and receiving the sensor signals and the status report from these units.

Figure 14 shows the MATLAB/SIMULINK simulation model of the HPS; a lot of sub models are put together to compose the main model. To put into practice the EM we have to control the overall system and implement the general EM algorithm on the PMC.

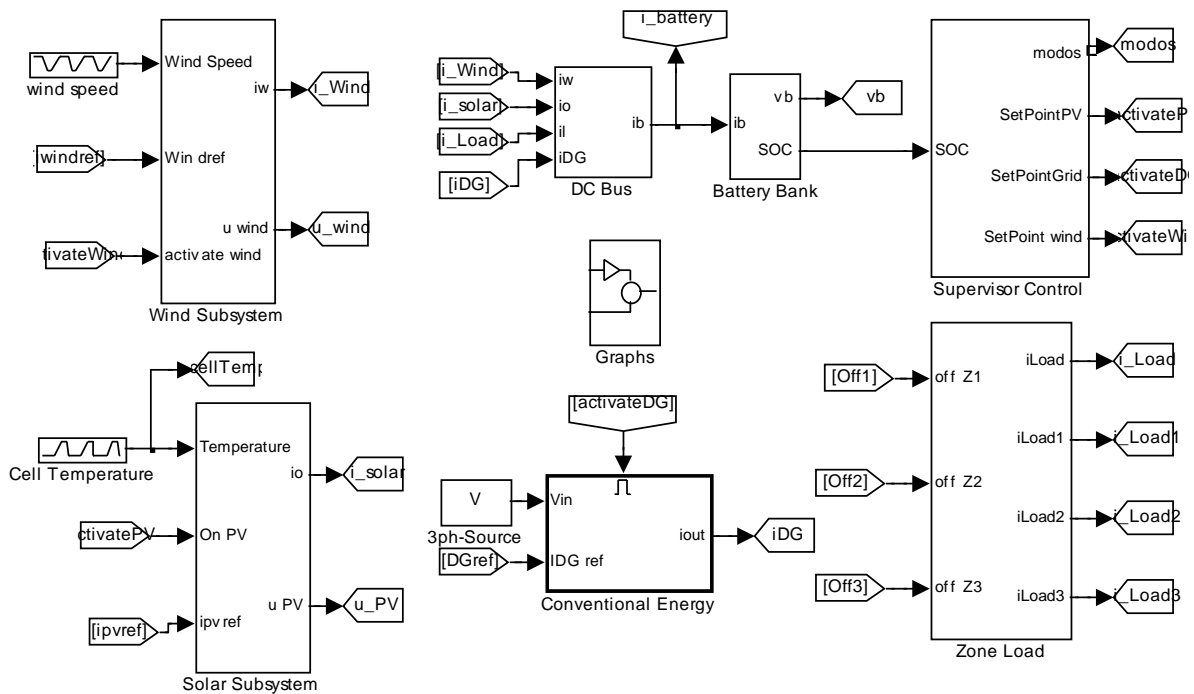


**Figure 14** Matlab/Simulink Simulation model of the HPS.

### 3.2 Wind Turbine

The wind turbine model used in this work was proposed in [26] by Valenciaga et al. On this model, the turbine is linked to the battery bank through a diode bridge rectifier and a DC/DC converter. Figure 15 shows the MATLAB/SIMULINK simulation model of the wind subsystem.

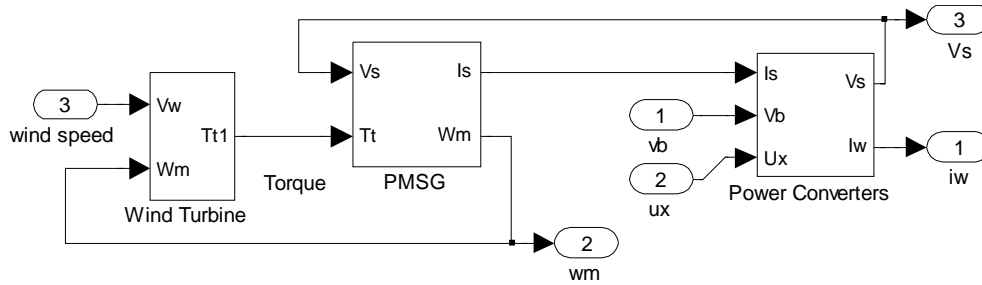


**Figure 15** Simulink model of the wind subsystem.

The mechanical power generated by a turbine is proportional to the air density ( $\rho$ ), the power coefficient of the rotor ( $C_p$ ), the cube of the wind speed ( $v$ ), and the swept area ( $A$ ) as show below.

$$P_t = C_p(\lambda)\rho Av^3 \quad (3.1)$$

The power coefficient value, depends upon the aerodynamics of the rotor blades, the blades angle, and the wind velocity, and could be described in terms of the tip-speed ratio  $\lambda$  which is given by:

$$\lambda = \frac{r\omega_m}{v} \quad (3.2)$$

where,  $r$  is the blade length, and  $\omega_m$  is the angular shaft speed.

The wind turbine torque is given by:

$$T_t = \frac{P_t}{\omega_m} = \frac{1}{2} C_t(\lambda)\rho Arv^2 \quad (3.3)$$

where,  $C_t(\lambda) = \frac{C_p(\lambda)}{\lambda}$ , is the torque coefficient of the turbine.

The expression of the electrical angular speed, corresponding to the minimum shaft speed below which the system cannot generate is given by:

$$\omega_{e \text{ lim}} = \frac{V_s}{\phi_m} \quad (3.4)$$

where,  $\phi_m$  is the flux linked by the stator windings, and  $V_s$  is the line voltage on the Permanent Magnet Synchronous Generator (PMSG). Figure 16 depicts the MATLAB/SIMULINK simulation model of the wind turbine.

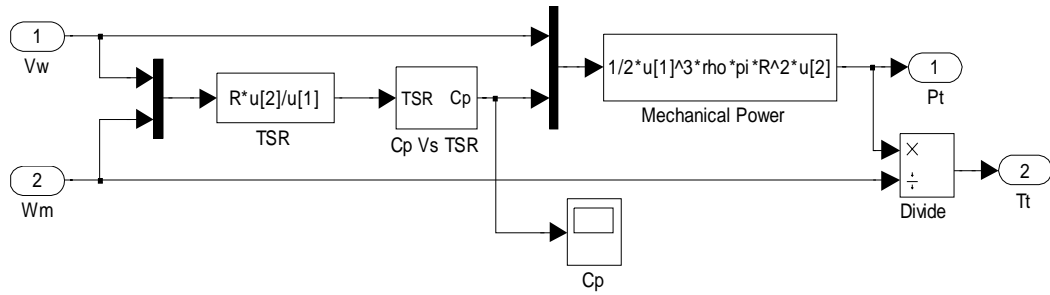


Figure 16 Simulink model of Wind Turbine.

The PMSG dynamic model in a rotor reference frame is given by the following equations [26], and the Matlab/Simulink simulation model is shown in Figure 17.

$$\dot{i}_q = -\frac{R_s}{L} i_q - \omega_e i_d + \frac{\omega_e \phi_m}{L} - \frac{\pi v_b i_q u_x}{3\sqrt{3}L \sqrt{i_q^2 + i_d^2}} \quad (3.5)$$

$$\dot{i}_d = -\frac{R_s}{L} i_d + \omega_e i_q - \frac{\pi v_b i_d u_x}{3\sqrt{3}L \sqrt{i_q^2 + i_d^2}} \quad (3.6)$$

$$\dot{\omega}_e = \frac{P}{2J} \left( T_t - \frac{3P}{2} \phi_m i_q \right) \quad (3.7)$$

where  $i_q$  and  $i_d$  are, respectively, the quadrature current and the direct current;  $L$  and  $R_s$  are the per phase inductance and resistance of the stator windings;  $P$  is the PMSG number of poles;  $J$  is the inertia of the rotating parts;  $\phi_m$  is the flux linked by the stator windings; and  $u_x$  is the control signal.

The voltage  $V_s$  is externally imposed by the DC/DC converter as a function of the duty cycle, and is described by:

$$V_s = \frac{\pi v_b}{3\sqrt{3}} u_x \quad (3.8)$$

If we assume an ideal static conversion, the current at the output of the DC/DC converter could be determined as shown in the next equation.

$$i_w = \frac{\pi}{2\sqrt{3}} \sqrt{i_q^2 + i_d^2} u_x \quad (3.9)$$

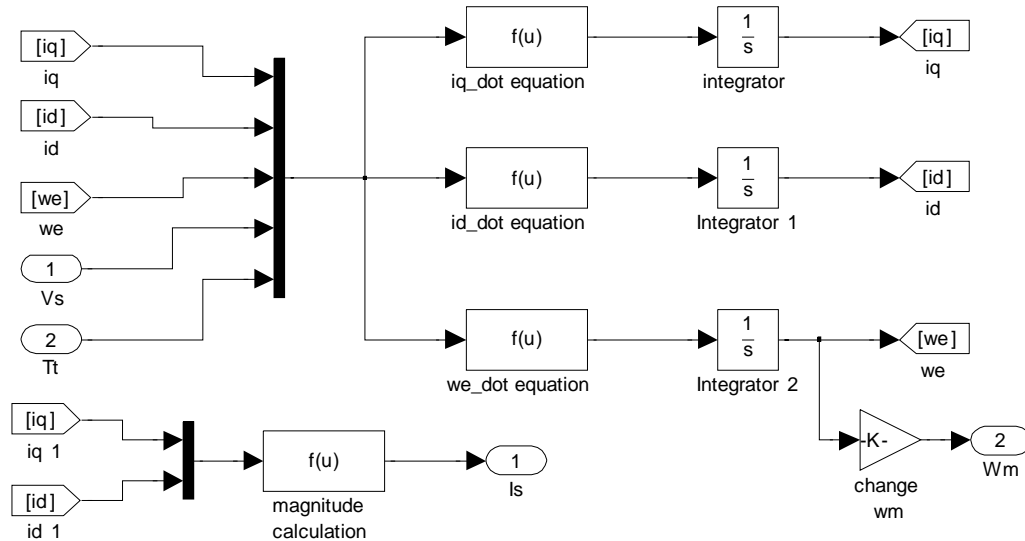


**Figure 17** Simulink model of Permanent Magnet Synchronous Generator.

The parameters used in the simulations are in Table 2.

**Table 2** Wind turbine and PMSG parameters.

PMSG nominal power	5KW
P	28
$R_s$	0.3676 $\Omega$
L	3.55mH
$\phi_m$	0.2867Wb
J	7.856Kg m <sup>2</sup>
R	1.84m

### 3.3 Photovoltaic Panel

The photovoltaic power model that we used in this work was proposed in [50]. This model depends on several cell parameters and on variable environment conditions such as the temperature over the solar panel  $T$ , the characteristic constant for the I-V curves  $b$ , the percentage of effective intensity of the light over the solar panels  $\alpha$ , the open circuit voltage  $V_{oc}$ , the short circuit current  $I_{sc}$ , and a shading linear factor  $\gamma$ . This model was selected because it uses the electrical characteristics provided by the solar panel data sheet, and its electrical behavior could be modeled by a nonlinear current source connected with the intrinsic cell series resistance. In this model, the I-V and P-V relation of the solar panel are:

$$i_{pv} = \alpha I_{max} \tau_i - \alpha I_{max} \tau_i e^{\left( \frac{V_{pv}}{b(\gamma\alpha + 1 - \gamma)(V_{max} + \tau_v)} - \frac{1}{b} \right)} \quad (3.10)$$

$$P_{pv} = V \cdot i_{pv} = \alpha I_{max} V \tau_i - \alpha I_{max} V \tau_i e^{\left( \frac{V_{pv}}{b(\gamma\alpha + 1 - \gamma)(V_{max} + \tau_v)} - \frac{1}{b} \right)} \quad (3.11)$$

Where

$$\alpha = \frac{E_i}{E_{iN}} \quad (3.12)$$

$$\frac{V_{oc} - V}{V_{oc}} = \frac{I_{sc} - I}{I_{sc}} \quad (3.13)$$

The shading linear factor is the percent of maximum voltage loss from a maximum to minimum intensity of light. The open-circuit voltage mark of the solar panels array for an effective intensity of light less than 20% over the solar panel is [50].

$$\frac{V_{oc} - V}{V_{oc}} = \frac{I_{sc} - I}{I_{sc}} \quad (3.14)$$

$$\frac{V_{oc} - V}{V_{oc}} = \frac{I_{sc} - I}{I_{sc}} \quad (3.15)$$

$$\frac{V_{oc} - V}{V_{oc}} = \frac{I_{sc} - I}{I_{sc}} \quad (3.16)$$

The PV panel is developed around a DC bus and it is connected through a DC/DC buck converter which is described by the following equations [15]:

$$\frac{V_{oc} - V}{V_{oc}} = \frac{I_{sc} - I}{I_{sc}} \quad (3.17)$$

$$\frac{V_{oc} - V}{V_{oc}} = \frac{I_{sc} - I}{I_{sc}} \quad (3.18)$$

where is the battery voltage, is the current injected on the DC bus, is the voltage level on the PV panel array terminals, and is the control signal.

Figure 18 shows the MATLAB/SIMULINK simulation model of the solar panel.

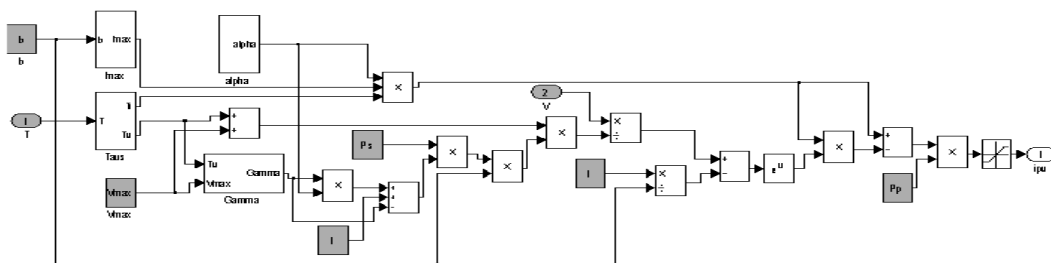


Figure 18 Simulink model of the solar panel.

The datasheet for the SLK60M6 panel is presented in appendix A, and summarized on Table 3. The maximum power generated by the panel is 279.7W; the array that we used have two panels in series to set the voltage and two panels in parallel to set the current.

**Table 3** Photovoltaic Module Specifications.

SLK60M6	
Isc	7.52A
Voc	37.2V
Iop	6.86A
Vop	30.6V
b	0.07292
TCi	2.2mA/°C
TCv	-127mV/°C
Vmin	32.55V
Vmax	37.312V

The total power generated by the PV array is 559.48W, the maximum current is 15 A, and the maximum operation voltage is 74.4V as shown in Figure 19.

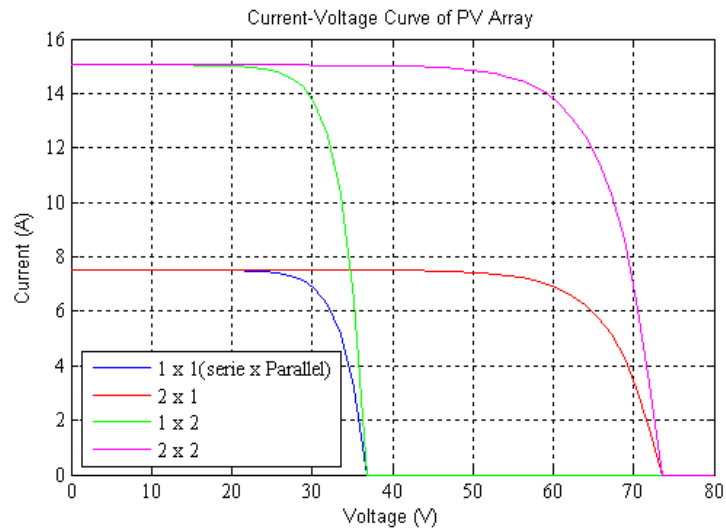


**Figure 19** Current-Voltage curve of PV array

### 3.4 Battery Bank

The battery model that we used was developed by [53]. This model is capable of modeling the steady state and the dynamic behavior of the battery.

The battery model is modeled by two circuit diagrams which are coupled via a current controlled current source and a nonlinear voltage controlled voltage source as shown in Figure 20.

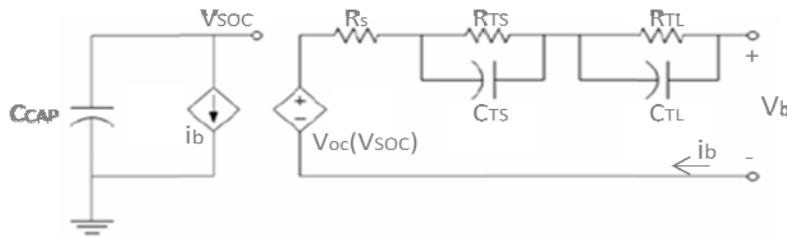


**Figure 20** Battery Model adapted from [53].

The state of charge (SOC) of the battery is represented by a large capacitor in the left hand side circuit; the model of the transient behavior and voltage-current relationship of the battery was represented by two RC circuits and series resistance on the right hand side of the diagram.

The state space model of the circuit is given by [51]:

(3.19)

where  $C_{TL}$  and  $R_{TL}$  are the capacitance and resistance in the long transient RC circuit,  $C_{TS}$  and  $R_{TS}$  are the capacitance and resistance in the short transient RC circuit,  $R_S$  is the series resistance,  $g$  is the nonlinear SOC function. The input  $u$  is the current entering the battery, and the output  $y$  is the voltage across the battery terminals.

The model was implemented in Simulink as shown in Figure 21. The relationship of nonlinear SOC was implemented via a lookup table with a set of ten values range from full charge to complete discharge [51].

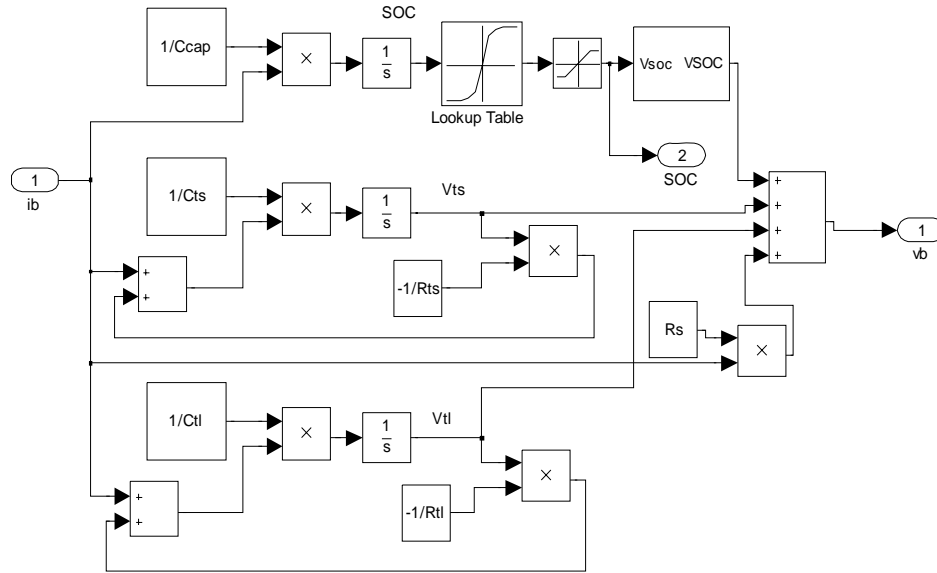


**Figure 21** Simulink model of Li-Ion Battery.

All the parameters in the model are multivariable functions of SOC, current, cycle number and temperature, and can be calculated following the next equations [53].

$$C_{CAP} = 3600 * Capacity * f_1(cycle) * f_1(temp) \quad (3.20)$$

where Capacity is the nominal capacity in Ahr and  $f_1(\text{cycle})$  and  $f_2(\text{temp})$  are cycle number and temperature dependent correction factors, respectively. For this simulation model, the  $f_1(\text{cycle})$  and  $f_2(\text{temp})$  are set to one, and the battery capacity is 22 Ahr.

The open-circuit Voltage  $V_{OC}$  is changed to different capacity levels.

$$V_{OC(SOC)} = -1.031e^{-35SOC} + 3.685 + 0.2156SOC - 0.1178SOC^2 + 0.3201SOC^3 \quad (3.21)$$

All the extracted RC parameters are constants around 20%-100% SOC and vary exponentially surrounded by 0%-20% SOC caused by the electrochemical reaction inside the battery.

$$R_{S(SOC)} = 0.1562e^{-24.37SOC} + 0.07446 \quad (3.22)$$

$$R_{TS(SOC)} = 0.3208e^{-29.14SOC} + 0.04669 \quad (3.23)$$

$$C_{TS(SOC)} = -725.9e^{-13.51SOC} + 703.6 \quad (3.24)$$

$$R_{TL(SOC)} = 6.603e^{-155.2SOC} + 0.04984 \quad (3.25)$$

$$C_{TL(SOC)} = -6056e^{-27.12SOC} + 4475 \quad (3.26)$$

The parameters used in the simulation of the Battery bank are in Table 4.

**Table 4** Parameters of the Battery Bank

$C_{CAP}$	80000 F
$C_{TS}$	600 F
$C_{TL}$	5000 F
$R_{TS}$	0.05 $\Omega$
$R_{TL}$	0.05 $\Omega$
$R_S$	0.05 $\Omega$
$V_{SOC0}$	48 V

# Chapter 4

---

## 4. Hierarchical Controller for a HPS

The main objective of the HPS is to satisfy the requirements of the electrical loads at the same time as maximizing the utilization of renewable energy sources while optimizing the operation of the battery bank and the conventional generators.

The developed control strategy consists of a hierarchical two level structure: *individual control units* for the individual energy conversion systems and a *supervisory controller* which determines the reference currents for the DC/DC converters and the SOC of the battery bank for energy management.

### 4.1 Individual Control Units

Each energy conversion system has an individual control unit in order to operate it according to the system needs. The system energy requirements are delivered to these units through signals coming from the supervisory controller. However, the supervisory controller takes into account the limits of the energy conversion systems to which it is delivering a command signal.

On this work, there are three different individual control units. The wind and the solar subsystems are controlled using SMC following [15,26]. The control strategy for the battery bank was developed in [2].

#### **4.1.1 SMC for a Wind Turbine**

The wind subsystem acts under supervisor control commands whichever supplying the total load or tracking the operation point of maximum power conversion. This subsystem is turned on in all modes of operation because is designated as the principal energy source. The impulse for this design choice was that it was taken from the perspective of applications in geographical areas with affluent wind regimes. However, we could considerate the solar subsystem as the main generator source and the wind subsystem as the secondary role.

##### ***4.1.1.1 Sliding Mode controller Design***

The main objective is to control the power produced by the wind subsystem into the DC bus to satisfy the total demand (the load and the battery charge requirements  $I_{bref}$ ) [26].

In this case, the control is just used to reject the unwanted internal forces that draw the system apart from the sliding surface.

#### 4.1.1.2 Modes of Operation

For this subsystem, there are two modes of operation as described in [26]. The first occurs when the wind subsystem could generate enough power to satisfy the total power demand.

$$P_{wref1} = V_b(i_L + I_{bref}) \quad (4.1)$$

The second mode of operation occurs when the maximum energy captured from the wind is not enough to satisfy the total demand. For this case, we make as a power reference the optimum power extracted by the turbine minus losses.

$$P_{wref2} = P_{wopt} - P_{losses} \quad (4.2)$$

$$P_{wref2} = K_{opt}\omega_m^3 - \frac{3}{2}(i_q^2 + i_d^2)r_s$$

where

$$K_{opt} = \frac{C_t(\lambda_{opt})\rho AR^3}{2\lambda_{opt}^2} \quad (4.3)$$

$\lambda_{opt}$  is the tip speed ratio that maximizes the power extracted to the wind.

The boundary between the operation modes of the wind subsystem is given by the angular shaft speed of the boundary point, and is obtained by equating the mechanical power references of both modes of operation (Equation 4.1 and 4.2), that is:

$$P_{wref1} + \frac{3}{2}(i_q^2 + i_d^2)r_s = K_{opt}\omega_m SW^3 \quad (4.4)$$

resulting the following function for the delimiting electrical angular speed:

$$\omega_{m\ SW} = \sqrt[3]{\frac{P_{w\ ref1} + \frac{3}{2}(i_q^2 + i_d^2)r_s}{K_{opt}}} \quad (4.5)$$

Figure 22 shows the operation points of both sliding surfaces. The decision to work in one mode of operation or the other can be taken by comparing the measured speed with the boundary speed  $\omega_{m\ SW}$  as follow:

$$\omega_m \geq \omega_{m\ SW} \Rightarrow \text{First mode of operation}$$

$$\omega_m < \omega_{m\ SW} \Rightarrow \text{Second mode of operation}$$

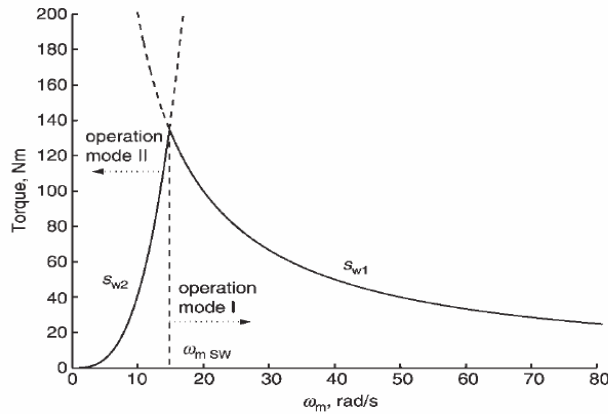


**Figure 22** Operation Points of both sliding surfaces [54].

*a) Sufficient Wind Regime*

On this mode of operation, the main objective of the wind subsystem is to regulate the power produced by the wind turbine following  $P_{w\ ref1}$ .

To accomplish this objective, the sliding surface  $h_1$  was written in terms of currents on the battery bank.

$$h_1 = P_{wref1} - P_w = V_b (I_{bref} + i_L - i_w) \quad (4.6)$$

The switched control signal produces an unwanted deviation in  $T_e$ , and a high ripple on the current of the DC/DC converter. To avoid this problem, following [26], we added an integrator to the input  $u_x$ , channel turning  $u_x$  into a new state variable and the integrator input signal  $w$  becomes the new input to the system. In consequence, the algebraic dependence between the input of the system and the sliding surface is broken.

The dynamic model of the extended system is shown in Equation 4.7 [26] and the block diagram is presented in Figure 23.

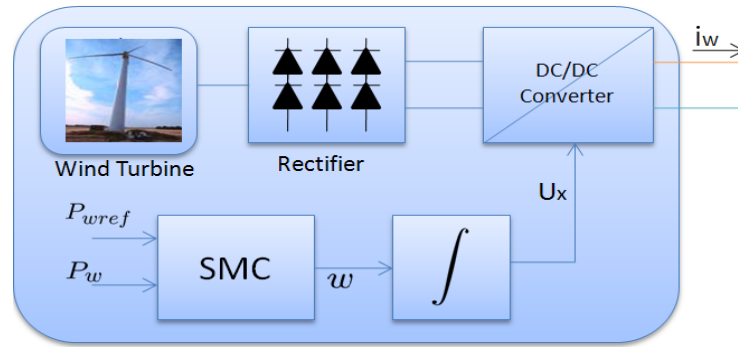


**Figure 23** Block diagram of controlled wind subsystem

$$\dot{x} = \begin{bmatrix} \dot{\omega}_e \\ \dot{u}_x \end{bmatrix} = \begin{bmatrix} f_1(x) \\ f_2(x) \end{bmatrix} + \begin{bmatrix} g_1(x) \\ g_2(x) \end{bmatrix} w \quad (4.7)$$

$$\begin{bmatrix} \dot{\omega}_e \\ \dot{u}_x \end{bmatrix} = \begin{bmatrix} \frac{P}{2J} (T_t - T_{elin}) \\ 0 \end{bmatrix} + \begin{bmatrix} 0 \\ 1 \end{bmatrix} w$$

where the electrical torque of PMSG is given by  $T_{elin} = K(\omega_e - \omega_{elim})$  and the switched control law is given by:

$$w = \begin{cases} w_1^+ = \frac{-|f_1(x)|}{4} \left[ \frac{-18L^2\phi_m^2 u_x \omega_e + 2\pi\sqrt{3}L^2 u_x^2 \phi_m v_b}{\sqrt{3D}\phi_m R_s + 9\phi_m^2 R_s^2 - 36C + 10B - 2A} + 1 \right]^2 & \text{if } h_1 \geq 0 \\ w_1^- = \frac{|f_1(x)|}{4} \left[ \frac{18L^2\phi_m^2 u_x \omega_e + 2\pi\sqrt{3}L^2 u_x^2 \phi_m v_b}{\sqrt{3D}\phi_m R_s + 9\phi_m^2 R_s^2 - 36C + 10B - 2A} + 1 \right]^2 & \text{if } h_1 < 0 \end{cases} \quad (4.8)$$

where

$$A = \pi^2 L^2 v_b^2 u_x^2$$

$$B = \pi\sqrt{3}L^2 \phi_m v_b \omega_e u_x$$

$$C = L^2 \phi_m^2 \omega_e^2$$

$$D = 27\phi_m^2 R_s^2 - 108C + 24B - 4A$$

#### b) *Insufficient Wind Regime*

On this mode, the system is not able to operate on the sliding surface  $h_1$ , and it is necessary to incorporate a secondary sliding surface  $h_2$  whose main objective is to extract the maximum power available from the wind turbine.

$$h_2 = P_w - P_{w\text{ref}2} \quad (4.9)$$

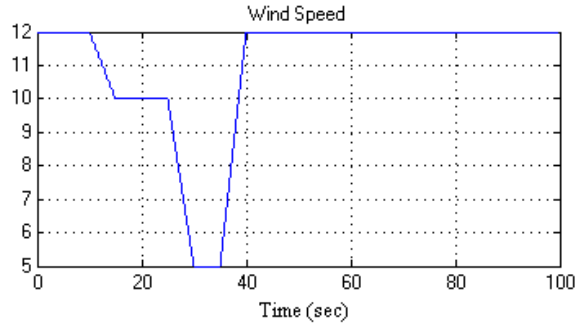
and the switching input signal is given by

$$w = \begin{cases} w_2^+ > 0 & \text{if } h_2 \geq 0 \\ w_2^- < 0 & \text{if } h_2 < 0 \end{cases} \quad (4.10)$$

#### **4.1.1.3 Simulation Results**

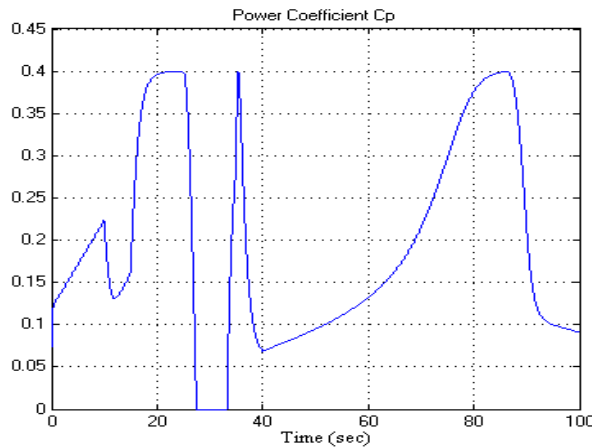
In order to test the operation of wind subsystem, two scenarios were simulated and evaluated. Over the first 25 seconds, there is a sufficient wind for the wind turbine to work well (the minimum wind speed recommended for this turbine is 10 m/s), between 30 and 38

seconds the wind speed was reduced to simulate insufficient wind power mode (See Figure 24). For all scenarios, the load is a variable current source.



**Figure 24** Wind Speed

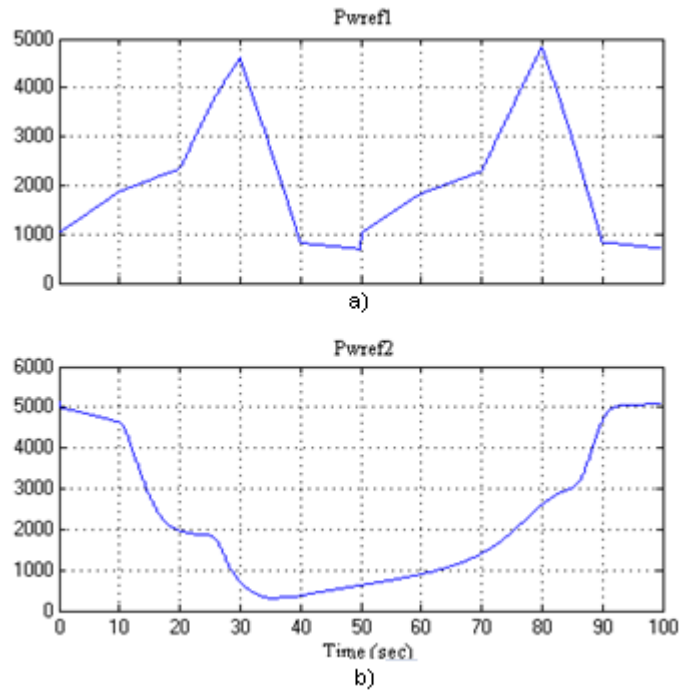
Figure 25 depicts the power coefficient of the wind turbine. If the wind speed was reduced under the operation limit of wind turbine, the power coefficient decreases to zero for a few seconds until the wind speed increases again, in other words, the rotation of the rotor would stop because the wind speed at the rotor front would reduce to zero.



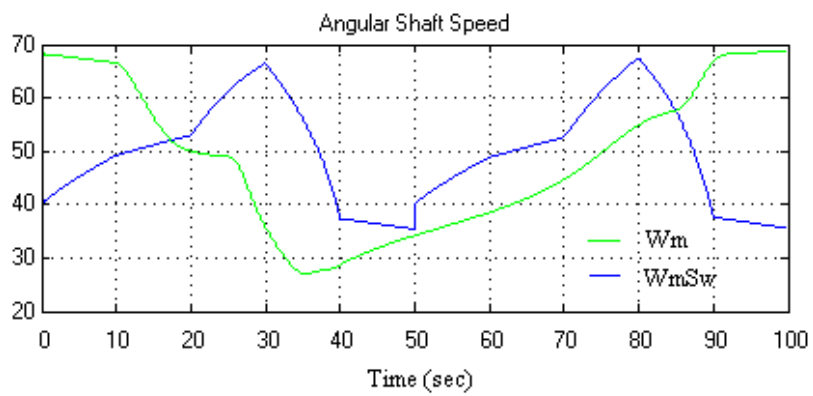
**Figure 25** Power Coefficient of wind turbine

Figure 26a shows that the power reference of the wind turbine to follow the first generation mode, and Fig. 26b to follow the second generation mode. Figure 27 presents the decision criteria to change the mode of operation; if the angular shaft speed of the boundary

point  $\omega_{m\ SW}$  is higher than the angular shaft speed  $\omega_m$ , the mode of operation is mode 2 or insufficient wind generation; else, the mode of operation is mode 1.

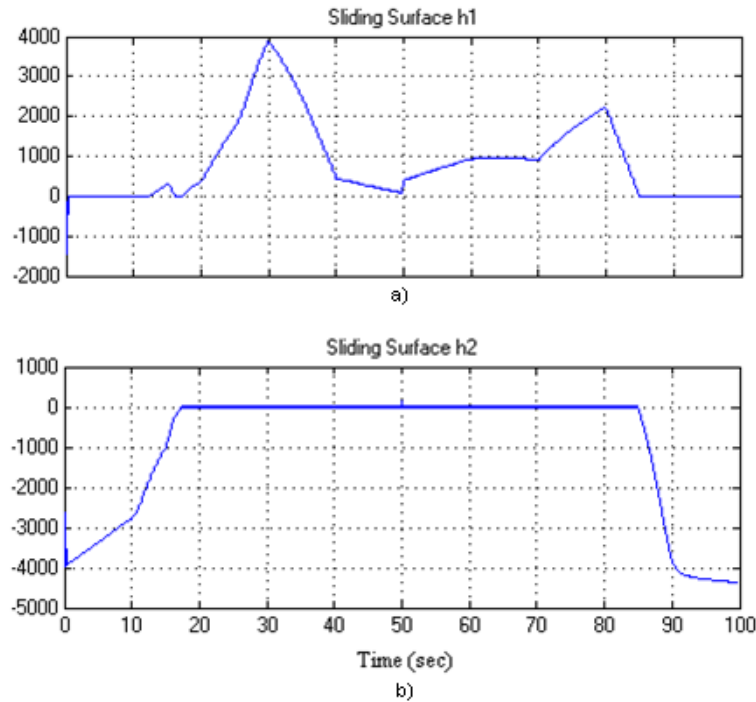


**Figure 26** Power Reference of wind subsystem. a) Mode 1 b) Mode 2



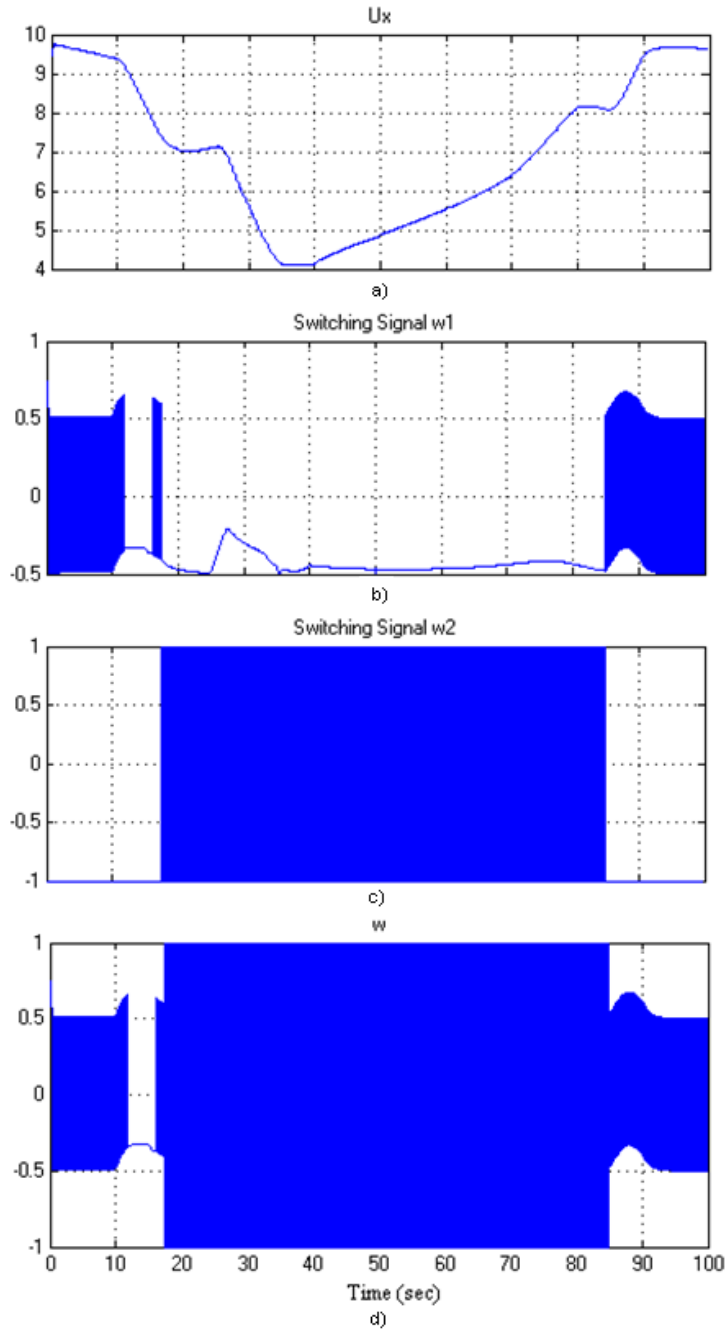
**Figure 27** Angular Shaft Speed

Figure 28 shows the sliding surfaces of both modes of operation of wind subsystem; Fig 28a presents the evolution of the sliding surface  $h_1$ , and Fig. 28b shows the evolution of  $h_2$ ; the sliding surfaces must be zero for their respective mode of operation.



**Figure 28** Sliding surfaces of wind turbine. a) 1<sup>st</sup> mode b) 2<sup>nd</sup> mode of generation.

Figure 29 shows the control signals for the wind subsystem; Fig. 29a presents the signal  $u_x$ , Fig 29b shows the switching signal  $w_1$ ; due to the design based on passivity considerations, exist the variation of the switching control values  $w_1^+$  and  $w_1^-$ . Fig 29c presents the switching signal  $w_2$ ; the reaching time depends on the tuning of the switching control values  $w_2^+$  and  $w_2^-$ . Finally Fig 29d depicts the total control signal  $w$ . It is important to mention that such minimum effort switching control law result in a chattering reduction of the output current of the DC/DC converter.



**Figure 29** Control signals of wind subsystem

Finally, Figure 30 depicts the currents present on the DC bus. Fig. 30a presents the wind current, we could observe when there is not enough power from the wind source, and the wind turbine can't follow the set-point. Fig. 30b shows the PV current, it was set to a constant current of 10A, on this case, the wind subsystem is complementing the

photovoltaic generation. Fig. 30c shows the load current, which when added to the battery reference (20A) makes the total demand. Fig. 30d illustrates the current on the battery bank, we could observe when there is enough power to supply the total demand it is on recharge cycle and set the current to 20A, but when the power is insufficient, it supplies power to the load. This happens between 22 to 38 seconds and between 70 to 83 seconds.

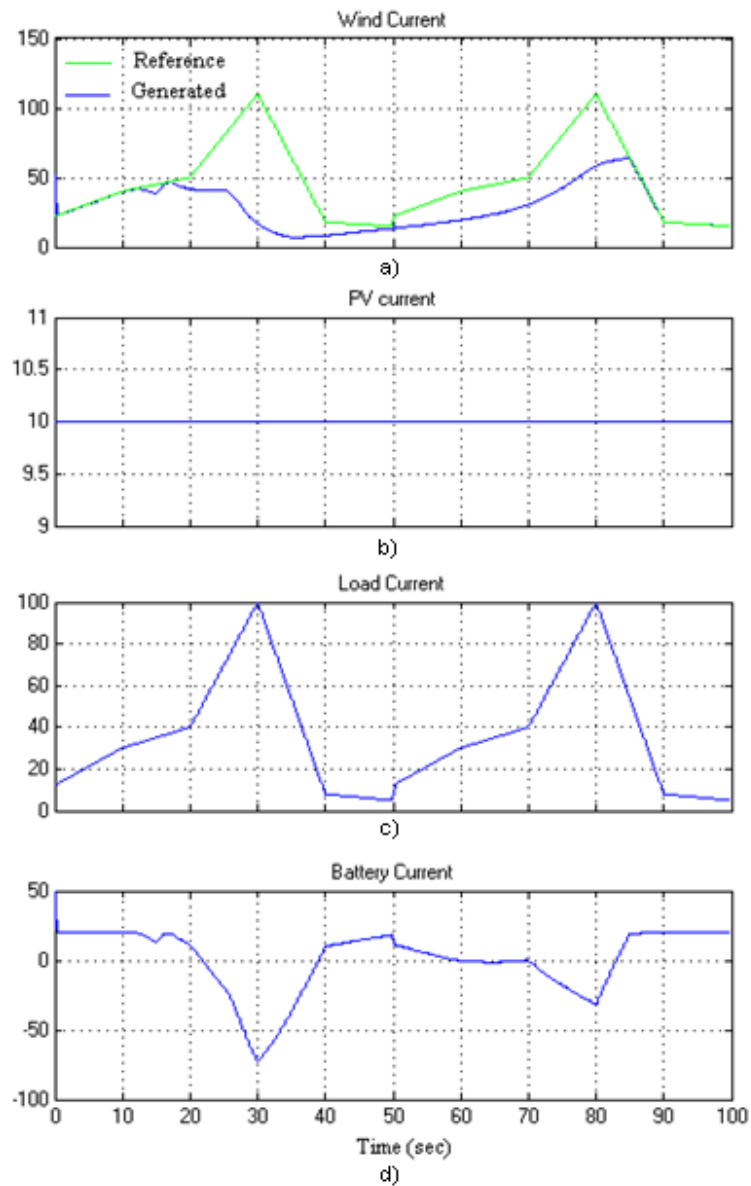


**Figure 30** DC bus Currents (Wind subsystem)

## 4.1.2 Power Control of a Photovoltaic Array using SMC

The solar subsystem acts under supervisor control commands using whichever regulating power or tracking the PV to maximum power operation point. This subsystem starts its operation when the wind power generation is not enough to satisfy the total demand. This subsystem is functioning on all modes except mode 1, because it is established as secondary energy source.

### 4.1.2.1 Sliding Mode Controller Design

The main objective of SMC is to control the power generated by the PV array to satisfy the total power demand (The load and the Battery Bank). For an efficient recharge and to maximize the battery life, the recovery cycle is expected to be done under a given constant current  $I_{bref}$ .

### 4.1.2.2 Modes of Operation

For the PV array, we set two modes of operation following [15]. The first occur when the PV array is capable of generating enough power to satisfy the total power demand.

$$P_{ref} = v_b(i_L + I_{bref} - i_w) \quad (4.11)$$

The second mode of operation occurs when the Panel is unable to generate enough power to supply the power reference. In this mode, the PV operates on the Maximum Power Operation Point (MPOP).

In MPOP, the instantaneous and incremental conductance of the array has different sign and the same absolute value. This condition arises from [50]:

$$\frac{\partial P_{pv}}{\partial V} = i_{pv} - \frac{V i_{pv} - \alpha V I_{max} \tau_i}{b(\gamma\alpha + 1 - \gamma)(V_{max} + \tau_v)} \quad (4.12)$$

The previous equation is the derivative of Equation 3.11 with respect to the voltage. Taking the derivatives of equation 3.10 we obtained the dynamic equations for Current of the PV array [50].

$$\frac{\partial i_{pv}}{\partial V} = \frac{i_{pv} - \alpha I_{max} \tau_i}{b(\gamma\alpha + 1 - \gamma)(V_{max} + \tau_v)} \quad (4.13)$$

The decision to work in one mode of operation or the other is taken by comparing the power that the array would generate if operating at the MPOP and  $P_{ref}$ . This is illustrated on Figure 31, and could be expressed as a fictitious power  $P_f = -\frac{\partial i_{pv}}{\partial V_{pv}} V_{pv}^2$  in the following way [15]:

$$P_f \geq P_{ref} \Rightarrow \text{First mode of operation}$$

$$P_f < P_{ref} \Rightarrow \text{Second mode of operation}$$

a) *Sufficient Power Generation Conditions*

In this mode, the cell temperature and the isolation are sufficient to satisfy  $P_{ref}$ . To accomplish this objective, the sliding surface was written in terms of currents on the battery bank [15].

$$h_1 = i_L + I_{bref} - i_w - i_o \quad (4.14)$$

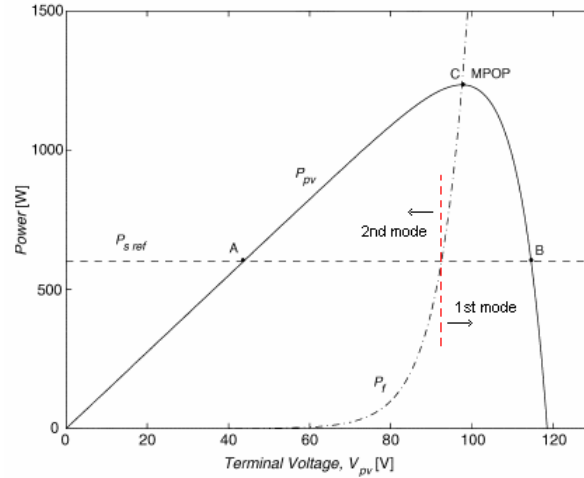


**Figure 31** Zones of operation for control modes under sufficient power generation conditions [15].

and the switch control signal is:

$$u = \begin{cases} 1 & \text{if } h_1 \geq 0 \\ 0 & \text{if } h_1 < 0 \end{cases} \quad (4.15)$$

*b) Insufficient Power Generation conditions*

The control objective is to operate the PV cell at the MPOP because the cell temperature and the isolation are insufficient to satisfy  $P_{ref}$ . In order to satisfy the Equation 4.12, the sliding surface must be [15]:

$$h_2 = \frac{\partial I_{pv}}{\partial V_{pv}} + \frac{I_{pv}}{V_{pv}} \quad (4.16)$$

and the switched control signal must be:

$$u = \begin{cases} 0 & \text{if } h_2 \geq 0 \\ 1 & \text{if } h_2 < 0 \end{cases} \quad (4.17)$$

in this case, the battery bank recharging is made at  $I_b$  instead of  $I_{bref}$ .

### 4.1.2.3 The control Law

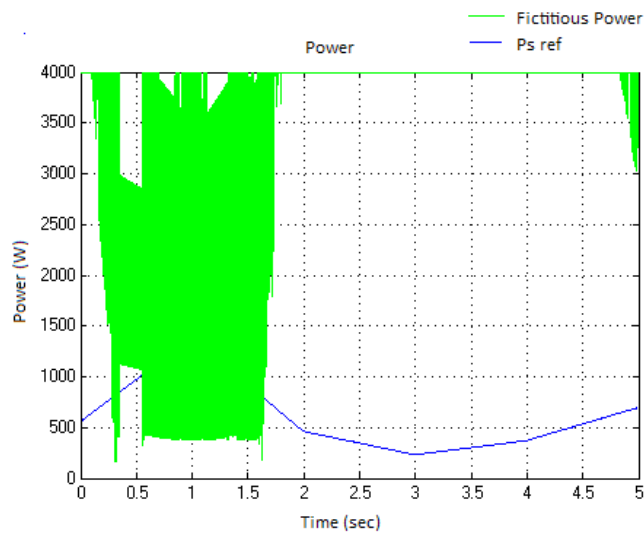
The final control law comprises the two modes of operation that could be summarized as follow [15]:

$$u = \begin{cases} \text{if } -\frac{\partial I_{pv}}{\partial V_{pv}} V_{pv}^2 \geq P_{ref} \\ \text{then } \begin{cases} 1 \text{ if } h_1 \geq 0 \\ 0 \text{ if } h_1 < 0 \end{cases} \\ \text{if } -\frac{\partial I_{pv}}{\partial V_{pv}} V_{pv}^2 < P_{ref} \\ \text{then } \begin{cases} 0 \text{ if } h_2 \geq 0 \\ 1 \text{ if } h_2 < 0 \end{cases} \end{cases} \quad (4.18)$$

with  $h_1 = i_L + I_{bref} - i_w - i_o$  and  $h_2 = \frac{\partial I_{pv}}{\partial V_{pv}} + \frac{I_{pv}}{V_{pv}}$ .

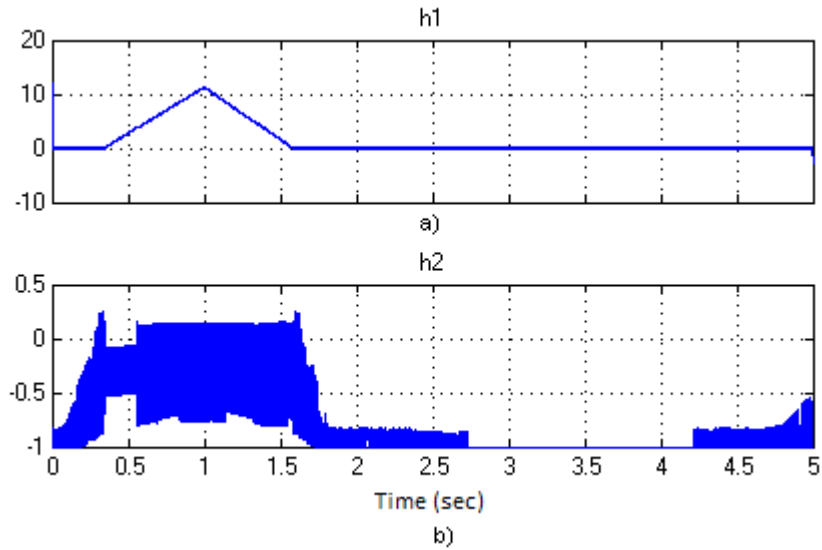
### 4.1.2.4 Simulation Results

The performance of the PV controller was evaluated through computer simulations. Figure 32 shows the fictitious power against the power reference. If the fictitious power is lower or equal to reference power, the PV controller acts in mode 2 else it acts in mode 1.



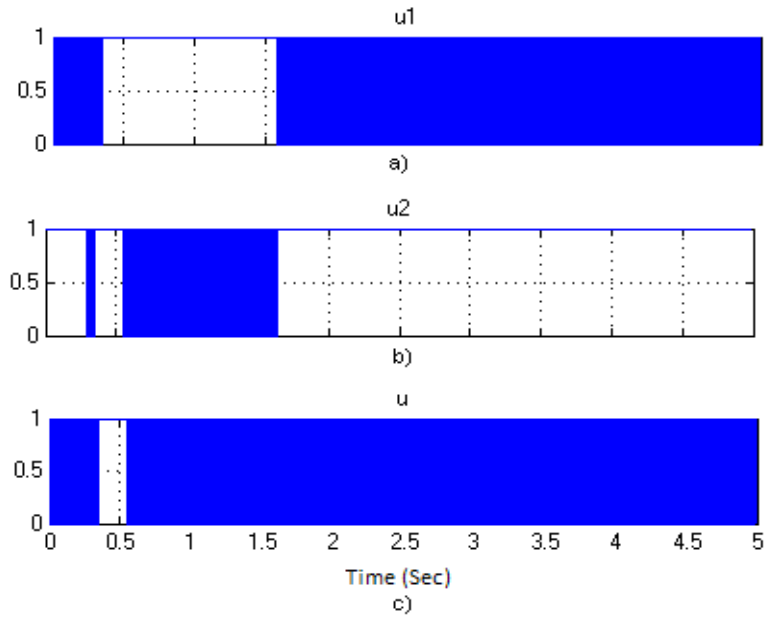
**Figure 32** Power signals to decide mode of operation of solar subsystem.

Figure 33a depicts the sliding surfaces  $h1$  for the first mode of generation, and Fig. 33b shows  $h2$  for the second mode of generation. We could observe the mode of operation by looking at the sliding surfaces.



**Figure 33** Sliding surfaces of solar subsystem.

Figure 34 shows the control signals of the PV array. Fig 34a shows the control signal  $u1$  for the PV array when it is under first mode of generation and Fig 34b shows control signal is  $u2$  for the second mode of operation. Fig 34c shows the signal  $u$  corresponds to total control action of PV array ( $u1+u2$ ). The reaching mode operates, keeping the switched in a permanent position, closed or open, so that the fastest rate of convergence is assured.



**Figure 34** Control signals of solar subsystem.

Finally, Figure 35 depicts the currents present on the DC bus. Fig. 35a presents the wind current fixed at 20A, on this case, the solar subsystem is complementing the wind generation. Fig 35b shows the PV current, we could observe the second mode of operation because the reference signal is higher than the generated signal, and it means that is not enough power from the PV array to satisfy the power demand. Fig 35c shows the load current, which adding the battery reference (20A) makes the total demand. Fig 35d illustrates the current on the battery bank, we could observe that when there is enough power to supply the total demand, it is on recharge cycle and set the current to 20A, but when the power is insufficient it supplies power to the load.

#### **4.1.3 Control Strategy for the Battery Bank and the Grid**

The main objective of this control unit is to make the decision to charge, or discharge the battery bank, and to manage the current provided by the grid.

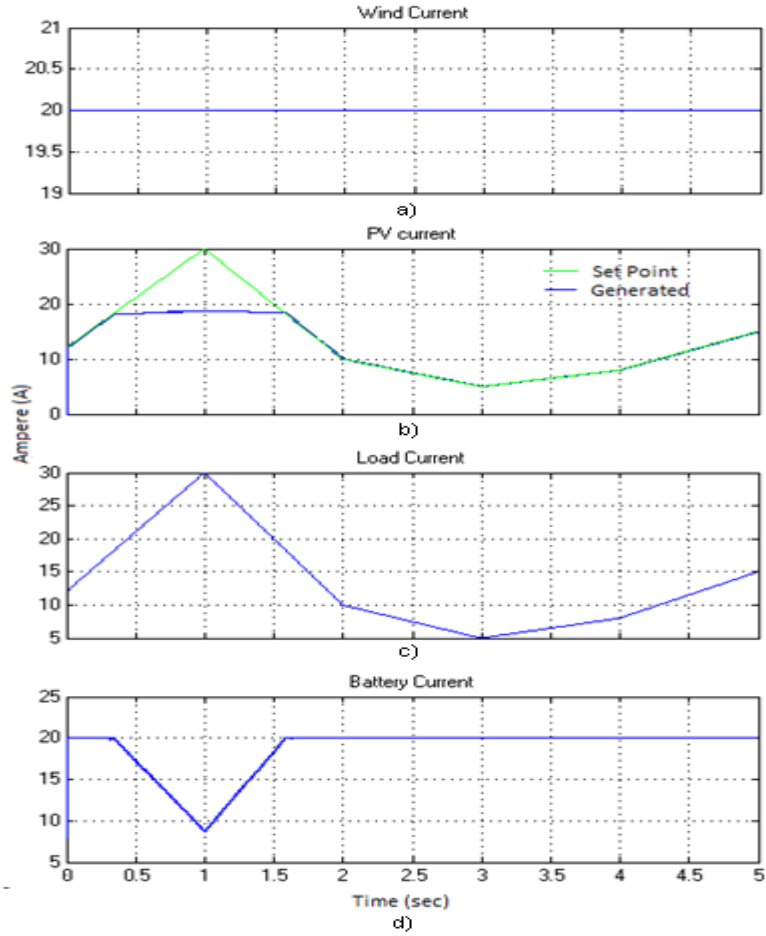


**Figure 35** DC bus currents

Here, the reference bank current  $I_{bref}$  could take two values. If the battery bank current  $I_b$  is positive, it charges the battery bank and  $I_{bref}$  is set to a positive value. If the battery bank is fully charged,  $I_{bref}$  must be reduced to zero [2].

When the battery bank current is negative, it means that the battery bank is supplying energy. If the energy available on the BB is insufficient, the Grid is able to supply the power needed by the load [2].

#### **4.1.3.1 Controller Design**

First, we have to define the magnitude of the charge and discharge currents; they always have to be less or equal to these values. Second, the State of Charge (SOC) of the Battery Bank is supposed to always stay within defined upper and lower limits. These limits are given by:

$$I_{bref+} = \text{Maximun Charging Current}$$

$$I_{bref-} = \text{Maximun Discharging Current}$$

$$Q_{max} = \text{Upper Limit of SOC}$$

$$Q_{min} = \text{Lower Limit of SOC}$$

#### **4.1.3.2 Modes of Operation**

For the Battery Bank, we set two modes of operation. The first occurs when the battery current is positive (charging mode), and the second occurs when the battery current is negative (discharging mode).

a)  $I_b$  is positive

In this mode, the power generated by the renewable energy system is higher than the power required by the load, so the extra power is handled as follow [2]:

- The extra power will be stored in the Battery Bank as long as SOC is less than  $Q_{max}$  and  $I_b$  is a smaller amount than  $I_{bref+}$ .

- If  $I_b > I_{bref+}$ , then the Battery bank is charged by  $I_{bref+}$ , and the extra power is reduced from the PV and wind subsystems through the individual control units.
- If  $SOC = Q_{max}$ , means that the battery bank is fully charged and the extra power must be reduced from the PV and Wind subsystems, i.e. the reference for the controllers is set to zero.

b)  $I_b$  is negative

In this case, the load demand is higher than the power available from the Wind and PV subsystems, so the battery bank and the Grid must supply the extra power needed. Depending upon the SOC of the Battery Bank and the magnitude of  $I_b$ , supplying the extra demand is complete according to the next hierarchical order [2]:

- Only through the Battery Bank as long as these conditions are satisfied:

$$SOC > Q_{min} \quad (4.19)$$

$$|I_b| \leq I_{bref-}$$

- Through the Battery Bank and the Grid: this occurs when the load demand is higher than the battery discharge limitations, so the Grid is able to provide the extra current. The conditions that has to be satisfied are:

$$SOC > Q_{min} \quad (4.20)$$

$$|I_b| > I_{bref-}$$

- Only through the Grid: if the battery bank is completely discharged, this is  $SOC = Q_{min}$ , the Grid must supply the extra power needed. The strategy implemented is called *slope-on strategy* (see Figure 36), in which the grid start level occurs when the SOC is equal to a level higher than  $Q_{min}$ , defined by the battery; when that level  $Q_{min} * X$  is reached, the grid starts taking the load progressively from the battery. The grid current starts increasing with the same slope so that the total current contribution from in cooperation battery bank and the grid making  $I_b = 0$  [2].

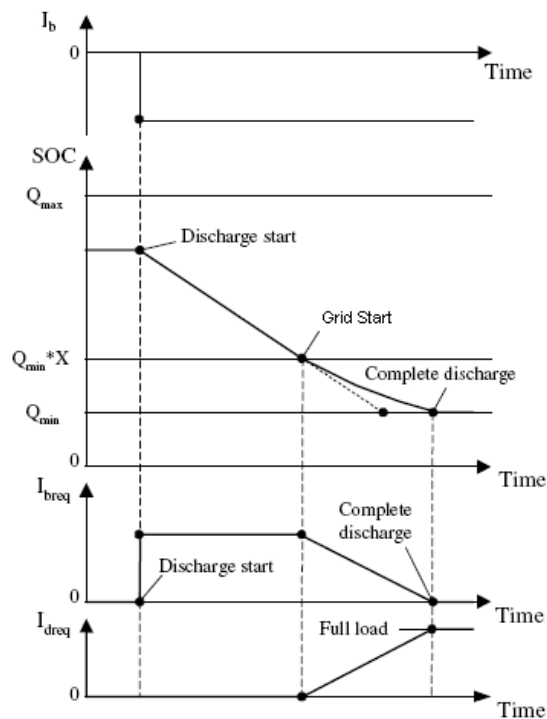


**Figure 36** Implementation of slope-on strategy adapted from [2].

### 4.1.3.3 Simulation Results

The performance of the Battery Bank and the Grid was evaluated through Matlab simulations. For this results, the upper and lower limit of SOC are:

$$Q_{max} = 1$$

$$Q_{min} = -1$$

But, we are going to consider that the battery is fully charged at 76% of SOC and the Diesel Start Point is at -0.76% of SOC, that is:

$$Q_{max} = 0.7613$$

$$Q_{min} * X = -0.7613$$

The maximum charging current, and the maximum discharge current was set to these values:

$$I_{bref+} = 20A$$

$$I_{bref-} = -20A$$

Figure 37(a) shows the Battery Bank current, Fig. 37b shows the Grid current and Fig. 37c shows the State of Charge of the Battery Bank. On this example, the Battery was totally discharged, and the Grid supplies the extra power demand; on recharge cycle, the battery was recharged until 20A. At 3.8, 8.5, and 13 seconds, the battery bank starts to discharge; the grid is able to supply energy at 4, 8.7, and 13.5 seconds because the battery bank

reaches the maximum discharge current. At 0, 5.8, and 10.1 seconds, the grid supply energy because the SOC is  $Q_{min} * X$  or lower.

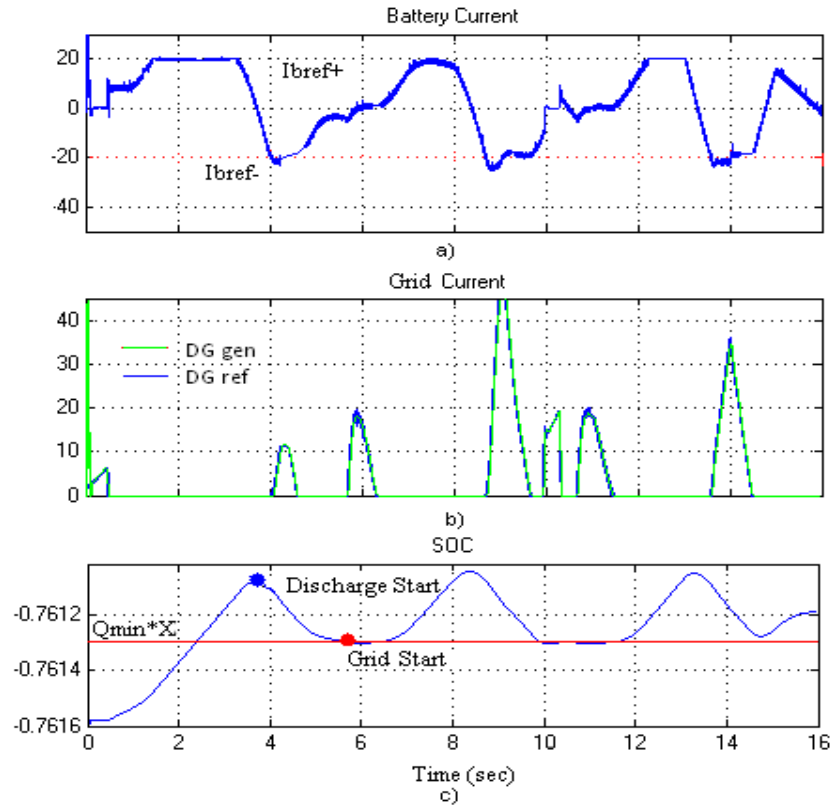


**Figure 37** Battery Bank and Grid currents when the battery is discharged.

Figure 38a shows the Battery Bank current, Fig. 38b the Grid current and Fig. 38c the State of Charge of the Battery Bank. On this example, the Battery was fully charged, and the grid supplies energy only when the battery bank reaches the maximum discharge current. Between 1.6 to 3.5 seconds  $I_b=0$  and the renewable generators only produce the power necessary to satisfy the load demand (Battery is not a part of the total demand), when the SOC is lower than  $Q_{max}$ , the battery is recharged at 20A.

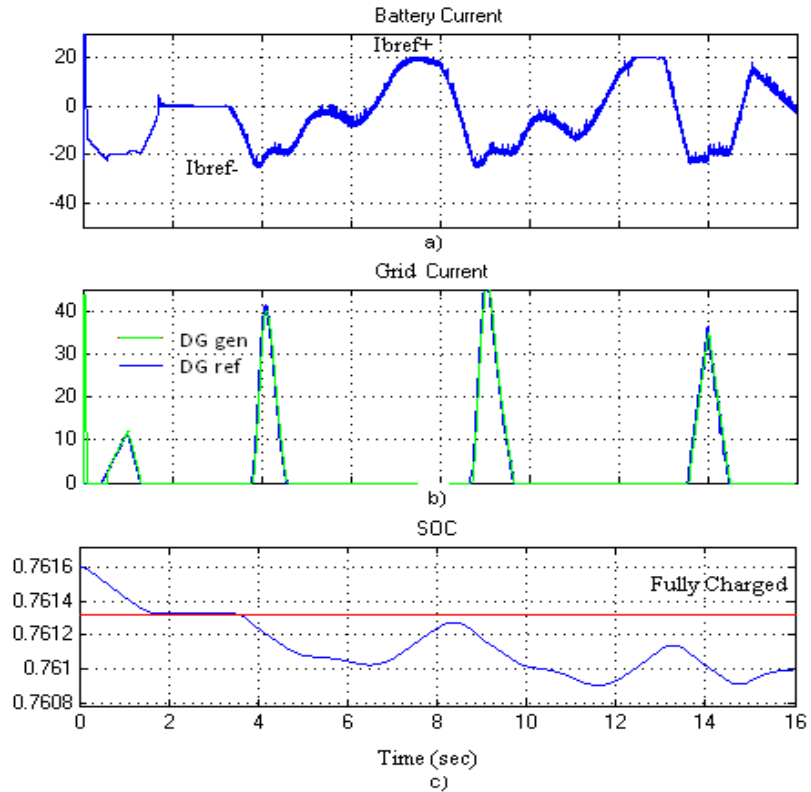


**Figure 38** Battery Bank and Grid currents when the battery bank is fully charged.

#### 4.1.4 On- Off Control for the Load

This control was developed by us to connect or disconnect a particular load or zone from the total power demand. The main reason to do that is to protect the generation sources when there is insufficient generation capacity to meet the demand.

If the total demand is higher than the total generated power, the loads will be disconnected on a sequence order depending of some priorities established a priori.

##### 4.1.4.1 The control law

In our simulation, the lowest priority load is zone three, and the highest is zone one (zone one always needs to stay connected).

$DG_{max}$  is the maximum current generated by the Grid. The Load currents for each zone are  $i_{L1}$ ,  $i_{L2}$ , and  $i_{L3}$ .

The criteria to disconnect load three is described as follow:

$$if(i_{L1} + i_{L2} + i_{L3}) - i_{gen} > DG_{max}$$

$$Load_3 = Off$$

*else*

$$Load_3 = On$$

The criteria to disconnect load two is described as follow:

$$if(i_{L1} + i_{L2}) - i_{gen} > DG_{max}$$

$$Load_2 = Off$$

*else*

$$Load_2 = On$$

$$i_L - i_{gen} < DG_{max}$$

#### **4.1.4.2 Simulation Results**

In this example, the grid only could generate 20A, so if the total demand is higher than the maximum current generated, the load zones will be disconnected.

Figure 39 shows the control signals for each load zone; Fig 39a is always zero, because the first zone is on all the time; Fig 39b depicts the on-off signal for zone two, the

signal is set to one only if the third zone is already off. Fig 39c presents the on-off control signal to third load zone, if the signal is set to one, the load is turned off.

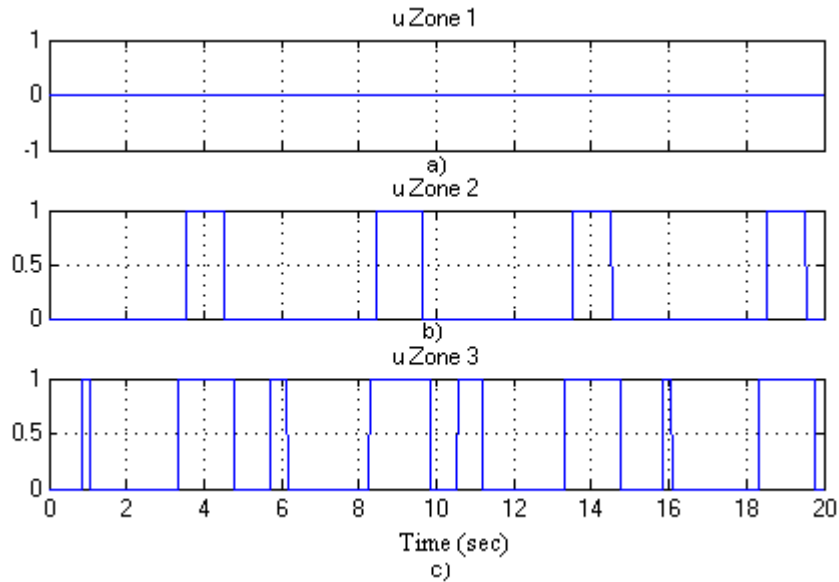


**Figure 39** Control signal for load zones.

Figure 40a shows the Grid current; for this example, the grid was turned on all the time. Fig. 40b depicts the total demand (without control techniques), and the total current demand present on the system. Fig. 40c presents the current demanded for each zone.

## 4.2 Supervisor Control Strategy

The system is composed by a wind subsystem, a solar subsystem, a connection to te grid, a battery bank, and loads as described before. The main objective of the supervisor control is to satisfy the load power demand and to maintain the state of charge (SOC) of the battery bank.

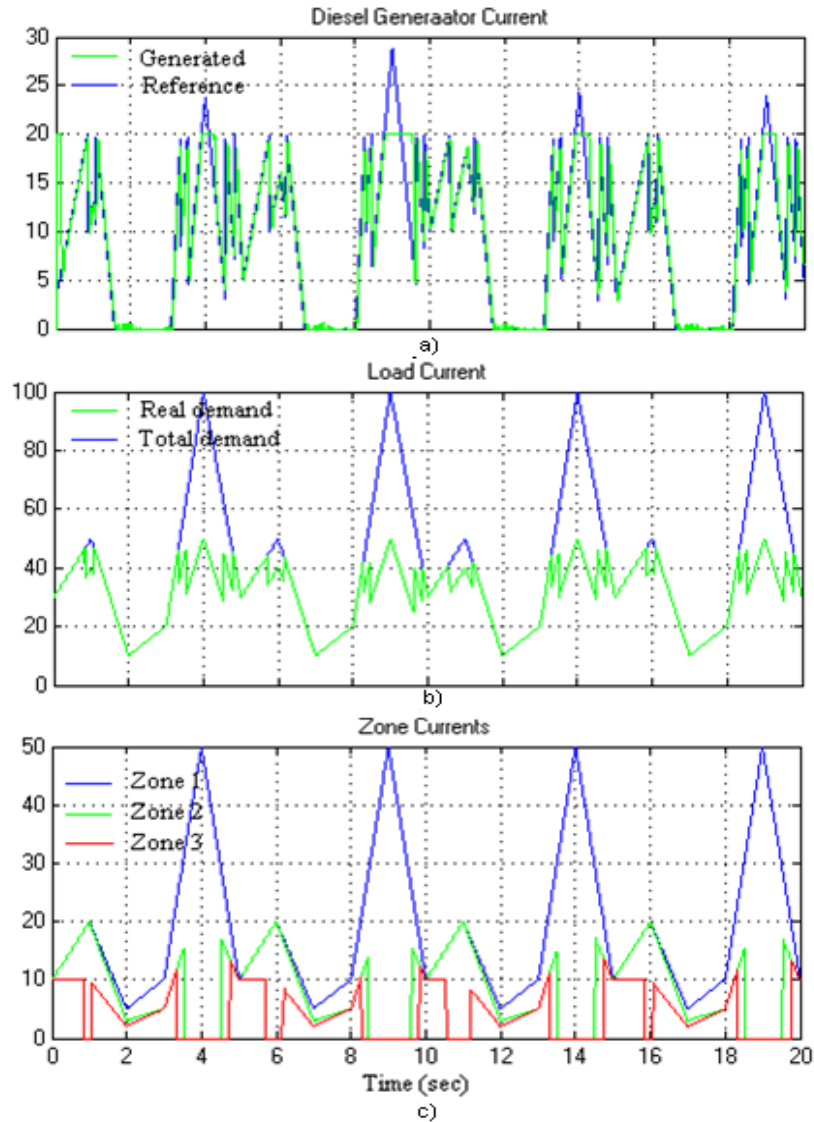


**Figure 40** Grid and Load currents.

The supervisor control determines the operation mode of each generation subsystem. Fundamentally, these operation modes are determined by the energy balance between the total demand (load and battery bank) and the total generation (wind, solar, and grid).

To design the supervisory controller, we select the wind subsystem as the main generator role; the complementary roles are in charge of solar subsystem and the grid respectively.

The complete diagram of HPS including the interaction with the supervisory controller is presented in Figure 41. The supervisor inputs are measure variables as the currents and voltages outputs of the subsystems in the HPS and the SOC of the battery bank. The supervisor outputs are the signals to activate or deactivate each subsystem. The general scheme for inputs and outputs is shown in Figure 42.

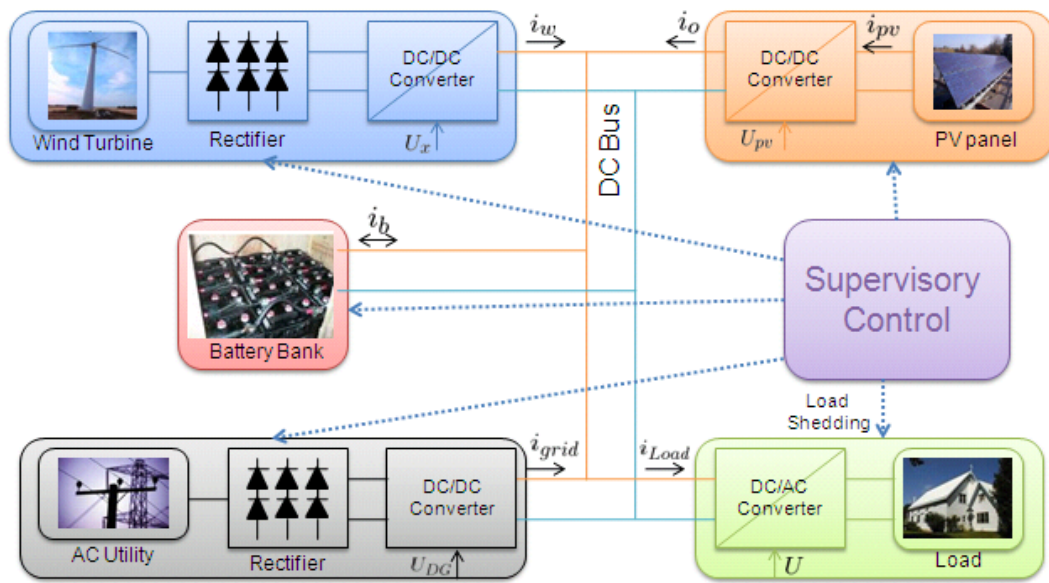


**Figure 41** Supervisory controller interaction model.

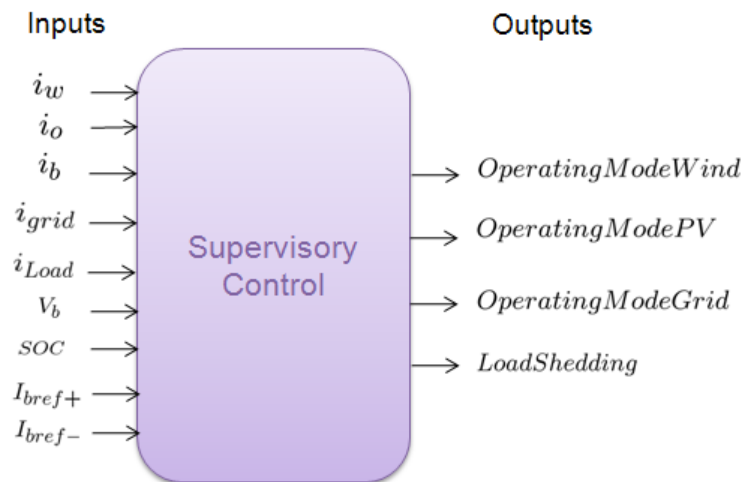


**Figure 42** Scheme for inputs and outputs in the supervisor control.

#### 4.2.1 Modes of Generation

To accomplish the objective, we select five modes of operation as follow. The main idea of the first three modes was proposed in [1], the latest two modes were added to accomplish the supervisor technique of HPS, and was proposed in [2]. Mode 3 was modified to match the battery bank control strategy with the supervisor control. Mode 4 and mode 5 were modified because they were proposed for Diesel generators, but we changed it by connection to the grid.

##### 4.2.1.1 Supervisory controller: Mode 1

Mode one occurs when the wind generation is enough to satisfy the total demand. The solar subsystem and the grid are inactive even as the battery bank is in recharge mode at maximum charging current if it is discharged or at zero current if it is fully charged, and

the wind subsystem is set to power regulation. This mode is running until the maximum available wind power is exceed by the total power demand [1].

$$Mode\ 1: \text{ if } \{\omega_m \geq \omega_{msw}\} \left\{ \begin{array}{l} \text{Wind Subsystem} \rightarrow \left\{ \begin{array}{l} \text{Power Regulation} \\ P_{wref1} = V_b(i_L + I_{bref}) \end{array} \right. \\ \text{Solar Subsystem} \rightarrow \text{Inactive} \\ \text{Battery Bank} \rightarrow \left\{ \begin{array}{l} \text{Recharge Cycle} \\ I_{bref+} \end{array} \right. \\ \text{Grid} \rightarrow \text{Inactive} \\ \text{Zone Load} \rightarrow \text{Inactive} \end{array} \right.$$

#### 4.2.1.2 Supervisory Controller: Mode 2

On this mode, the wind generation is not enough to satisfy the total demand, and it is set by the supervisor control to operate at the point of maximum energy conversion. The solar subsystem is set to follow a power reference required to complement the wind subsystem and together satisfy the total power demand. The battery bank is part of the total power demand, because is in recharge cycle, and its current is always the battery reference current [1].

$$Mode\ 2: \text{ if } \left\{ \begin{array}{l} \omega_m < \omega_{msw} \\ -\frac{\partial I_{pv}}{\partial V_{pv}} V_{pv}^2 \geq P_{ref} \end{array} \right. \left\{ \begin{array}{l} \text{Wind Subsystem} \rightarrow \left\{ \begin{array}{l} \text{Maximum Power Conversion} \\ P_{wref2} = K_{opt}\omega_m^3 - \frac{3}{2}(i_q^2 + i_d^2)r_s \end{array} \right. \\ \text{Solar Subsystem} \rightarrow \left\{ \begin{array}{l} \text{Power Regulation} \\ P_{sref} = v_b(i_L + I_{bref} - i_w) \end{array} \right. \\ \text{Battery Bank} \rightarrow \left\{ \begin{array}{l} \text{Recharge Cycle} \\ I_{bref+} \end{array} \right. \\ \text{Grid} \rightarrow \text{Inactive} \\ \text{Zone Load} \rightarrow \text{Inactive} \end{array} \right.$$

#### 4.2.1.3 Supervisory Controller: Mode 3

On this mode, the wind and the solar subsystems are set to operate at their maximum energy conversion points, and the battery bank is set to supply power to the load instead to receive energy. This mode is maintained as long as the state of charge of the

battery is greater than a minimum required [1] or the battery current is higher than the maximum discharging current [2].

$$\text{Mode 3: if } \left\{ \begin{array}{l} \omega_m < \omega_{msw} \\ -\frac{\partial I_{pv}}{\partial V_{pv}} V_{pv}^2 < P_{ref} \\ |I_b| \leq I_{bref-} \\ i_L < i_{gen} \end{array} \right. \left\{ \begin{array}{l} \text{Wind Subsystem} \rightarrow \left\{ \begin{array}{l} \text{Maximum Power Conversion} \\ P_{wref2} = K_{opt} \omega_m^3 - \frac{3}{2} (i_q^2 + i_d^2) r_s \end{array} \right. \\ \text{Solar Subsystem} \rightarrow \left\{ \begin{array}{l} \text{MPOP tracking} \\ \frac{\partial I_{pv}}{\partial V_{pv}} + \frac{I_{pv}}{V_{pv}} = 0 \end{array} \right. \\ \text{Battery Bank} \rightarrow \text{Able to supply power to the load} \\ \text{Grid} \rightarrow \text{Inactive} \\ \text{Zone Load} \rightarrow \text{Inactive} \end{array} \right.$$

#### 4.2.1.4 Supervisory Controller: Mode 4

In this case, the load demand is higher than the power available from renewable sources, and the battery bank current is equal or higher than maximum discharging current. The supervisor control turns on the grid to provide the extra current [2]. On this mode, the battery current is always the maximum discharging current.

On this mode, the On-Off control for the load may be activated if the total current demand is highest than the total current generated by the renewable energy and the grid.

$$\text{Mode 4: if } \left\{ \begin{array}{l} \omega_m < \omega_{msw} \\ -\frac{\partial I_{pv}}{\partial V_{pv}} V_{pv}^2 < P_{ref} \\ |I_b| > I_{bref-} \\ SOC > Q_{min} \\ i_L > i_{gen} \end{array} \right. \left\{ \begin{array}{l} \text{Wind Subsystem} \rightarrow \left\{ \begin{array}{l} \text{Maximum Power Conversion} \\ P_{wref2} = K_{opt} \omega_m^3 - \frac{3}{2} (i_q^2 + i_d^2) r_s \end{array} \right. \\ \text{Solar Subsystem} \rightarrow \left\{ \begin{array}{l} \text{MPOP tracking} \\ \frac{\partial I_{pv}}{\partial V_{pv}} + \frac{I_{pv}}{V_{pv}} = 0 \end{array} \right. \\ \text{Battery Bank} \rightarrow \left\{ \begin{array}{l} \text{Supplying power to the load} \\ I_{bref-} \end{array} \right. \\ \text{Grid} \rightarrow \text{Able to supply power to the load} \\ \text{Zone Load} \rightarrow \text{Active} \end{array} \right.$$

#### 4.2.1.5 Supervisory Controller: Mode 5

On this mode, the total demand is more than the power available from wind and solar subsystems, and the battery bank is discharged. The supervisor control allows the grid

to starts taking the load gradually from the battery to supply the power demand [2]. On this mode, the battery current is always zero.

The On-Off control for the load may be activated if the total current demand is highest than the total current generated by the system.

$$\text{Mode 5: if } \begin{cases} \omega_m < \omega_{msw} \\ -\frac{\partial I_{pv}}{\partial V_{pv}} V_{pv}^2 < P_{ref} \\ SOC \leq Q_{min} \\ i_L > i_{gen} \end{cases} \begin{cases} \text{Wind Subsystem} \rightarrow \begin{cases} \text{Maximum Power Conversion} \\ P_{wref2} = K_{opt} \omega_m^3 - \frac{3}{2} (i_q^2 + i_d^2) r_s \end{cases} \\ \text{Solar Subsystem} \rightarrow \begin{cases} \text{MPOP tracking} \\ \frac{\partial I_{pv}}{\partial V_{pv}} + \frac{I_{pv}}{V_{pv}} = 0 \end{cases} \\ \text{Battery Bank} \rightarrow \begin{cases} \text{Completely Discharged} \\ I_b = 0 \end{cases} \\ \text{Grid} \rightarrow \text{Active} \\ \text{Zone Load} \rightarrow \text{Active} \end{cases}$$

#### 4.2.2 Operation Strategy

The operation strategy for the supervisor control of the HPS is shown in Figure 43 as a state transition diagram for each mode of the supervisory controller.

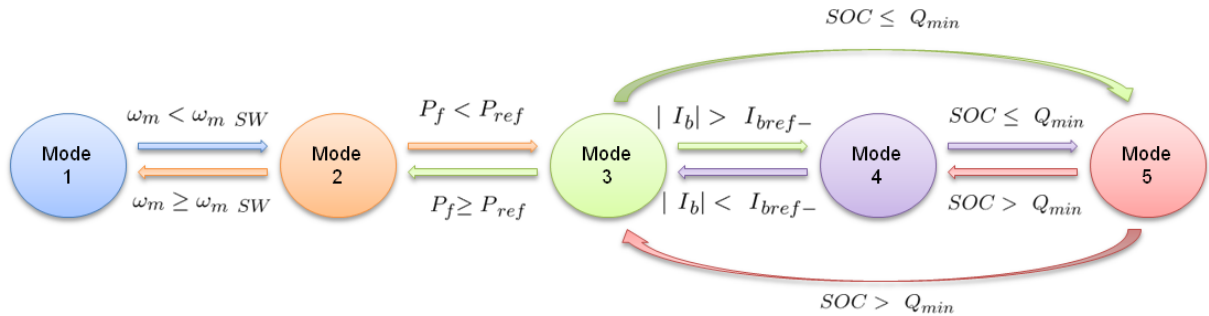


**Figure 43** Mode transition criteria for the supervisor control.

The supervisory controller can shed some loads if the total power demand is higher than what the overall system could supply. This strategy was not included as an operation mode because it depends basically of the load demand and not on the availability of the generation sources. Figure 44 shows the transition criteria to apply shedding load. This

criterion occurs only if the system is operating in mode 4 or mode 5. Figure 45 shows the Matlab/Simulink diagram for the supervisory controller.

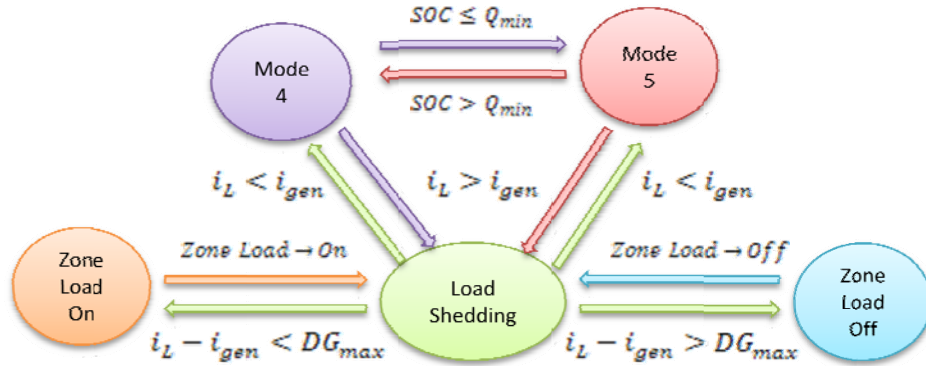


Figure 44 Load shedding scheme

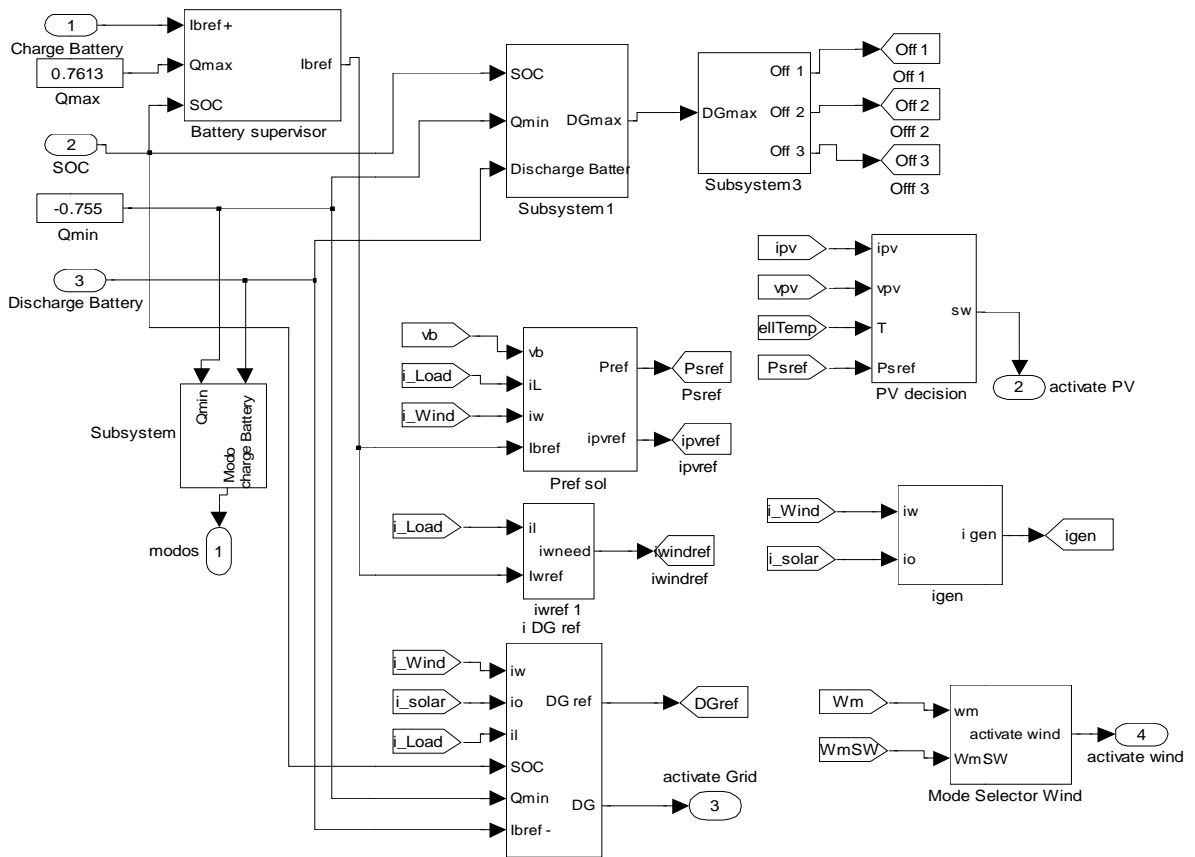


Figure 45 Matlab/Simulink Model of supervisory controller.

### 4.2.3 Simulation Results

This section presents the results of the full system including all modes of operation, all Individual Control Units, and the Supervisor Control. Two scenarios were evaluated to represent all the possible situations on the system behavior. First scenario was simulated with the battery bank fully charged and the second scenario with the battery bank totally discharged.

Both scenarios were simulated with the same parameters and perturbations to compare the performance of each subsystem and to evaluate the behavior of Supervisor Control.

Figure 46 shows *a)* the wind speed, with variations between 10-12 m/sec, and *b)* the cell temperature of PV array which varies between 30 – 50 °C. The three zones of the load were selected to force the HPS and the Supervisor Control to operate in all possible modes.

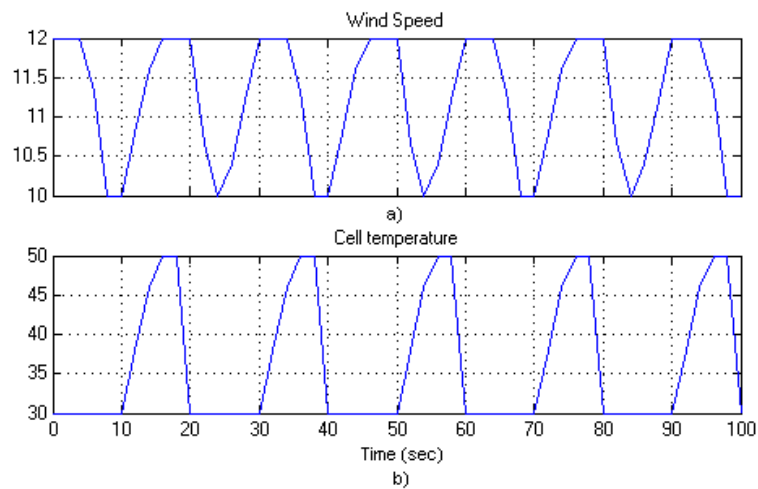


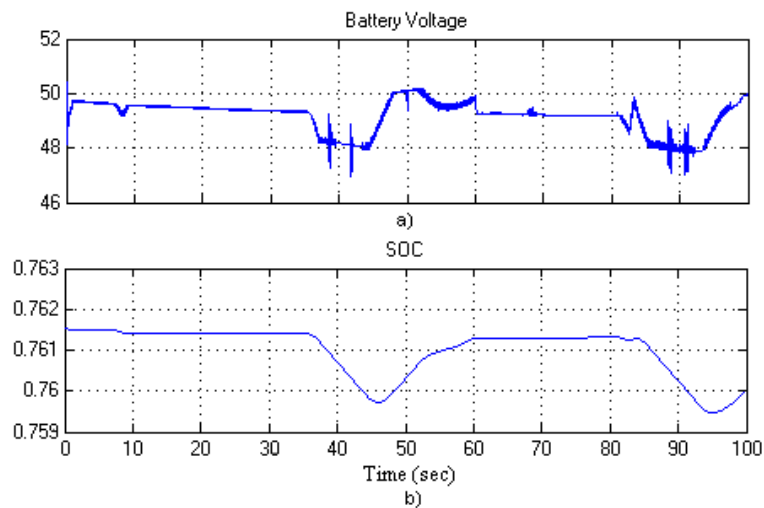
**Figure 46** a) Wind speed and b) Cell temperature variations

#### 4.2.3.1 Battery Bank Fully Charged

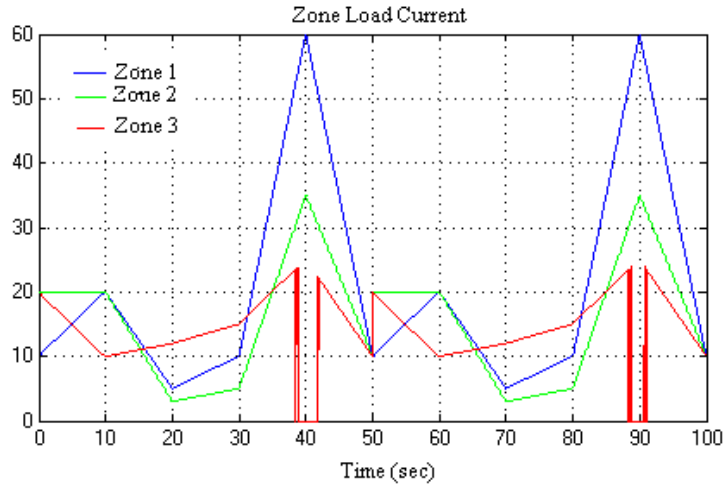
This corresponds to the first scenario to evaluate. The initial condition of the battery bank is fully charged (SOC = 0.7616); the upper limit to considerate a fully charged battery is 0.7613, so when the SOC of the battery is higher than this value, the battery reference current for the renewable source to charge the battery is zero.

Figure 47 shows *a)* the battery bank voltage and *b)* the SOC of the battery bank, on this graph we could observe the battery fully charged before four seconds, after this time, the battery still charged, but not at its maximum capacity. If the slope is positive, means that the battery bank is on charging mode, also it is on discharging mode.

Figure 48 depicts the current of each load zone. As we said before, the highest priority zone is the zone 1. The interruption on the current means that the corresponding zone was disconnected.



**Figure 47** Battery Voltage and SOC (Battery Bank Fully Charged).



**Figure 48** Load current divided by zones (Battery Bank Fully Charged).

Figure 49 shows *a)* the wind turbine and *b)* the Photovoltaic panel control signals. We could observe that PV array is not controlled when the HPS is in mode 1. The individual control signals and sliding surfaces of solar subsystem and wind subsystem are shown in Figure 50 and Figure 51 respectively.

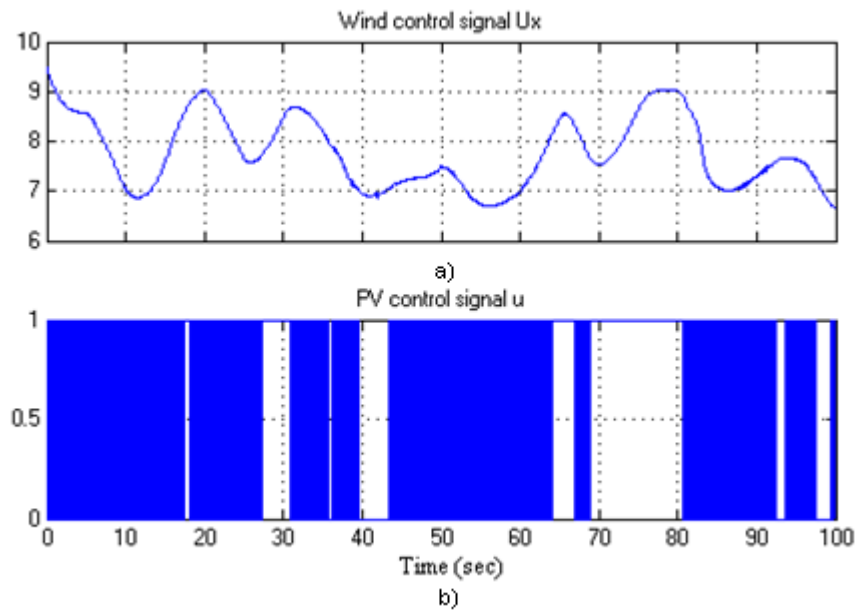


**Figure 49** Control signals of Wind Turbine and PV array (Battery Bank Fully Charged)

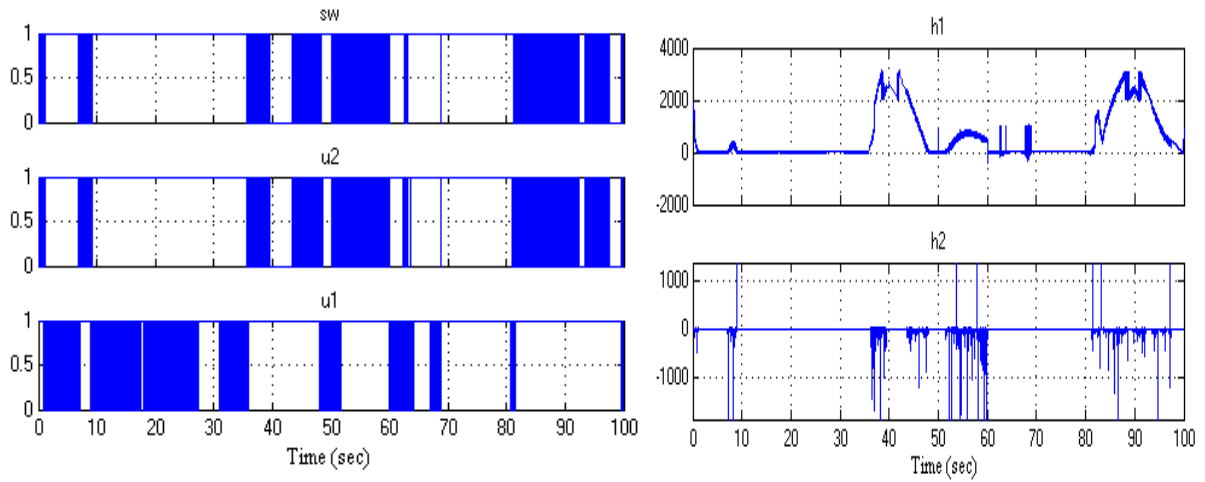


**Figure 50** Control signals and sliding surfaces of PV array

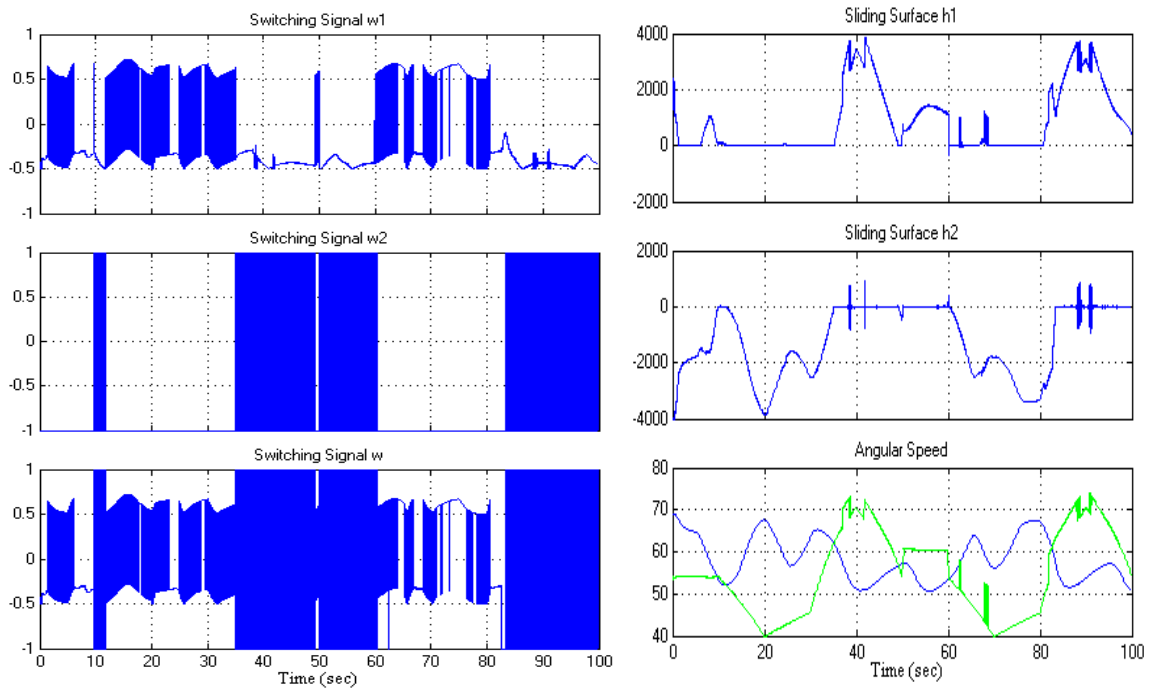


**Figure 51** Control signals and sliding surfaces of Wind Turbine

Figure 52 shows the DC bus current of HPS. Fig. 52a presents the wind current (Set-Point and generated current), at time 1.2 to 6.8, 13.8 to 35, and 60 to 81 seconds. It can be

observed that the reference signal is equal to generated signal. This means that the system is operating at mode 1 as shown in Fig. 52*f*; the maximum current generated by the wind subsystem is 75A. Fig. 52*b* presents the solar current. When the reference signal is equal to a generated signal and both signals are different from zero, it means that the system is operating at mode 2 else, system operates at mode 3 as shown in Fig. 52*f*. The maximum current produced by the panel is 17A. Fig. 52*c* shows the battery bank current. Because the battery initial condition was fully charged, when there are sufficient generation conditions, the battery reference current is set to zero, also is set to 20A. If the battery current does not exceed the maximum discharging current (-20A), it means that the system is working within the three first modes, else it is working on mode 4 as shown in graph six. Fig. 52*d* shows the grid current. This signal is activated only if the maximum discharge current of the battery bank was exceeded. This happens under this scenario because the battery bank is fully charged. The maximum current that the grid could produce is 25A, so when the grid reference is higher than this value, the on-off control made by supervisor control is activated to turn off one zone of the total load demand as shown in Fig. 52*e*. Fig. 52*f* presents the operation modes of supervisor control. On this scenario, mode five is impossible because the battery bank is fully charged.

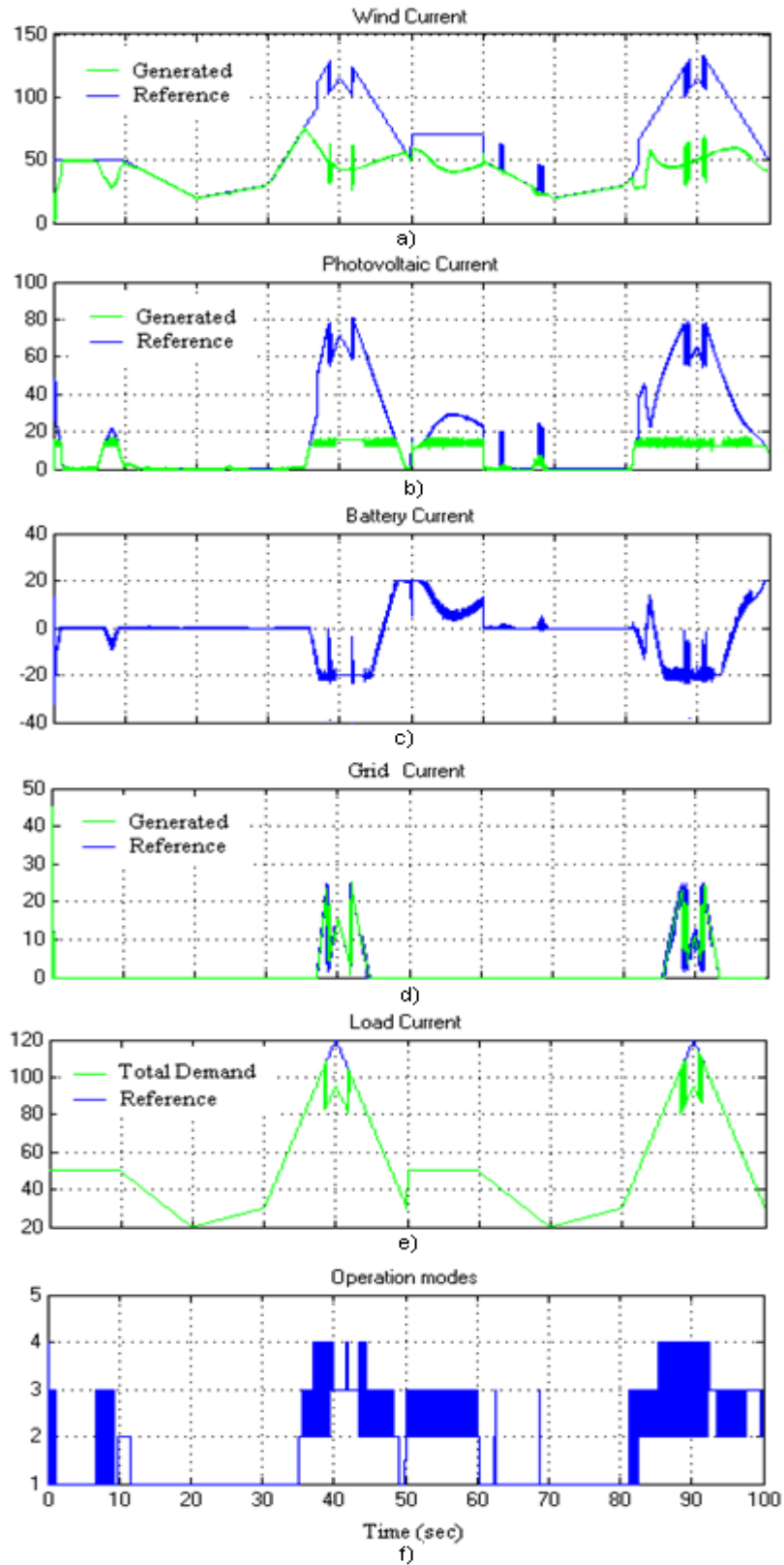
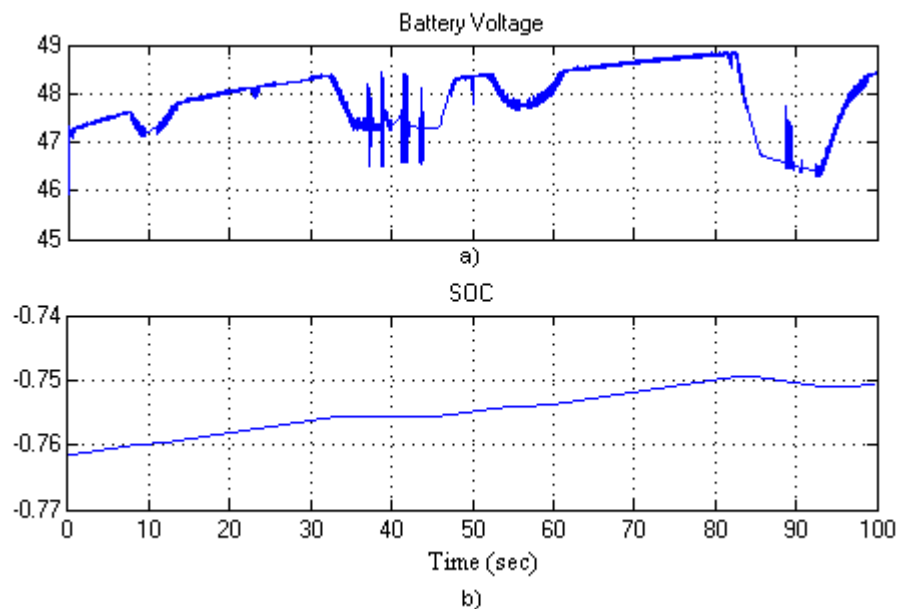


Figure 52 DC bus currents and operation modes (Battery Bank Fully Charged).

#### 4.2.3.2 Battery Bank Totally Discharged

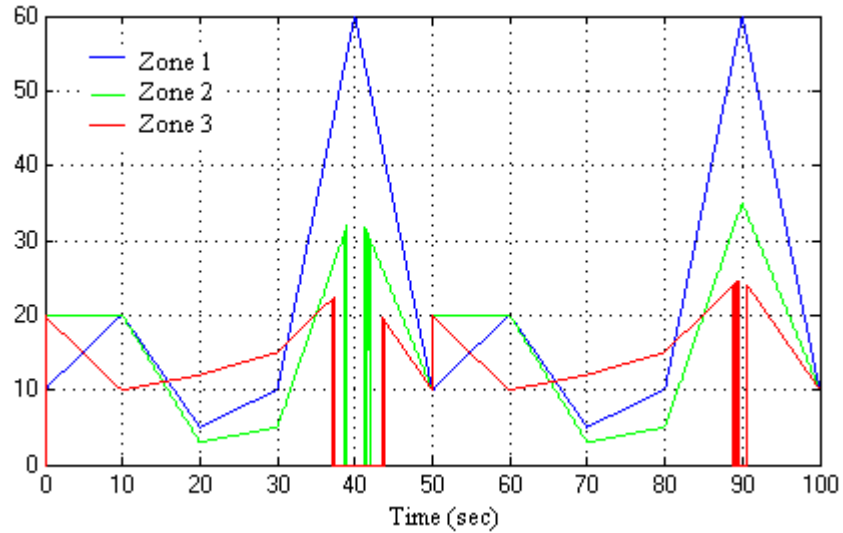
This corresponds to the second scenario to evaluate. The initial condition of the battery bank is totally discharged (SOC = -0.755); the limit to allow the grid generation because the battery is considered discharged is -0.755, so the battery reference current for the renewable source to charge the battery bank is the maximum charging current, in this case 20A.

Figure 53 shows the battery bank voltage and the SOC of the battery bank. On this graph we could observe the battery totally discharged. If the slope is positive, means that the battery bank is on charging mode, also it is on discharging mode. If the slope is constant, means that SOC is at lower limit so all the extra power needed by the load is given by the Grid, and the battery current is zero.



**Figure 53** Battery voltage and SOC (Battery Bank discharged)

Figure 54 depicts the current of each load zone. As we said before, the highest priority zone is zone 1. The interruptions on the current signal means that the respectively zone was disconnected. Figure 55 shows the wind turbine and the Photovoltaic panel control signals.



**Figure 54** Load current divided by zones (Battery Bank Discharged).

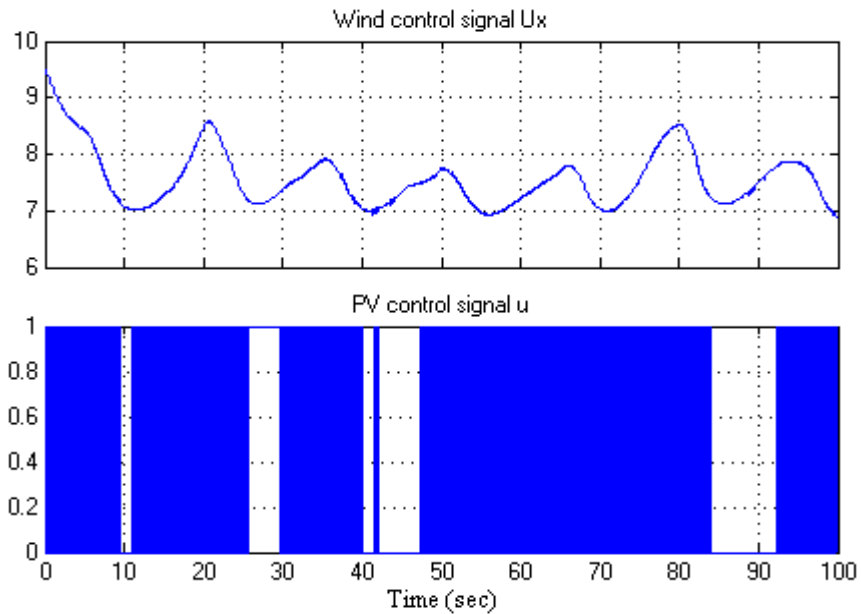


**Figure 55** Control signals of Wind Turbine and PV array (Battery Bank Discharged)

The individual control signals and sliding surfaces of solar subsystem and wind subsystem are shown in Figure 56 and Figure 57, respectively.

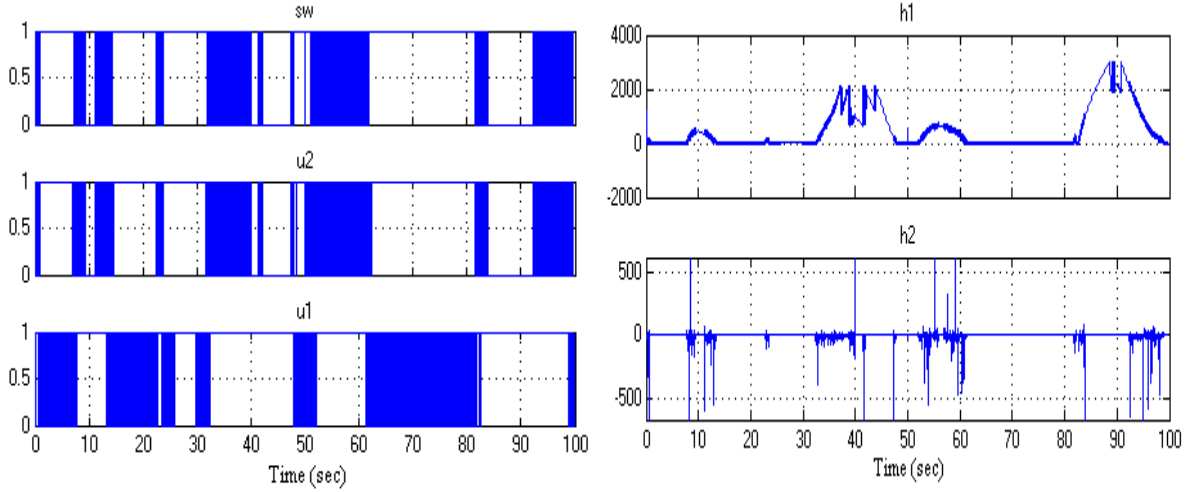


**Figure 56** Control signal and sliding surfaces of solar subsystem

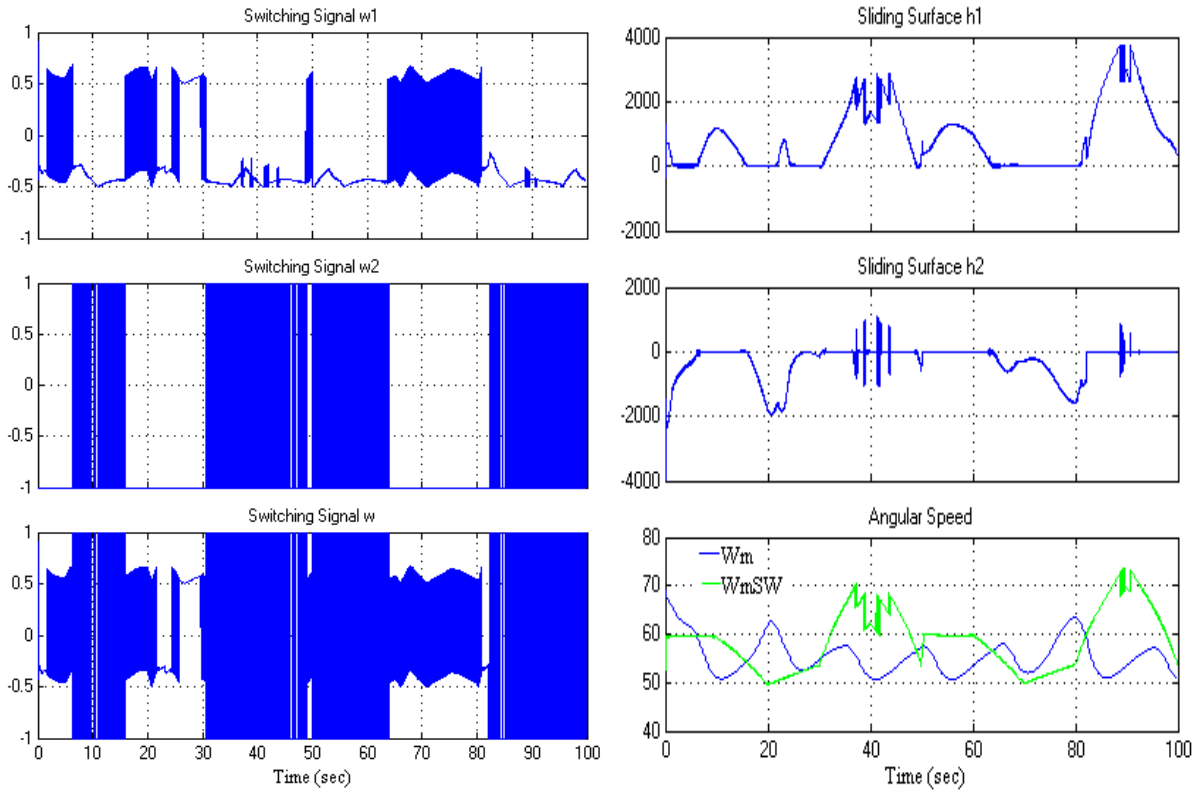


**Figure 57** Control signal and sliding surfaces of wind subsystem

Figure 58 shows the DC bus current of HPS: Fig. 58a presents the wind current (Set-Point and generated current). Between 2 to 6, 16 to 22, 24 to 31, and 64 to 81 seconds, we can observe that the reference signal is equal to generated signal. As shown before, that means that system is operating at mode 1 as presented in graph six. Fig. 58b illustrates the solar current with the same behavior of the previous example. Fig. 58c shows the battery bank current. Because the initial condition was totally discharged, when there are is enough generation from the renewable sources, the battery reference current is set to maximum charge current (20A), and the system works under the first three modes. If the battery current exceeds the maximum discharging current (-20A), the system works on mode 4. If the SOC of the battery is under  $Q_{min}$ , it means that the system works under mode 5 as shown in Fig. 58f. Fig. 58d shows the grid current. This signal is activated only if the maximum discharge current of the battery bank was exceeded or the SOC of the battery bank is charge to  $Q_{min}$ . The maximum current that the grid could produce is 25A, so when the diesel reference is higher than this value, the load shedding control is activated to turn off one or two zones of the total load as shown in Fig. 58e. Fig. 58f presents the operation modes of supervisor control. This scenario activates mode five because this mode depends on the lower limit of SOC of the battery.

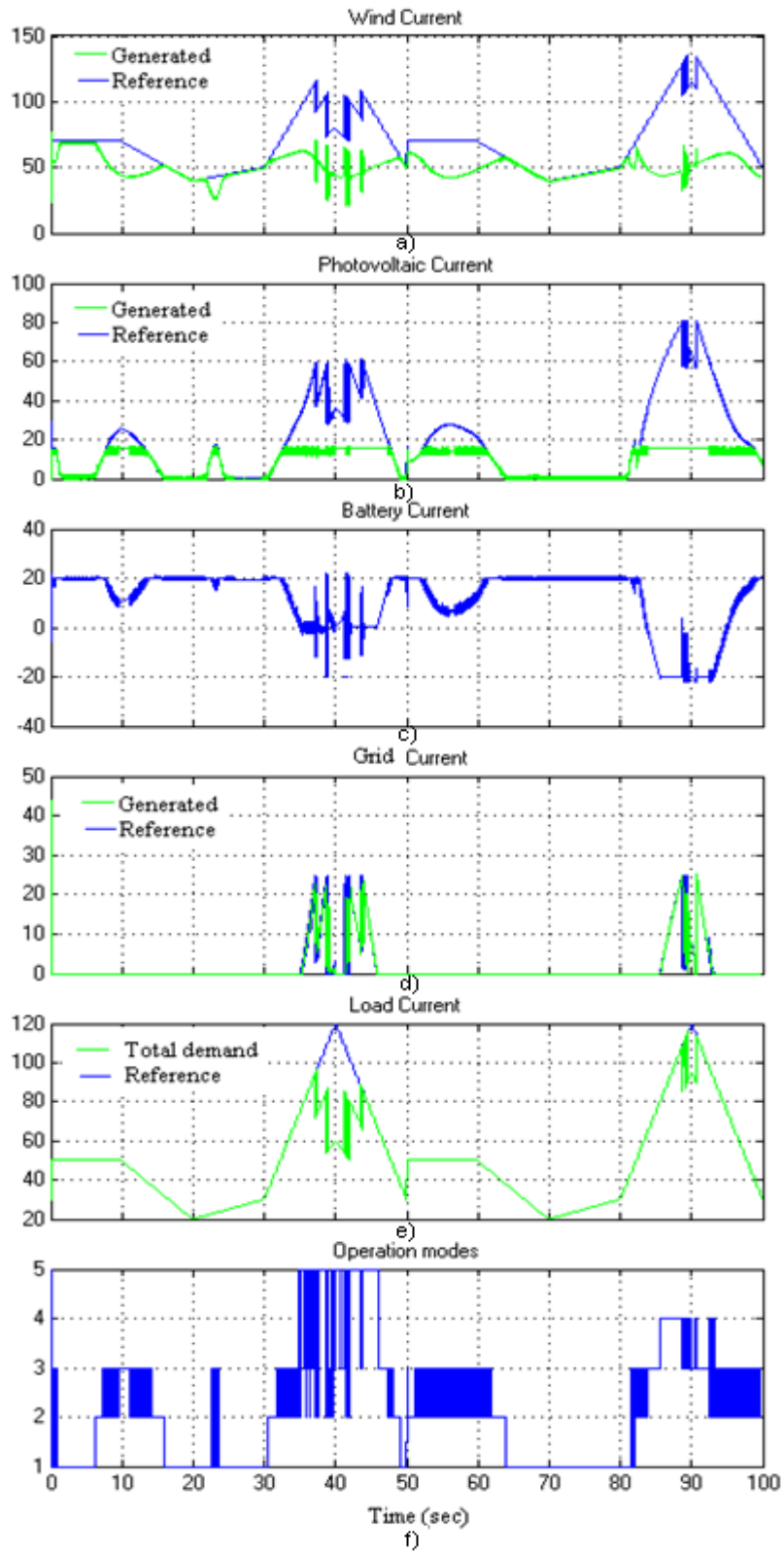


Figure 58 DC bus currents and operation modes (Battery Bank Discharged).

### 4.2.3.3 Sufficient power generation

In this example, we set a constant wind speed (12m/sec) and a constant cell temperature (30 °C) to simulate sufficient power regime for all system. The SOC of the battery bank is totally discharged as shown in Figure 59. The behavior of the overall system is similar to that described before. The main difference is that supervisor control moves between the three first modes. The grid only generates power in the beginning because the wind generation was not enough.

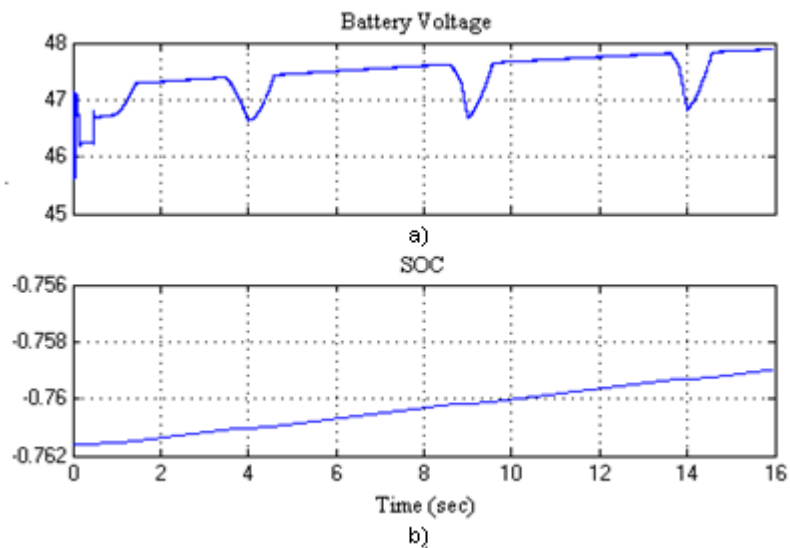


Figure 59 SOC of Battery Bank (Sufficient power regime)

Figure 60 shows the DC bus currents, the order of the graphs are the same as the previous example, and have a similar performance. Figure 61 presents the power of the PV array. If fictitious power is lower or equal to the reference power means that system is working in mode 3. Figure 62 shows the angular frequency of wind subsystem, as described before, it acts like a decision criteria to work in mode 1 or turn on the PV array to work in mode 2 or 3.

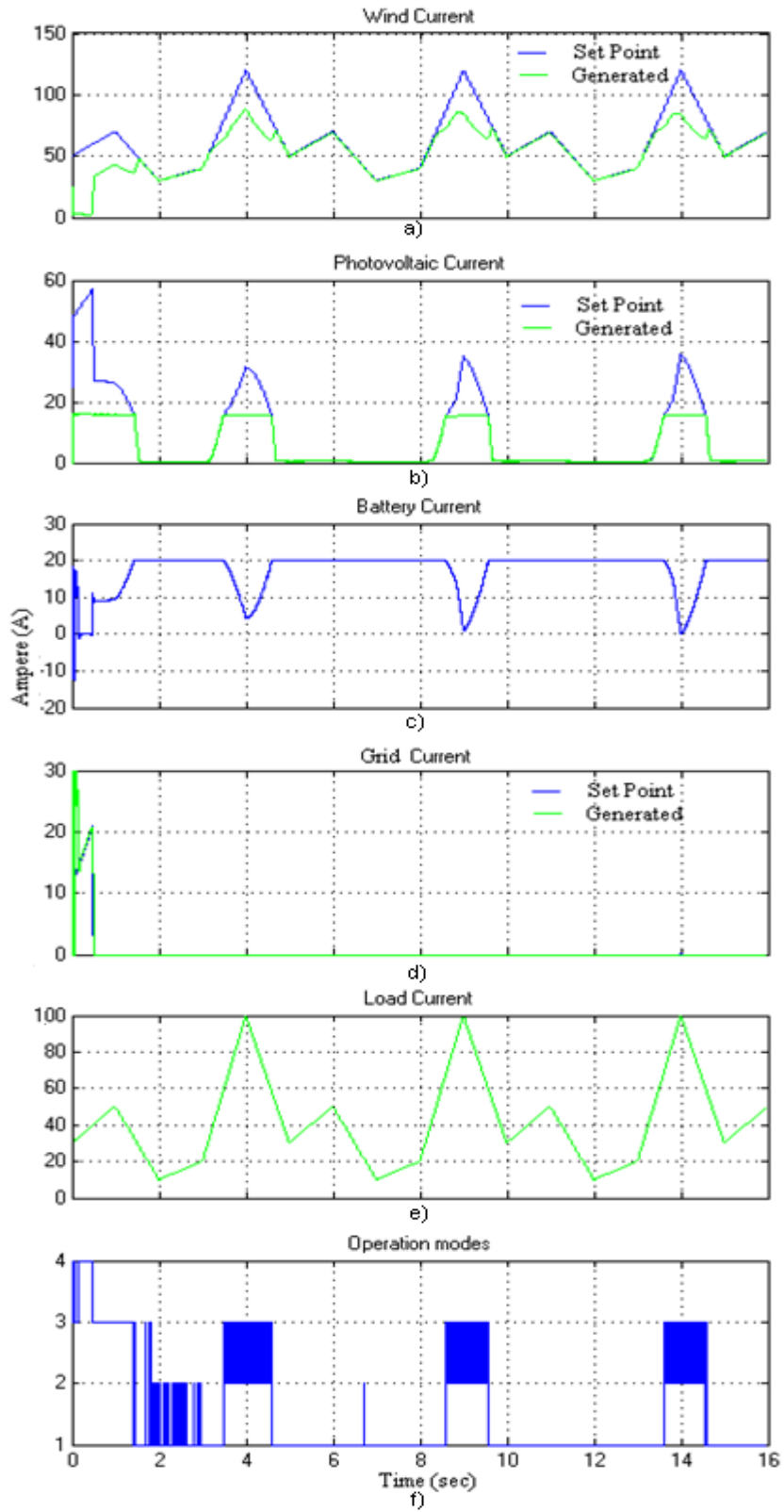
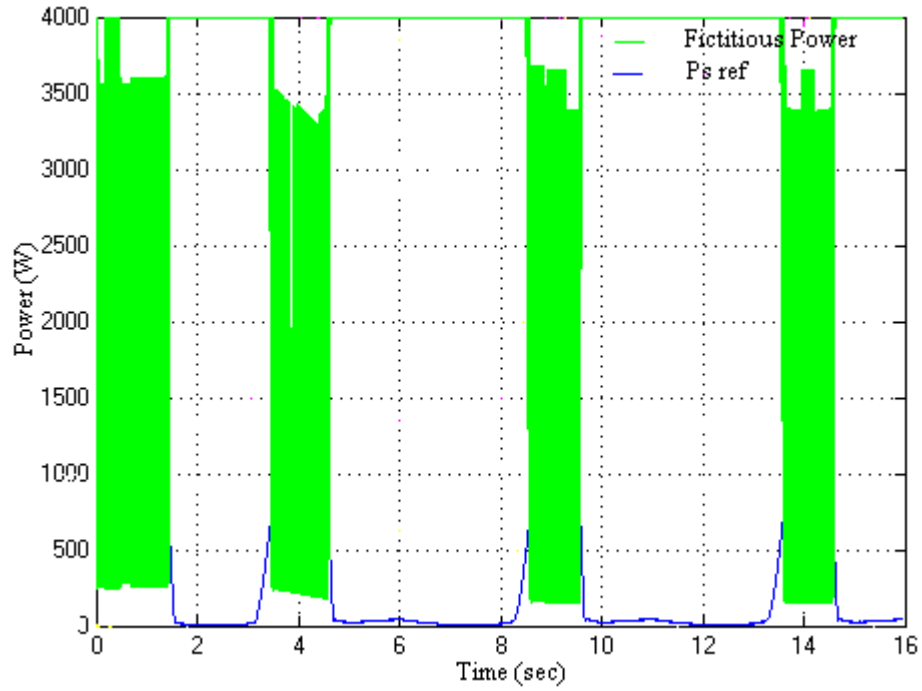
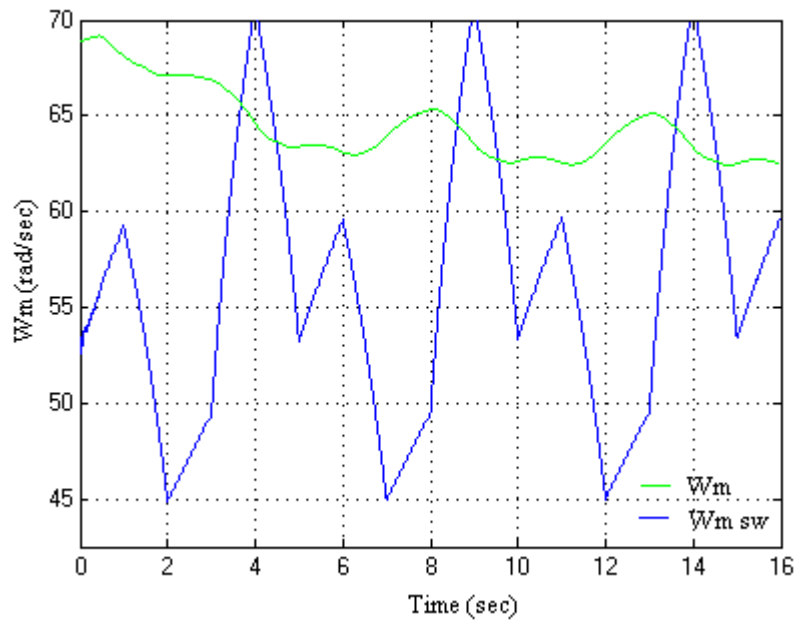


Figure 60 DC bus current of HPS (sufficient power generation)



**Figure 61** Power reference and fictitious power of PV array (sufficient generation power)



**Figure 62** Wind subsystem decision criteria (sufficient power regime)

Figure 63 and Figure 64 depict the PV array control signals for each generation mode, and their respective sliding surfaces. Figure 65 shows the control signals of renewable sources.

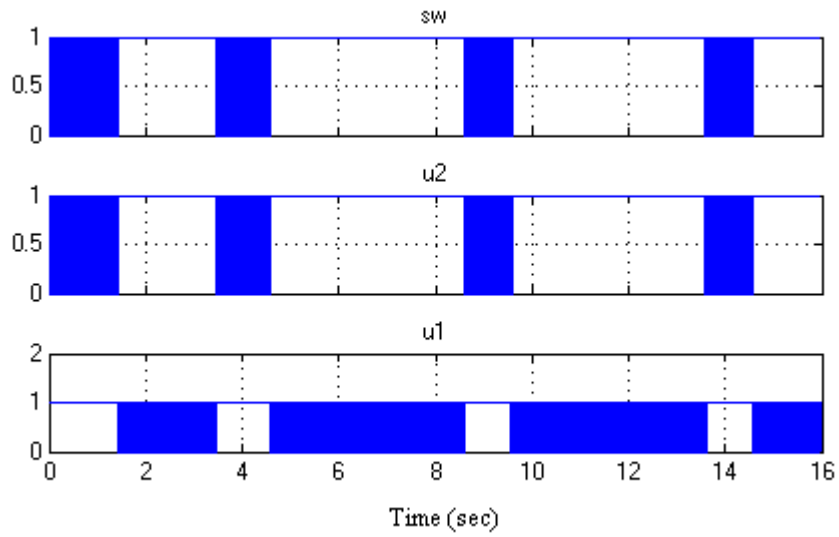


**Figure 63** PV array control signals (sufficient power generation)

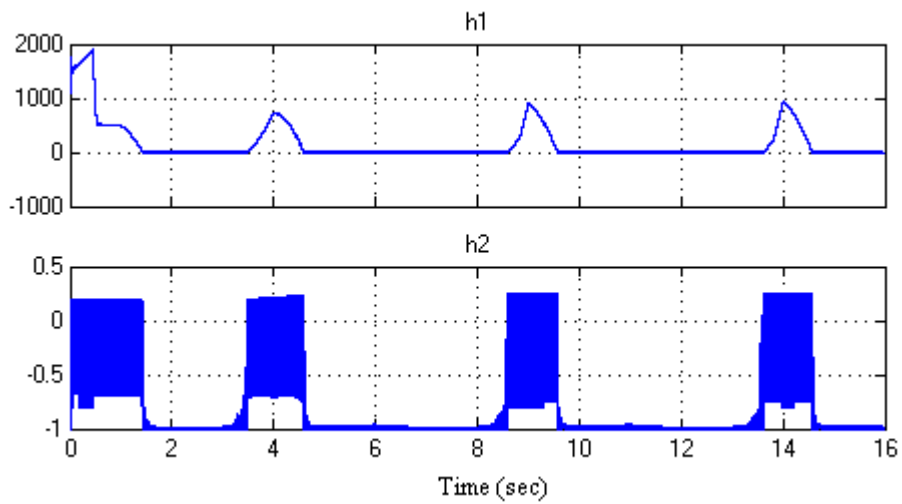


**Figure 64** PV array sliding surfaces (sufficient power regime)

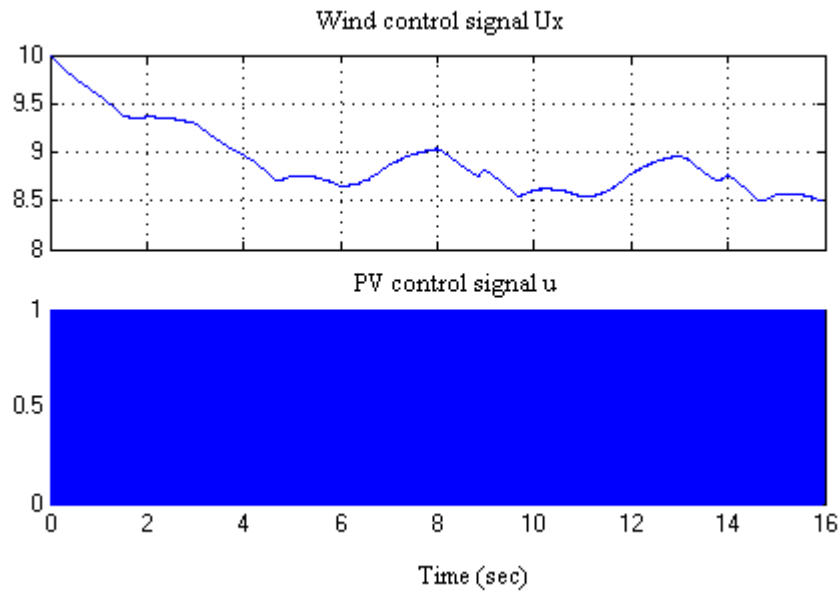


**Figure 65** Renewable energy control signals (sufficient power regime)

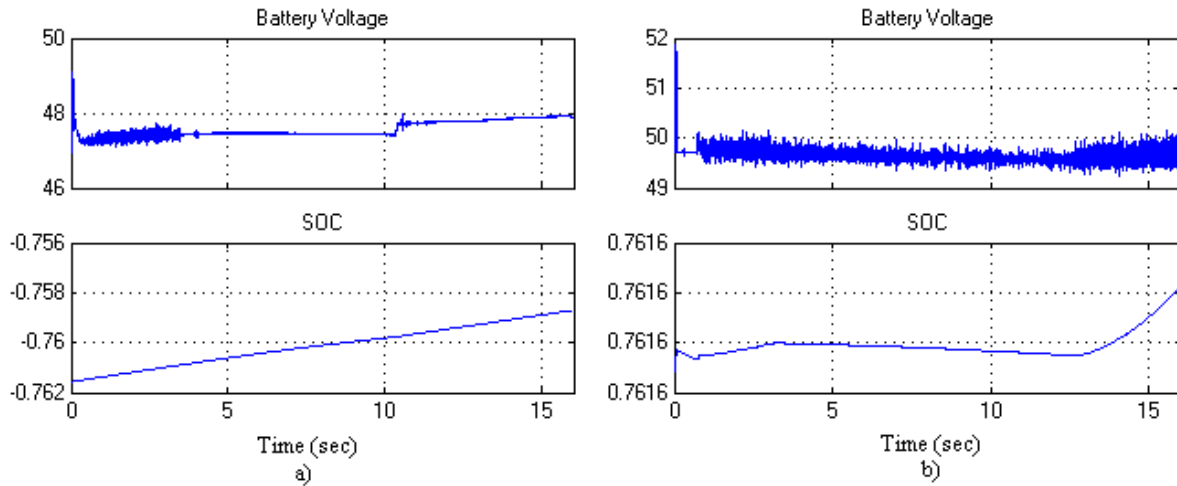
#### **4.2.3.4 Zonal EPDS**

In order to evaluate the supervisory controller behavior with a real load, we simulate the controller with a zonal EPDS, which is the DC part of the Integrated Power System (IPS) in [52].

Here, there were two zones. The first zone has a motor drive, and the second zone has a constant power load based on the classical buck converter. The power electronics converters control the power flows among the sources, loads, and power buses, following the commands of the PMC.

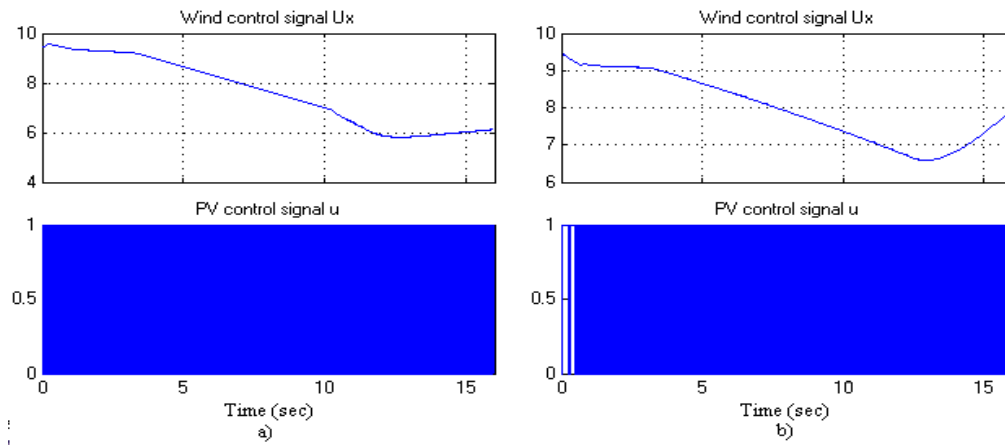
After the load there is a Boost converter in order to increase the operation voltage to the load. On this example, we simulate two scenarios: *a)* the battery bank is totally

discharged, and *b*) the battery bank is fully charged. Figure 66 shows the battery voltage and SOC of the battery bank for each case.



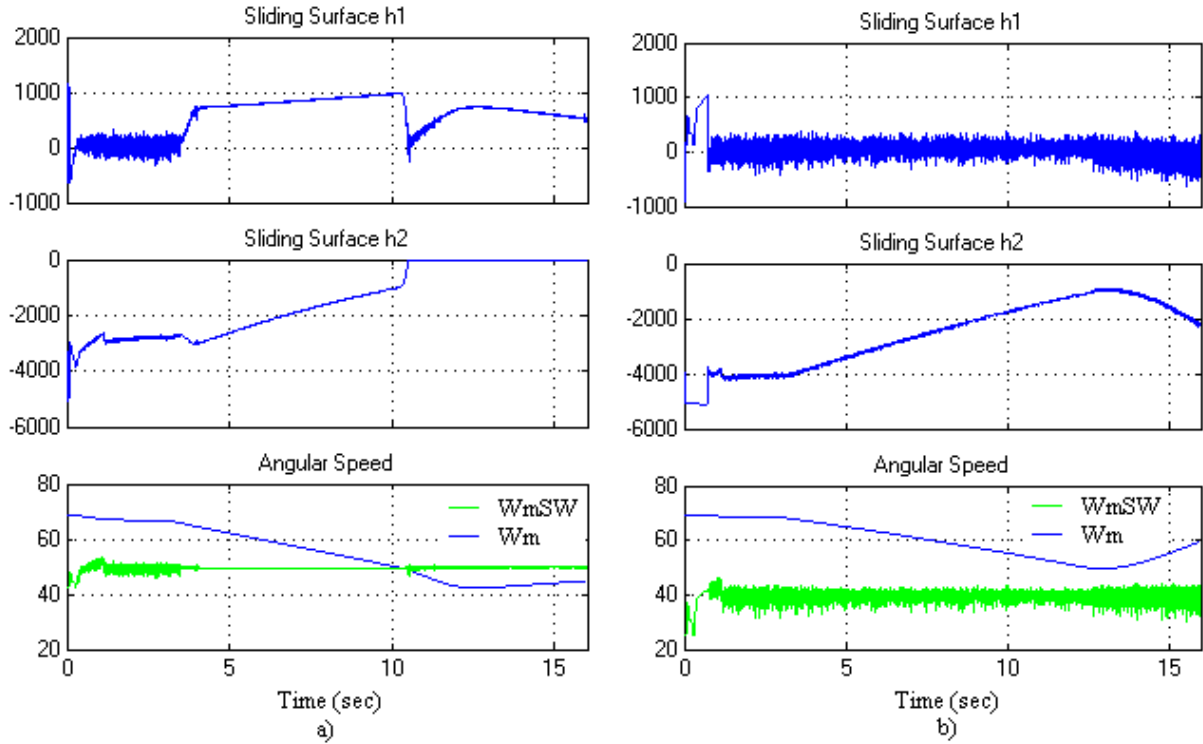
**Figure 66** Voltage and SOC of Battery Bank (a) totally discharged, (b) fully charged

Figure 67 shows the control signals for wind and solar subsystems for each state of the battery bank. In Fig. 67*a* the battery bank totally discharged, and the wind control signal is higher than Fig. 67*b* (battery bank fully charged), this means that in case *a*, the wind subsystem has to generate more power to satisfy the total demand.



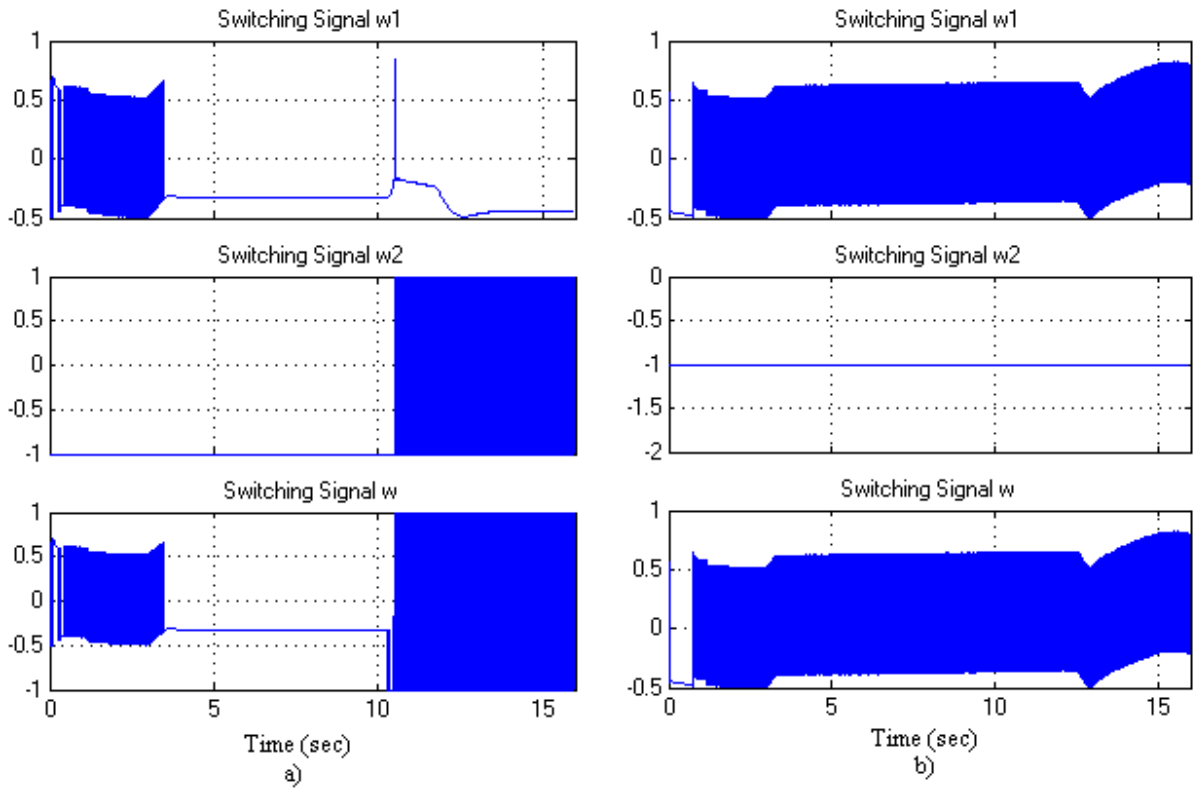
**Figure 67** Control signals of wind and solar subsystems with the battery bank (a) totally discharged, (b) fully charged

Figure 68 shows the sliding surfaces of wind subsystem. The second mode of operation only was activated if the battery bank is discharged, because the reference current for the wind turbine is higher than the case *b*. The angular shaft speed graph and Figure 69 confirms this statement.



**Figure 68** Sliding surfaces and angular speed of wind subsystem with battery bank (a) totally discharged, (b) fully charged

On other hand, Figure 70 and Figure 71 show the sliding surfaces and control signals for the solar subsystem, respectively. Only for the left side case, the supervisory control has to extract the maximum power from the PV subsystem.



**Figure 69** Control signals of wind subsystem with battery bank (a) totally discharged, (b) fully charged.

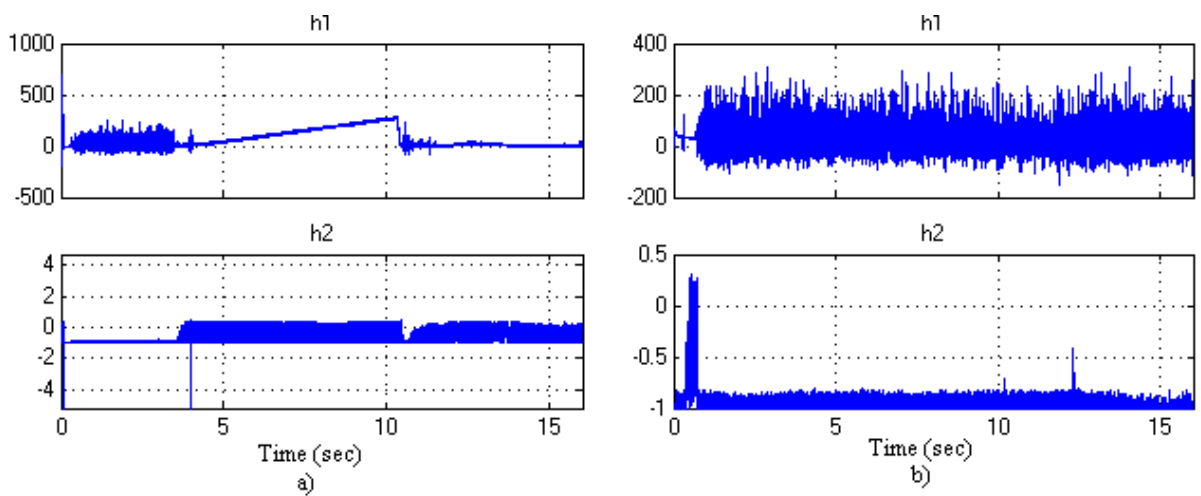


**Figure 70** Sliding surfaces solar subsystem with battery bank (a) totally discharged, (b) fully charged

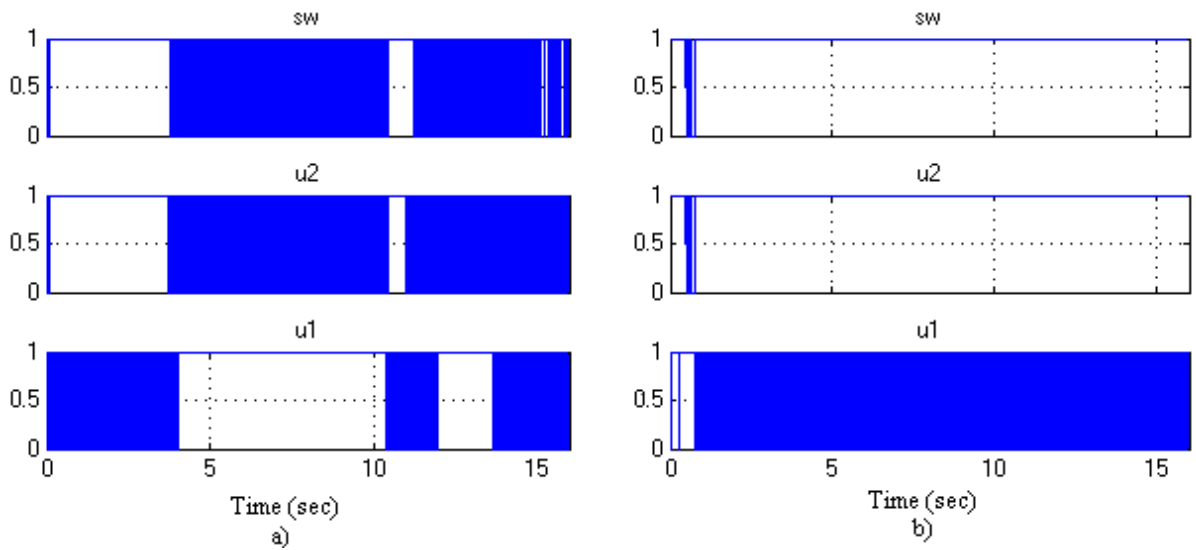


**Figure 71** Control signals of solar subsystem with battery bank (a) totally discharged, (b) fully charged.

Figure 72 shows the DC bus current of HPS. This example works between modes one and three, because the total demand is satisfied by the renewable energy. The battery bank does not supply energy to the load. In case *a*, the battery bank is in recharge mode at maximum recharging current (20A). In case *b*, the battery bank is fully charged, so the battery current is 0. The operation mode in case *b* is one, because the wind subsystem generate less power (the reference is lower than case *a*).

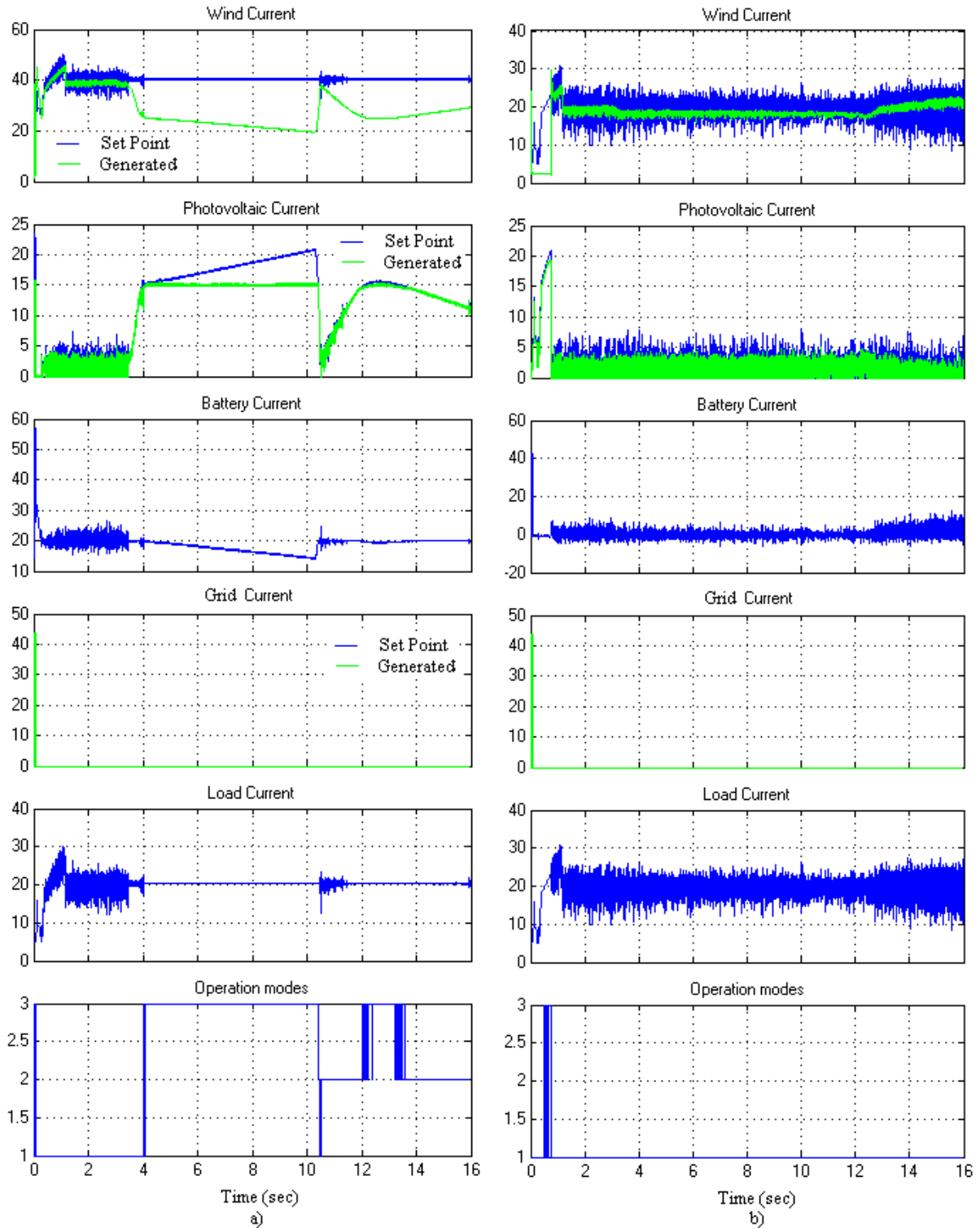


**Figure 72** DC bus current of HPS. The Battery Bank is (a) totally discharged, (b) fully charged.

#### 4.2.3.5 Changing source priority on supervisory controller

In this example, the hierarchical structure of the operation modes of supervisory controller was changed. The main generation role is in charge of the PV array and the second generation role is in charge of the wind subsystem. The simulations were made with the same simulation parameters of section 4.2.3.2.

Figure 73 shows *a)* the battery voltage and *b)* SOC of the battery bank. Figure 74 shows *a)* the control signal  $u_1$  of PV array on first mode of generation, and *b)* the control signal  $u_2$  to the second operation mode of PV array. Figure 75 shows the wind turbine control signals for *a)* first mode of generation *b)* second mode of generation, and *c)* the total control signal  $w$ . Figure 76 shows the control signals for the renewable sources *a)* wind turbine, and *b)* PV array.

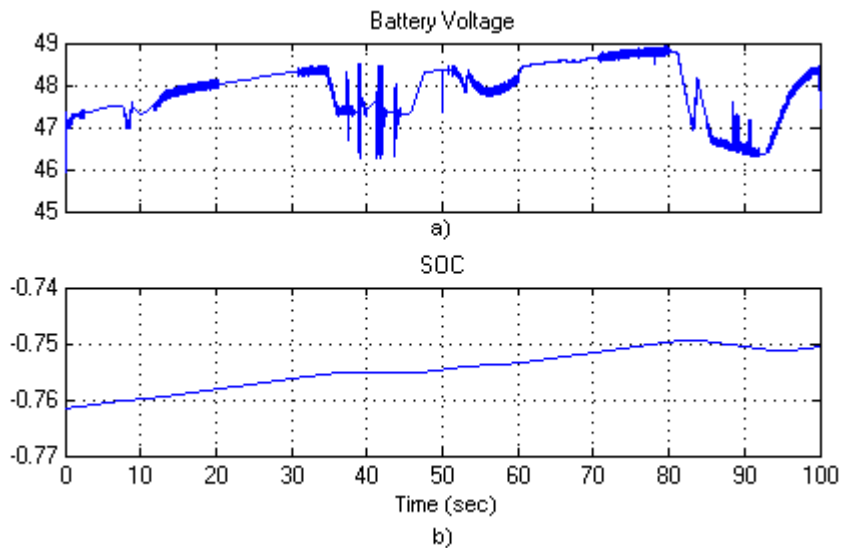


**Figure 73** Battery bank signals *a)* Voltage *b)* State of Charge

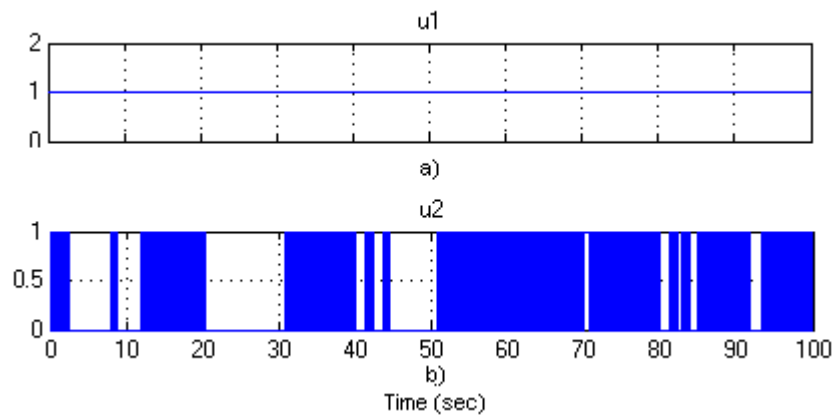


**Figure 74** PV array control signals

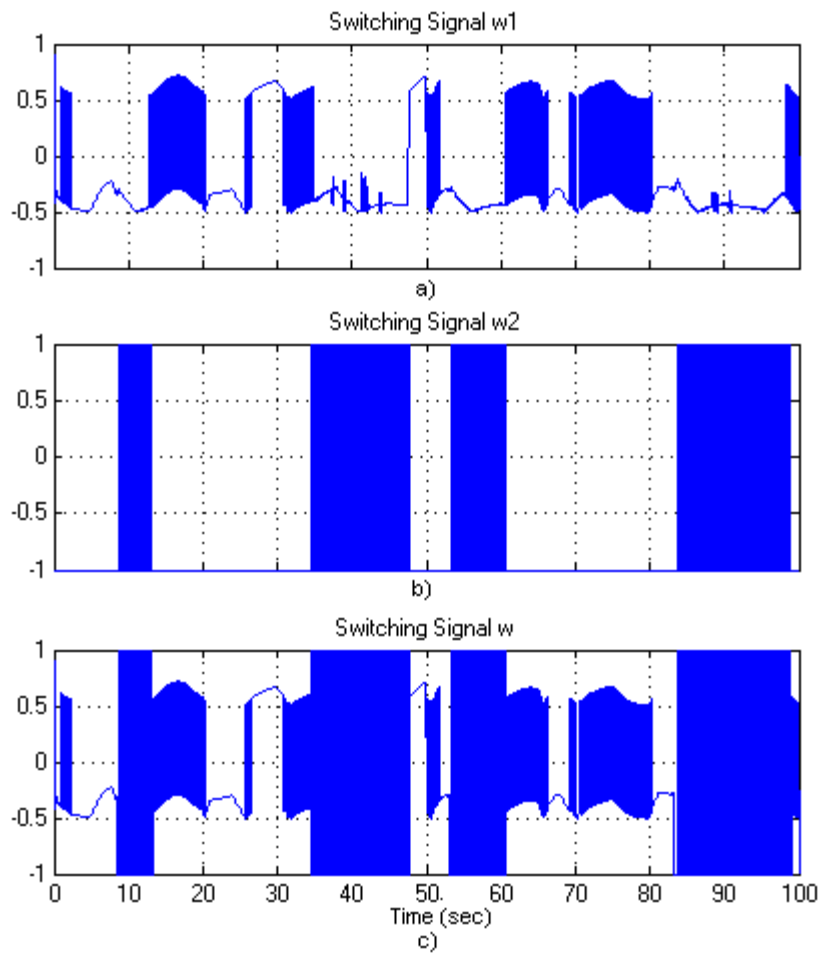


**Figure 75** Wind turbine control signals

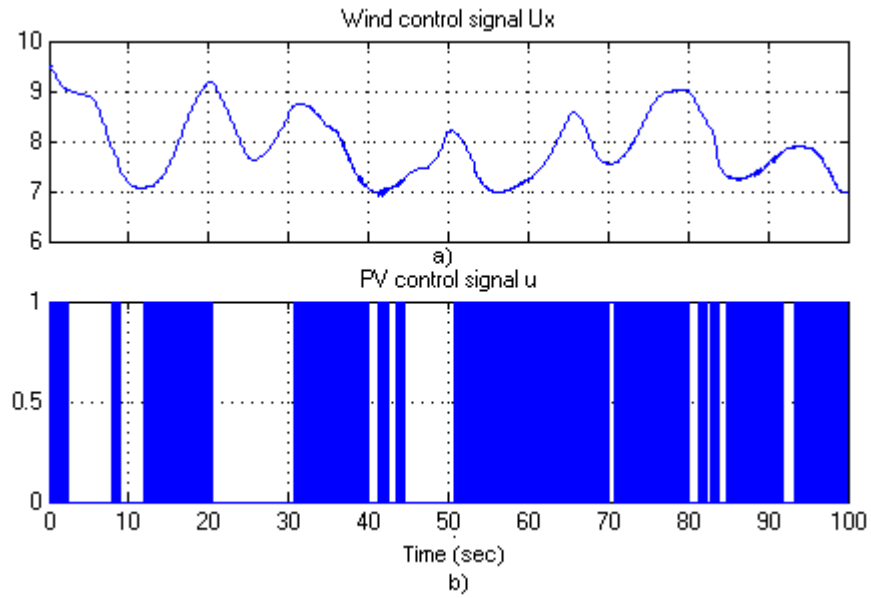


**Figure 76** Renewable sources control signals

Figure 77a shows the wind current, which in this case is the complementary generation source. Fig. 77b is the PV array current. In this case, it is the main generation role, so always is operating at MPOP to satisfy the demand. Fig. 77c is the battery bank current. The behavior is the same as described in previous examples. Fig. 77d is the grid current. Fig. 77e is the total demand current, and Fig. 77f shows the operation mode of the supervisory controller.

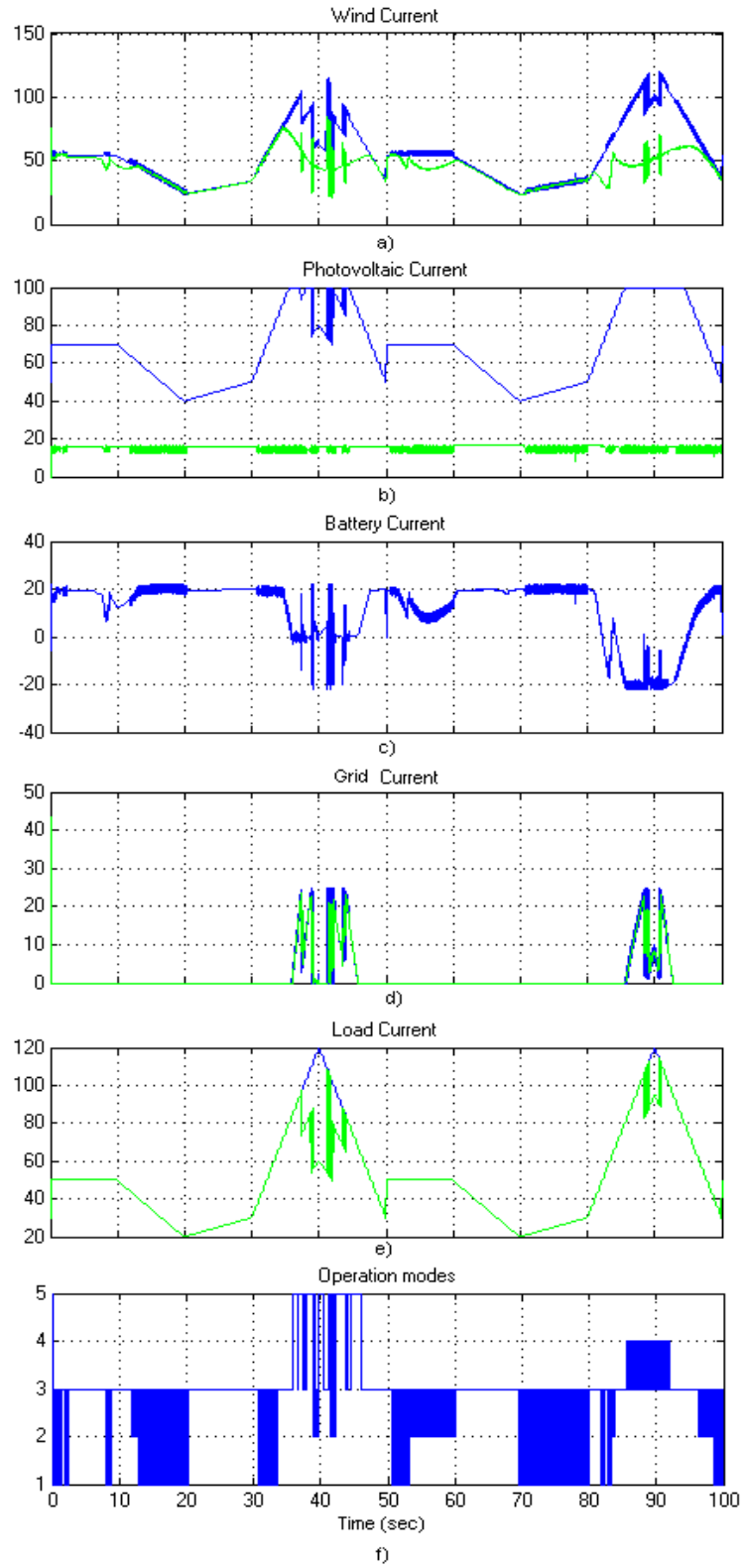
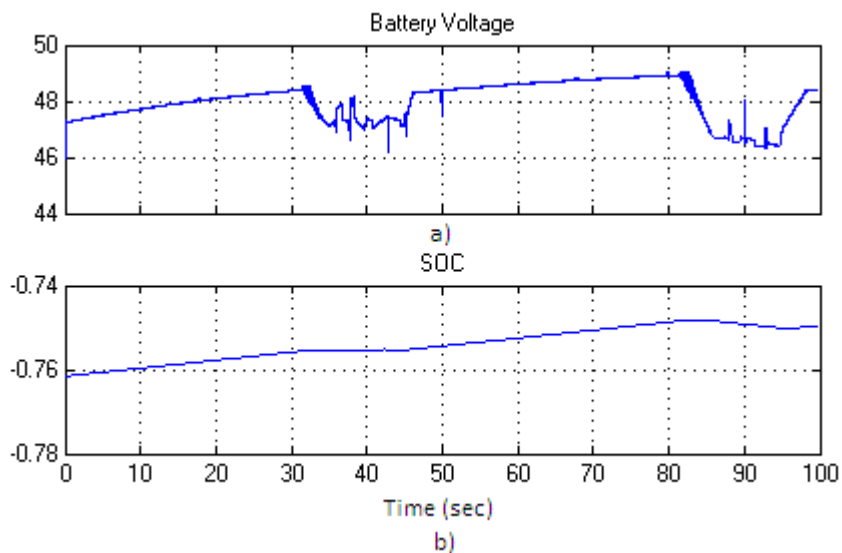


Figure 77 DC bus current

#### 4.2.3.6 Changing source priority on supervisory controller (4 PV panels)

In this simulation example, the hierarchical structure is the same as the one presented in the previous section. The main difference here is that the simulations were made with four panels in series and four panels in parallel in order for the PV to satisfy the load demand by itself.

Figure 78 shows *a)* the battery voltage and *b)* SOC of the battery bank. Figure 79 shows *a)* the control signal  $u1$  of PV array on first mode of generation; note that the solar subsystem is operating in both operation modes. Fig. 78*b* shows the control signal  $u2$  to the second operation mode of PV array. Figure 80 shows the wind turbine control signals for *a)* first mode of generation *b)* second mode of generation, and *c)* the total control signal  $w$ . Figure 81 shows the control signals for the renewable sources *a)* wind turbine, and *b)* PV array.



**Figure 78** Battery bank signals *a)* Voltage *b)* State of Charge

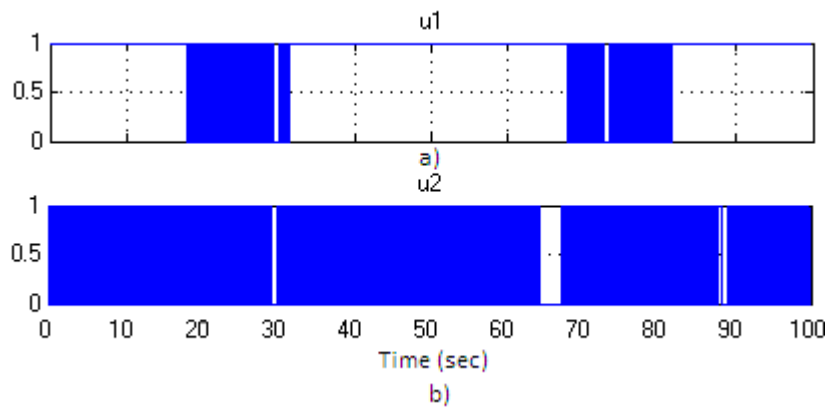


**Figure 79** PV array control signals

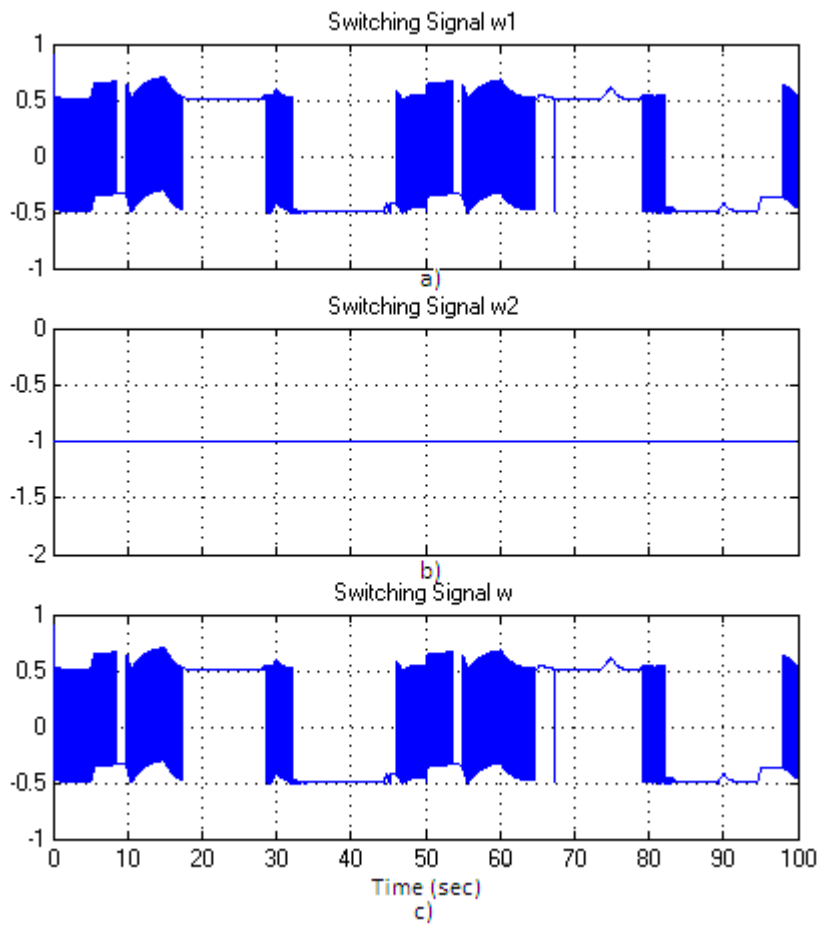


**Figure 80** Wind turbine control signals

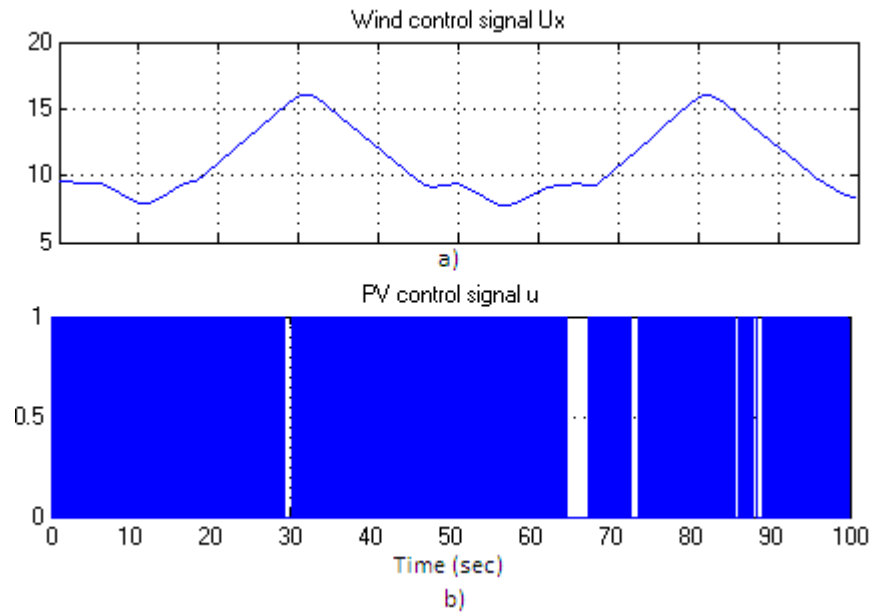


**Figure 81** Renewable sources control signals

Figure 82a shows the wind current, which, in this case, is the complementary generation source. Note that there is a time delay between when the wind turbine starts delivering energy to the system and when the generation command is given. Fig. 82b is the PV array current. In this case, it is the main generation role, so always is operating at MPOP to satisfy the demand. Fig. 82c is the battery bank current. Fig. 82d is the grid current. While the turbine starts, the deficiency in generation is supplied by the battery and the grid. Fig. 82e is the total demand current, and Fig. 82f shows the operation mode for the supervisory controller.

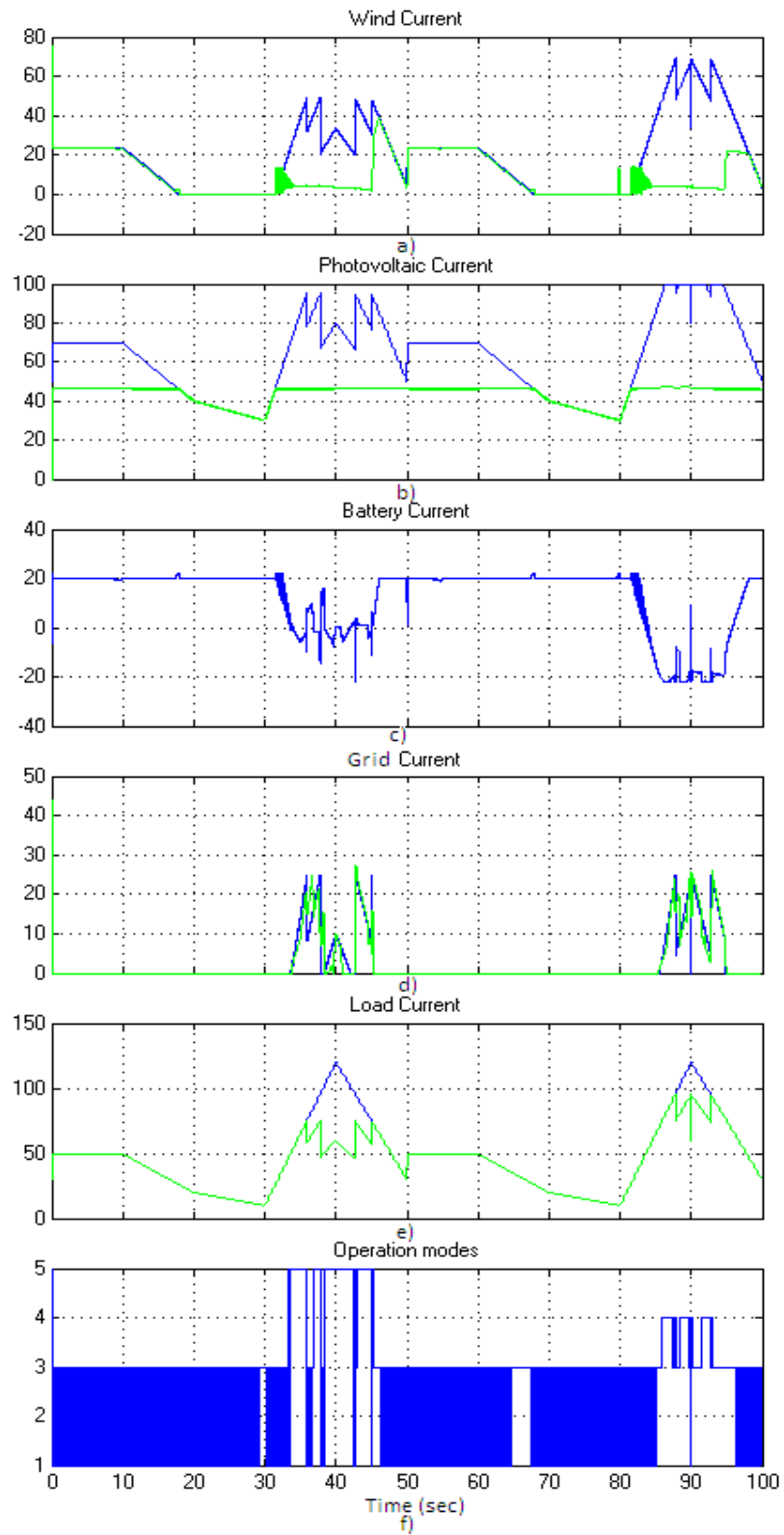


Figure 82 DC bus current

### **4.3 Conclusions**

This chapter presented the performance of a HPS controlled by a Hierarchical Control capable of managing all the energy resources of the system.

The results presented on the previous section, demonstrated that the designed control is capable to determining the operation mode of each subsystem presented on HPS. The criteria, to make the decisions, were based on measurable system variables such as shaft speed, currents, SOC, and power.

To accomplish the different control objectives (i.e., power regulation or maximum power conversion) in both (wind and solar subsystems), we use sliding mode control laws, for the energy management of the battery bank we used the SOC of the battery.

In the supervisory control scheme, we assumed that the main generation role would be carried out by the renewable energy, i.e., wind and solar subsystem respectively, while the traditional generation play a complementary role.

# Chapter 5

---

## 5. Control for a HPS using Model Predictive Control

As described on previous section, the main objective of the HPS is to satisfy the electrical loads at while as maximizing the use of renewable energy sources at the same time that the operation of the battery bank and the grid are optimized.

The control strategy is the same as described on chapter 4. It consists of a hierarchical two level structure: The main difference is that the PV individual control unit was controlled using MPC techniques, while the wind subsystem was controlled using SMC as shown before. The overall results are shown in section 5.3.

### 5.1 Dynamic Matrix Control (DMC)

In 1979, Cutler and Ramaker developed DMC; this type of MPC used as prediction model the step response [29]. The predictor will be

$$\hat{y}(t+k|t) = \sum_{i=1}^k g_i \Delta u(t+k-i) + f(t+k) \quad (5.1)$$

where,  $\Delta u(t)=u(t)-u(t-1)$ ,  $f(t+k)$  is the free response of the system, and  $G$  is the *dynamic matrix* given by

$$G = \begin{bmatrix} g_0 & 0 & \cdots & 0 \\ g_1 & g_0 & \cdots & 0 \\ \vdots & \vdots & \ddots & \vdots \\ g_{N_c-1} & g_{N_c-2} & \cdots & g_0 \\ \vdots & \vdots & & \vdots \\ g_{N_p-1} & g_{N_p-2} & \cdots & g_{N_p-N_c} \end{bmatrix} \quad (5.2)$$

The objective function and the input constraints are given by

$$J(N_p, N_c) = \sum_{k=1}^{N_p} [\hat{y}(t+k|t) - w(t+k)]^2 + \sum_{k=1}^{N_c} \lambda(k) [\Delta u(t+k-1)]^2 \quad (5.3)$$

subject to

$$u_{min} \leq u_{k|t} \leq u_{max}, \quad t \leq k$$

in vector notation, the objective function is given by

$$J = u^T [G^T G + \lambda I] u - 2e_o^T G u + e_o^T e_o \quad (5.4)$$

where  $u$  is the control signal,  $G$  is the Dynamic Matrix,  $\lambda$  is the control weighting factor, and  $e_o$  is the error between the prediction  $\hat{y}$ , and the reference trajectory  $w$ .

If there are no constraints, the control law is calculated by deriving the cost function and setting it to zero.

$$\frac{\partial J}{\partial u} = 0 \quad (5.5)$$

and the control law is given by

Put in practice, the regular method to use MPC is to calculate the control law using (5.6) and apply it to the process. If  $u$  violates the constraints it is set to its limits [32].

## 5.2 PV Controller Design using DMC

This section will discuss the control strategies for the different operation modes. This controller is part of the operational level, and the control objective for each operation mode has to be defined.

We have to define different operation points because the PV array behavior is non linear, for that reason, the different control objectives are controlled by a multi objective controller as shown in Figure 83.

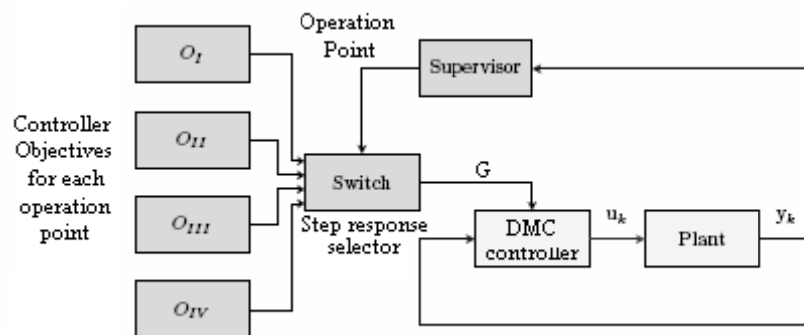


**Figure 83** Multi-objective controller.

The dynamic matrix  $G$  is built from the elements of the step response, the main difference on this strategy is that the matrix  $G$  needs to be calculated several times because the step response of a nonlinear system varies depending on the operating point.

Essentially, identical algorithm employed in linear systems can be in use, but  $G$  has to be updated every time the process characteristics change. On this scheme, the prediction matrix  $G$  is supplied by the step response selector.

The flow diagram of the constrained DMC algorithm implemented is presented on Figure 84.

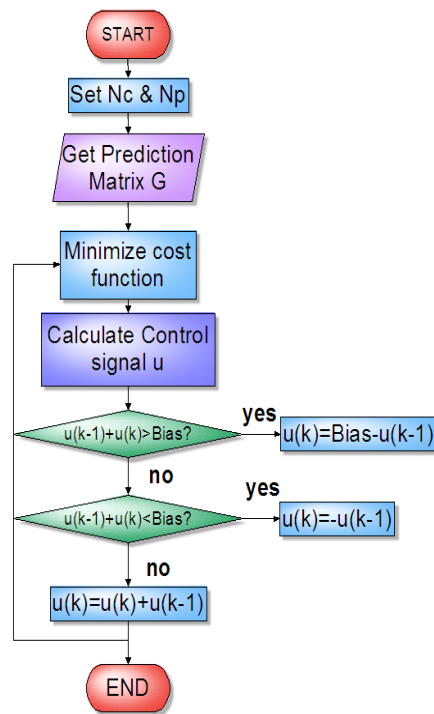


**Figure 84** DMC flow diagram including constraints on control signal.

We set seven operation points, each one is part of a different control objective, to develop the DMC controller for the PV array; this set of points was selected from I-V curve of the panel shown in Figure 3.

The power reference occurs when the PV array is capable of generating enough power to satisfy the total power demand and is given by equation 4.11, whilst the set point is given by the power generated by the PV panel given by the equation 3.11.

### 5.2.1 Simulation Results

Figure 85 shows the duty cycle of the DC/DC converter for the PV array. When the panel operates at maximum power conversion, the duty cycle is set to 0.8, because this point correspond to MPOP, a lower duty cycle means that the panel is going to generate less power.

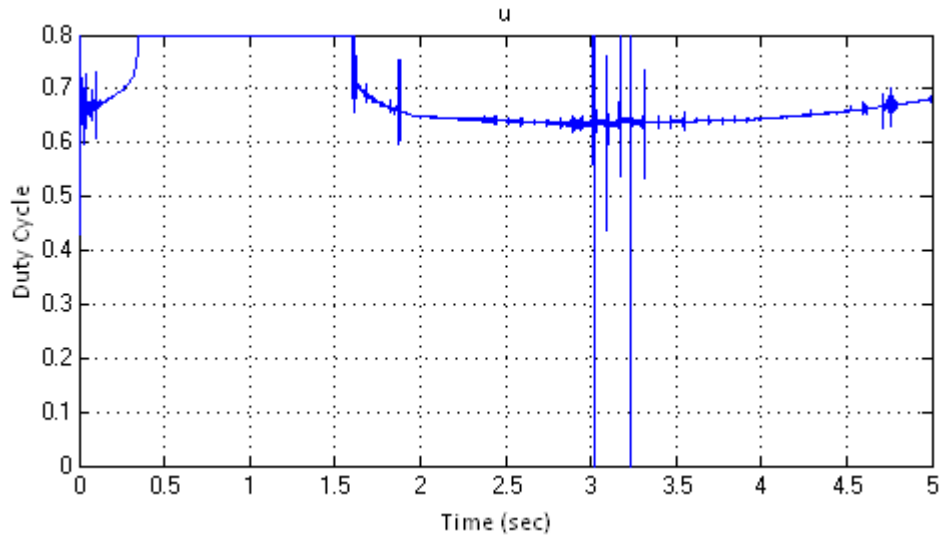


**Figure 85** DMC Control signal of PV array.

Figure 86 depicts the currents present on the DC bus. Fig. 86a presents a constant wind current fixed at 20A, on this case, the solar subsystem is complementing the wind generation. Fig. 86b shows the PV current. We could observe when there is not enough power from PV array to satisfy the power demand, so the system works on second mode of

operation, also the PV follows the reference. Fig. 86c depicts the total demand (load current, and battery reference current (20A)). Fig. 86d illustrates the current on the battery bank. We could observe when there is enough power to supply the total demand it is on recharge cycle and set the current to 20A, but when the power is insufficient, it is able to supply power to the load.

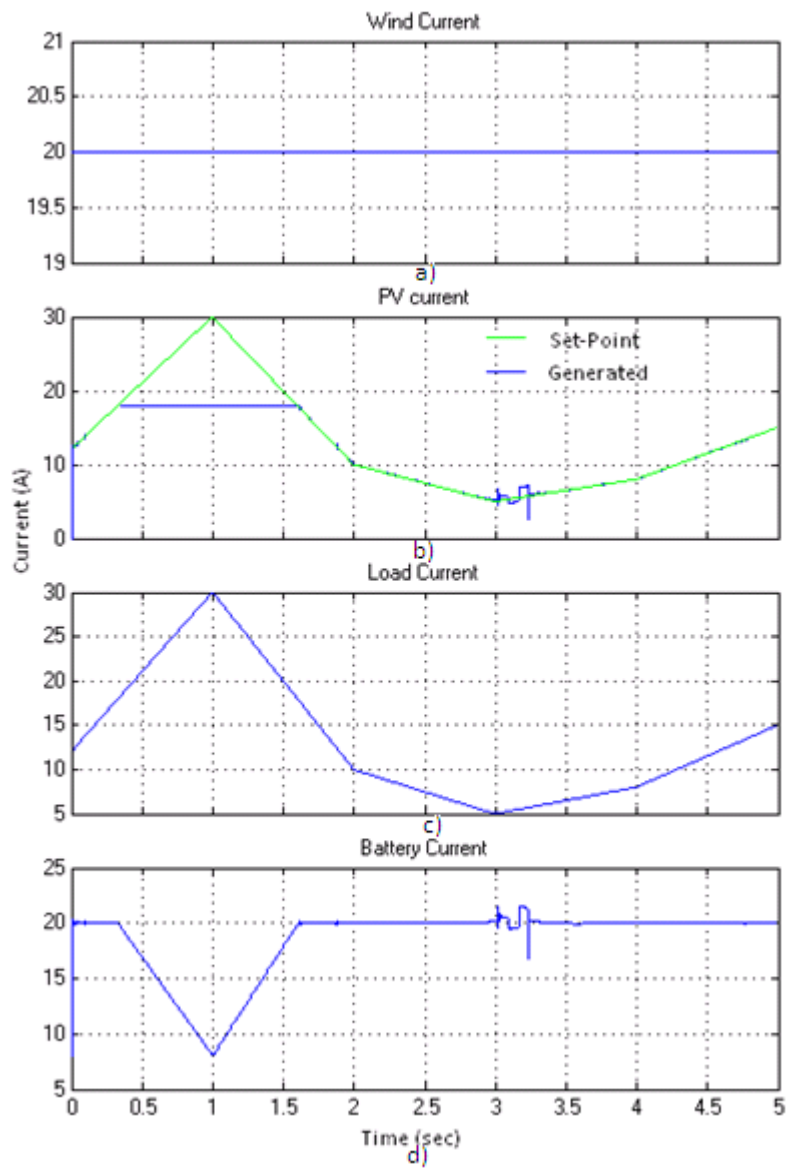


**Figure 86** DC bus currents (PV array with DMC)

### 5.2.2 MPC-PV against SMC-PV

The natural behavior of SMC for DC/DC converters include the switching signal of PWM, in other words, it is not necessary to include a PWM before the DC/DC converter. Furthermore, MPC work with the model; if the predicted model does not have the PWM, the controller can't predict the behavior of the system.

On other hand, we have to considerate the PWM restrictions for the MPC controller, because the control signal could not be faster than switching frequency of PWM, so we have to limit the bandwidth for the control. In SMC the switching frequency is inherent to the model.

Both examples (SMC and MPC) were simulated under the same circumstances. The control signal of MPC-PV has not a switching form; it sets the average of the duty cycle of the DC/DC converter as shown in Figure 85. On the other hand, the SMC-PV control signal has a switching for to generate the duty cycle of the DC/Dc converter as shown in Figure 34.

The behavior of MPC controller and SMC controller for the PV array is similar, the main difference occurs at 3 seconds. The MPC controller for PV array does not follow the reference current. This situation is presented because the MPC controller is not an optimal control, and the transition states between operation points are not been considered.

### 5.3 Wind Controller using DMC

We have to define different operation points because the wind turbine behavior is the most non linear in the system, for that reason, the different control objectives are controlled by a multi objective controller as described before.

We try to do the same technique described in the previous section to control the wind subsystem, but we had several problems to get the prediction matrix G because the subsystem step response has a time delay with a lot of noise that produce a bad behavior of the control system (see Figure 87).

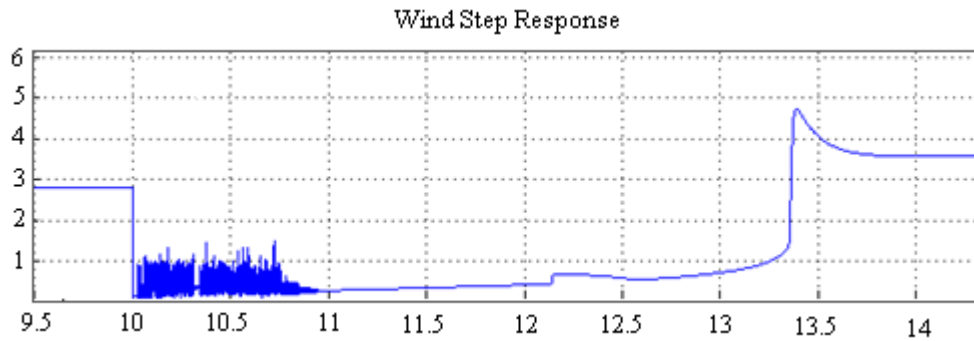


**Figure 87** Wind Turbine Step Response

The controller designed does not work appropriately, only works under some operation points.

### 5.4 Supervisory Controller

The performance of the PV controller was evaluated through computer simulations in two scenarios. The first scenario presents the PV panel controlled by a DMC with the

supervisory controller (wind subsystem was controlled by SMC), and the Battery Bank is fully charged. The second scenario has the battery bank totally discharged.

#### 5.4.1 Supervisor Control with battery bank fully charged

The initial condition of the SOC of the battery bank is  $SOC = 0.7616$ , this means that the battery bank is fully charged, so the fifth operation mode of the supervisory controller must never be activated. Figure 88 shows the battery bank voltage and the SOC of the battery bank.

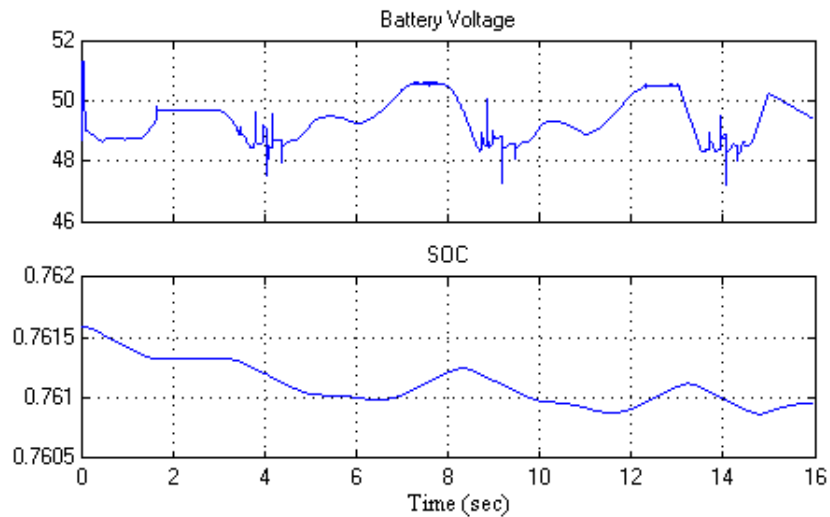


**Figure 88** Voltage and SOC of Battery Bank.

Figure 89 shows the wind control signal with SMC techniques, and the solar control signal using DMC method. On this graph we can observe that the PV control signal is more softly, and the control effort is lower than the PV control signal with SMC techniques.

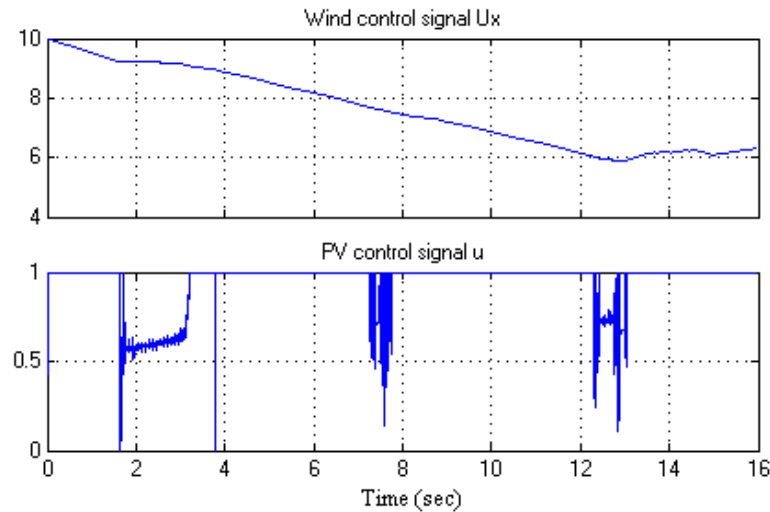


**Figure 89** Control signals PV (DMC) and WT (SMC).

Figure 90 depicts the currents present on the DC bus. Fig. 90a presents the wind current. On this case, the wind subsystem is controlled by SMC controller. Fig. 90b shows the PV current, the solar subsystem is complementing the wind generation and it is controlled by a DMC controller. Fig. 90c illustrates the current on the battery bank. We could observe that when there is enough power to supply the total demand, and the battery bank is fully charged, it is on recharge cycle and set the current to 0A or 20A. However when the power is insufficient, it is able to supplies power to the load. Fig. 90d shows the grid current. The grid supply power to the load only if the battery discharging current is higher than 20A. Fig. 90e depicts the total demand (load current, and battery reference current (20A)). Fig. 90f shows the operation modes of the supervisory controller.

The main difference between PV controller described in section 4.2.3.1 and this, is the PV array generated current using this control technique, the ripple on PV current is avoided. The principal reason is that the duty cycle is sent to the DC DC converter in an average form and not as a switching signal.

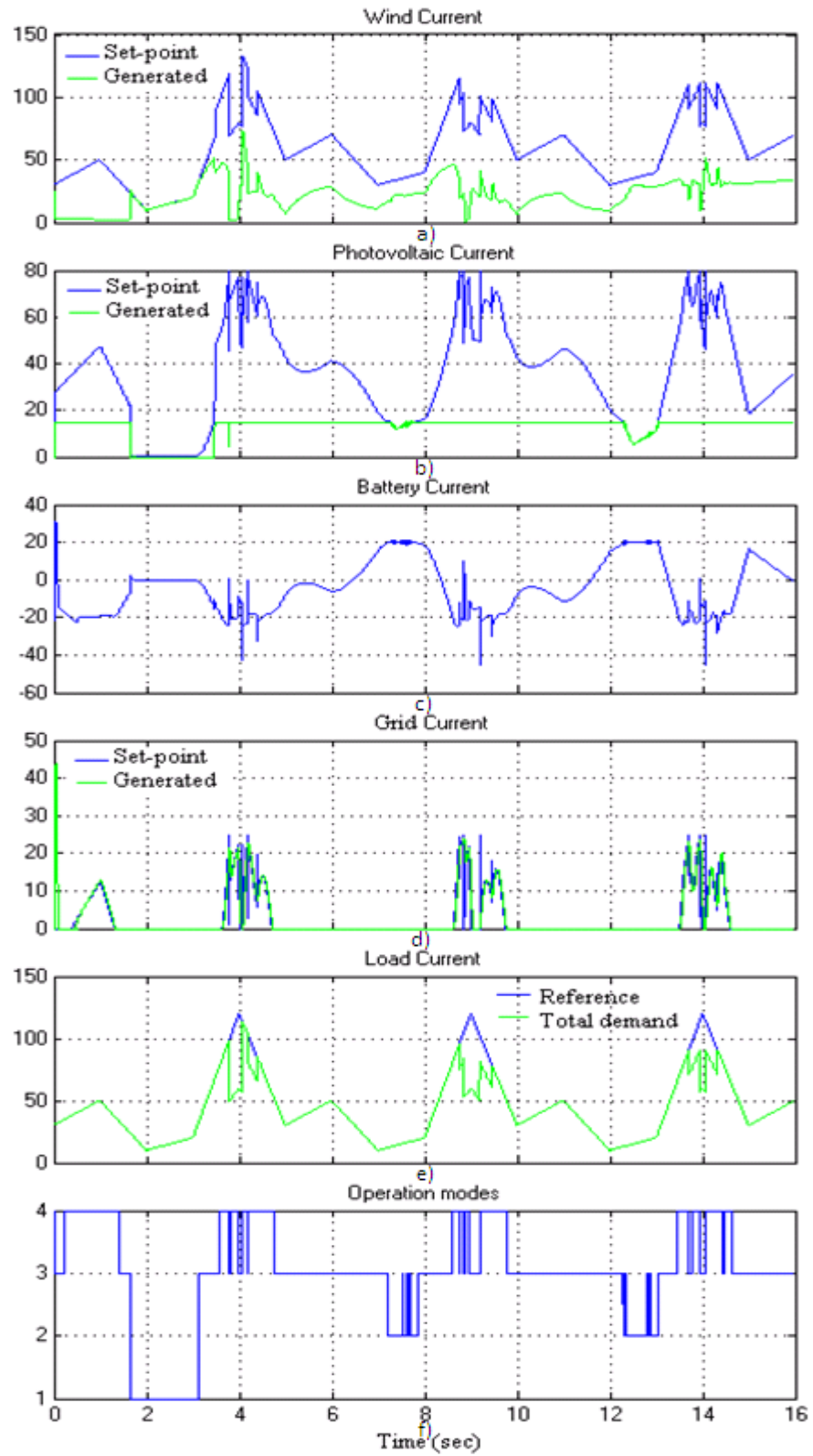
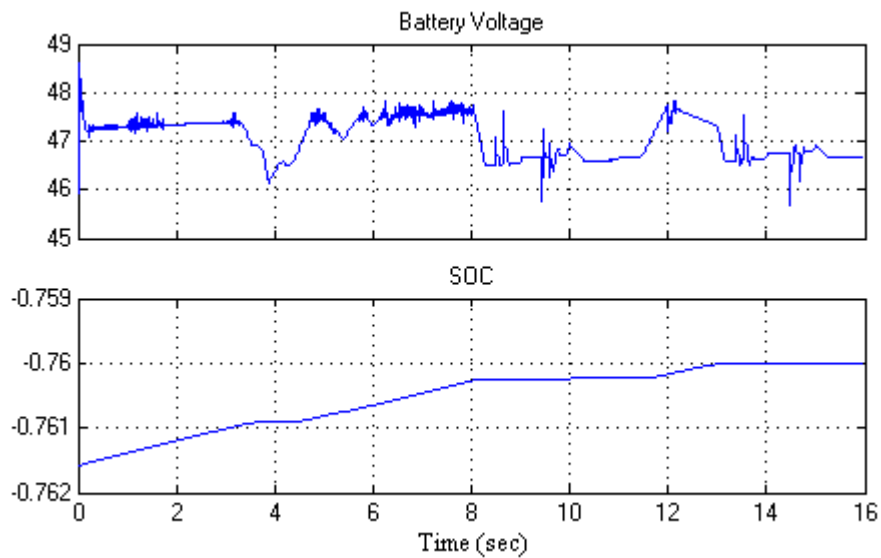


Figure 90 DC Bus current of HPS (PV controlled by DMC)

### 5.4.2 Supervisor Control with Battery Bank Totally Discharged

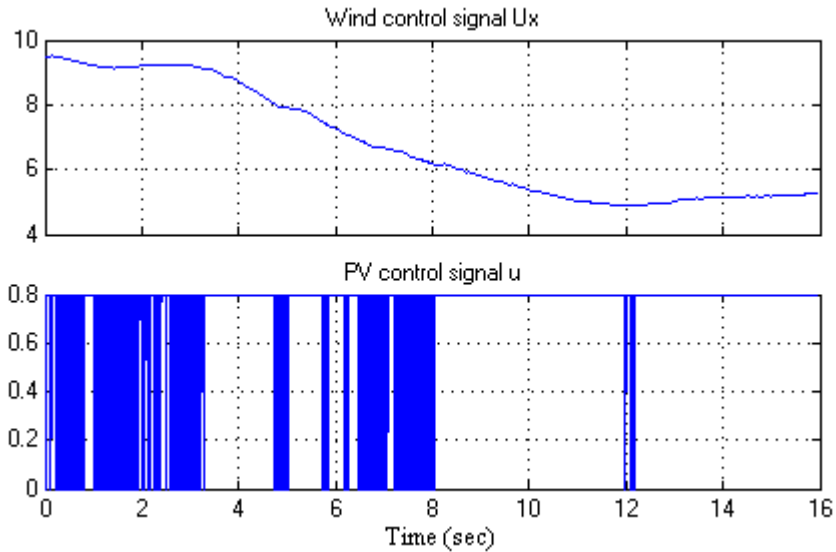
This corresponds to the second scenario to be evaluated. The initial condition of the battery bank is totally discharged (SOC = -0.755); the battery reference current for the renewable source to charge the battery bank is the maximum charging current, in this case 20A.

Figure 91 shows the battery bank voltage and the SOC of the battery bank. Notice on this graph that the battery is totally discharged. The battery behavior is the same as described in previous sections.



**Figure 91** Voltage and SOC of the Battery Bank

Figure 92 shows the control signal of wind subsystem using SMC techniques and the duty cycle of the DC/DC converter for the PV array using DMC techniques.



**Figure 92** Control signals of HPS

Figure 93 depicts the currents present on the DC bus. Fig. 93a presents the wind current. In this case, the wind subsystem is controlled by SMC controller. Fig. 93b shows the PV current, where the solar subsystem is complementing the wind generation and it is controlled by a DMC controller. Fig. 93c illustrates the current on the battery bank. It is observed that when there is enough power to supply the total demand it is on recharge cycle and set the current to 20A, but when the power is insufficient, it is able to supply power to the load. Fig. 93d shows the grid current. The grid supplies power to the load in two cases: (i) if the battery discharging current is higher than 20A, or (ii) if the SOC of the battery bank is under  $Q_{min}$ . Fig. 93e depicts the total demand (load current, and battery reference current (20A)). The sixth graph shows the operation modes of the supervisory controller.

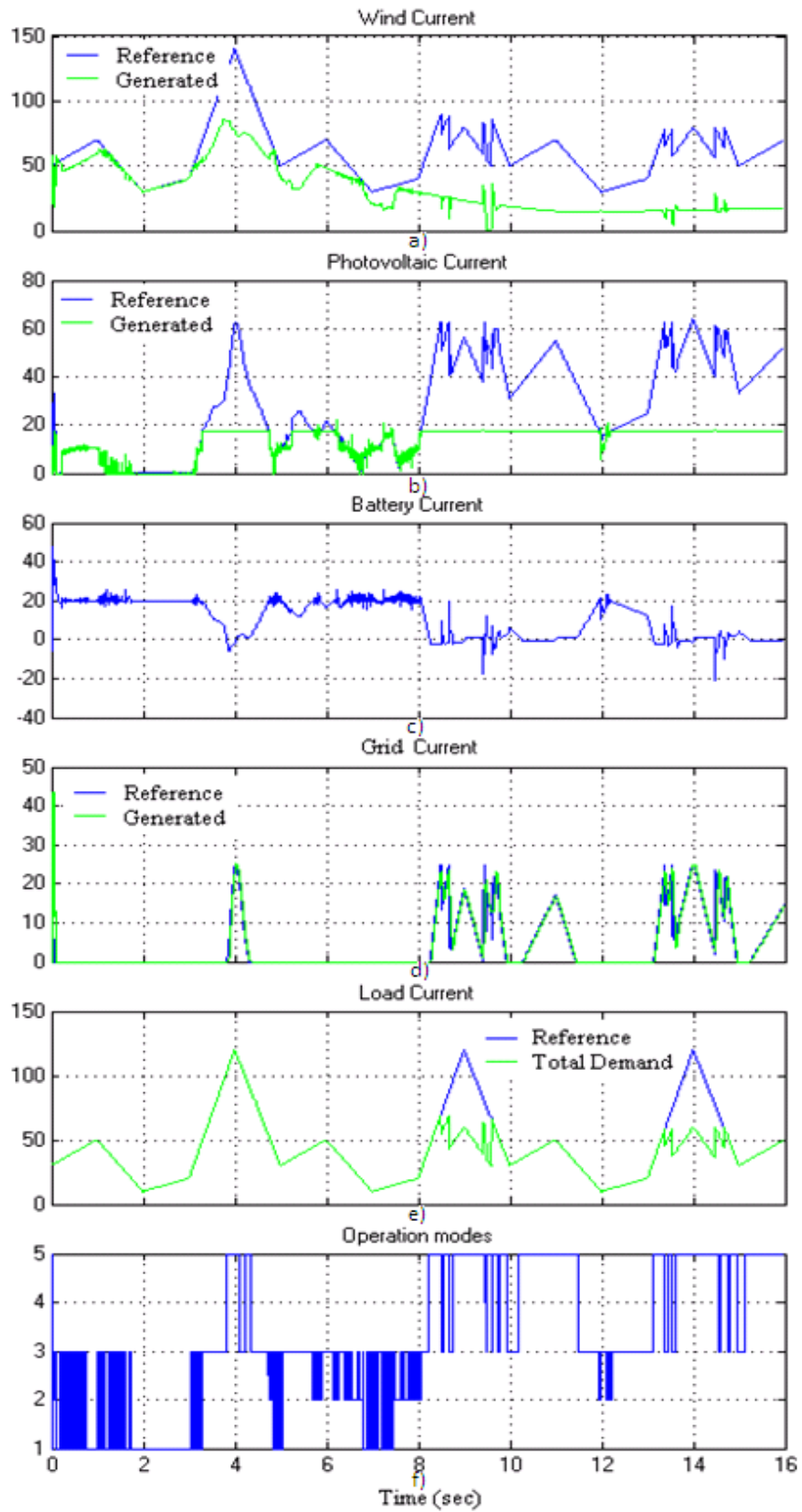


Figure 93 DC bus currents of HPS

## 5.5 Conclusions

The control implemented to PV array with DMC is a suboptimal control, because the strategy proposed here is an adaptation of a linear method; over each operation point the control strategy is linear, the transient between one point to other is not considered.

The battery behavior does not change if we use DMC technique to control the PV array, because the control laws are the same as described in section 4.1.3 so using one technique or other the battery bank acts in the same form.

On other hand, the DMC control is later than SMC for the same simulation, but the control effort is lower.

We try to do the same control technique with wind subsystem, but we had several problems to get the prediction matrix because the subsystem step response has a time delay with a lot of noise that produce a bad behavior of the control system.

To solve the optimization problem and to predict the process output in a nonlinear MPC, elevated computational capacity is necessary. This makes the approach not practical in a number of applications.

# Chapter 6

---

## **6. Conclusions and Future Work**

### **6.1 Summary of the work**

On this work we developed a Hierarchical Control of two levels. The highest level is a supervisory control with five modes of operation and a load shedding scheme in case of insufficient generation, in this case, we expanded the work of Valenciaga and Omari. The lowest levels have local control units to control the wind turbine, PV panels, and the battery bank using SMC and MPC techniques.

### **6.2 Conclusions**

A simulation model for a Hybrid Power System was developed to facilitate the study of the dynamics of HPS, and help in the development of control strategies to manage the system power flows under different generation and load conditions. The simulation model is modular in nature; each component is represented as a self-contained module (Wind Turbine, PV panels, Grid, Battery Bank, and Loads). The balance of energy is maintained by the controller to keep the system stable. The subsystems could be connected to form a complete HPS.

The wind speed and PV array cell temperatures can be modified to simulate the day variations. The Battery Bank was simulated in two states (charged or discharged). The load was a variable current source to force the system to operate in all modes. Different control strategies (SMC and MPC) were implemented to achieve the objective.

The control strategy for the EPDS is a hierarchical structure with two levels; the highest level is the supervisory controller which proved to be capable of handling and synchronizing the operation of the subsystems that compose the HPS. The lower level is compound by the local control units for each subsystem.

Sliding Mode Control and Model Predictive Control techniques have been considered to accomplish the control objectives at the subsystem level, particularly wind and solar subsystems. Nevertheless the applicability of the decision framework of the supervisor control is not limited to those particular control laws. In contrast, this technique is general, and allows the inclusion of any other local control law appropriate to attain the abovementioned control objectives.

On this work, the principal generation role was in charge of wind turbine, but this is not at all a rigid restriction of the control scheme. The decision algorithm of the supervisor control could be easily changed to set the solar subsystem as the main energy source and the wind subsystem as the secondary. The traditional generation sources either a fuel generator or AC utility is always going to play a secondary role.

## 6.3 Future Work

Future work can be committed towards:

- Implement a robust model of wind turbine, because the model used here had several inconsistencies. The model that we used is a linear model of the nonlinear wind turbine in order to apply the modern control design theory. However, the full model was reduced under some practical assumptions, for example, a factor omitted from the design modeling is the wind shear (the effect that rough terrain has on the turbulence on the wind)
- To develop the dynamic models with multiple resolutions to study different time scales over the HPS.
  - Testing the supervisor control using a larger version of a zonal system to represent the total demand. The supervisor control was tested with three ideal variable current sources, and the average zonal system, which not forced the supervisory to work in all operation modes.
- Introducing Power Quality issues as part of the decision making process of supervisor control. The supervisory controller must required quality of the supply, in terms of variations of voltage, frequency, and probability of loss of load. It is an essential condition for the choice of which generators should be in service.

- The load management (added or removed from the system) could be based on frequency variations.
- The load management must be more sophisticated Include control over the load (variable demand) by the supervisor.
- Avoid starting utility grid or diesel generators in situations of fast variations of power.
- Evaluate strategies where the HPS supplies power to the grid and net metering, and include it as an extra operation mode.

# References

1. Valenciaga, F and Puleston, P F. "Supervisor control for stand-alone hybrid power system using wind and photovoltaic energy". *IEEE transaction Energy Conversion*. Vol. 20. No2, pp. 398-405, June 2005.
2. Omari, Osama, Ortjohann, Egon and Morton, Danny. "An Online Control Strategy for DC Coupled Hybrid Power Systems". *IEEE Power Engineering Society General Meeting*. pp. 1-8, June 2007.
3. De Lemos Pereira, Alexandre. "Modular Supervisory Controller for Hybrid Power Systems". *Phd. Thesis. Riso National Laboratory, Roskilde*. University of Denmark, June 2000.
4. Roscia, M and Zaninelli, D. "Sustainability and quality through solar electric energy". *10th International conference on Harmonics and quality of Power*. Vol. 2, pp. 782-782, 2002.
5. Ross, M and Turcotte, D. "Bus configuration in Hybrid Systems". *Hybrid info Semiannual newsletter on photovoltaic hybrid power systems in Canada*. 7, pp. 2-5, Summer 2004.
6. Meinhardt, M and Cramer, G. "Past, Present and Future of grid connected Photovoltaic and Hybrid-PowerSystems". *IEEE Power Engineering Society Summer Meeting*. Vol. 2, pp. 1283-1288, July 2000.
7. Chang, Liuchen. "Wind Energy conversion Systems". *Canadian Review*. pp. 12-16, 2002.
8. Ross, M, Turcotte, D and Roussin, S. "Comparison of AC, DC, and AC/DC bus configurations for PV Hybrid Systems". *SESCI Conference*. 2005.
9. Wright, Alan D. "Modern Control Design for Flexible Wind Turbines". *Technical Report on National Renewable Energy Laboratory (NREL)*. pp. 1-223, July 2004.
10. Kraan, I. "Control Design for a Flexible Wind Turbine" (in Dutch). *Delft University of Technology*. 1992.
11. Bongers, P.M. "Modeling and Identification of Flexible Wind Turbines and a Factorizational Approach to Robust". *Ph.D thesis Department of Mechanical Engineering and Marine Technology, Delft University of Technology*. 1994.

12. Freeman, J.B and Balas, M.J. "An Investigation of Variable-Speed Horizontal-Axis Wind Turbines Using Direct Model-Reference Adaptive Control". *Proceedings of the 37th AIAA Aerospace Sciences Meeting and Exhibit*. pp. 66-76, 1999.
13. Bossanyi, E.A. "Adaptive Pitch Control for a 250 kW Wind Turbine". *Proceedings of the 9th BWEA Wind Energy Conference*. pp. 85-92, 1987.
14. Wikipedia, the free encyclopedia. "*Photovoltaics*". (September 2007). [Online] <http://en.wikipedia.org/wiki/Photovoltaics>.
15. Valenciaga, F, Puleston, P.F and Battaiotto, P.E. "Power Control of a Photovoltaic array in a hybrid electric generation system using sliding mode techniques". *IEE Proc. Control Theory Appl.* Vol. 148 No 6, pp. 448-455, November 2001.
16. Xantrex. "Battery Banks for Inverter Systems". *Smart Choice for Power*. pp. 1-22. April 2006.
17. Uykan, Zekeriya. "Hierarchical Control and Multimedia". Helsinki University of Technology, Control Engineering Laboratory. (September 2007). [Online] [http://www.control.hut.fi/Hyotyniemi/publications/97\\_report106/UYKAN/node1.html](http://www.control.hut.fi/Hyotyniemi/publications/97_report106/UYKAN/node1.html).
18. Henriksen, Lars C. "Model Predictive Control of a Wind Turbine". *Ph.D Thesis. Technical University of Denmark*. pp. 1-146. 2007.
19. Utkin, V.I. "Variable Structured Systems with Sliding Modes". *IEEE Transaction on Automatic control*. 1977, Vol. 22. N°2, pp. 212-222. April 1977.
20. Sira-Ramirez, H. "Sliding Motions in Bilinear Switched Networks". *IEEE Transaction on Circuits and Systems*. August 1987, Vol. 34. N°8, pp. 919-932. August 1987.
21. Sira-Ramirez, H and Ilic, M. "A Geometric Approach to the Feedback Control of Switch Mode DC-to-DC Power Supplies". *IEEE Transaction on Circuits and Systems*. Vol. 35. N°10, pp. 1291-1298. October 1988.
22. Venkataramanen, R. "Sliding Mode Control of Power Converters". *Ph.D Thesis. California Institute of Technology*. pp. 1-260. 1986.
23. Young, K.D, Utkin, V.I and Ozguner, U. A control engineer's guide to Sliding Mode Control. *IEEE Transaction on Control System Technology*. Vol. 7, pp. 328-342, May 1999.
24. Vazquez, N, et al. "Sliding Mode Control for DC/DC Converters: A new Sliding Surface". *IEEE International Symposium on Industrial Electronics*. Vol. 1, pp. 422-426. June 2003.

25. Ha, Q.P, et al. "Dynamic Output Feedback Sliding-Mode Control Using Pole Placement and Linear Functional Observers". *IEEE Transaction on Industrial Electronics*. Vol. 50 No. 5. October 2003.
26. Valenciaga, F, Puleston, P.F and Battaiotto, P.E. "Power Control of a Solar/Wind Generation System without Wind Measurement: A Passivity/sliding mode approach. *IEEE Transaction on Energy Conversion*. Vol. 18 No 4, pp. 501-507, December 2003.
27. Calvente, F. "Control en Modo Deslizante aplicado a Sistemas de Acondicionamiento de Potencia de Satélites". *Ph.D Thesis of Universidad Politecnica de Cataluña*. pp. 1-162, July 2001.
28. M., Qian. "Sliding Mode Controller Design for ABS System". *MS Thesis of Virginia Polytechnic Institute and State University*. pp. 42-51. April 1997.
29. Cutler, Charles R, Ramaker, Brian L and Prett, David M. "*Dynamic Matrix Control Method*". Patent number 4349869 Houston, Texas, United State, September 14, 1982.
30. Camponogara, E, Jia D. Krogh. B, Talukdar, S. "Distributed Model Predictive Control". *IEEE Control Systems Magazine*. Vol. 22, pp. 44-52, February 2002.
31. Rovnak, J A and Corlis, R. "Dynamic Matrix Based Control of fossil power plants". *IEEE transaction on energy conversion*. Vol. 6. 1991.
32. Camacho, Eduardo and Bordons, Carlos. "Model Predictive Control". New York : Springer Verlag, Second ed, pp. 277, 2006.
33. Qin, Joe S. and Badgwell, Thomas A. "A survey of industrial model predictive control technology". [ed.] Elsevier Science Ltd. *Control Engineering practice 11*. s.l.: Control Engineering practice 11, 2003, pp. 733-764.
34. Garcia, C E, Prett, D M and Morari, M. "Model predictive control: theory and practice—a survey". *Automatica (Journal of IFAC)*. Vol. 25, pp. 335-348, 1989.
35. Grieder, P, et al. "Computation of the constrained infinite time linear quadratic regulator". *Automatica*. Vol. 40 N°4. April 2004.
36. Rawlings, James B. "Tutorial overview of model predictive control". *IEEE Control Systems Magazine*. Vol. 20, pp. 38-52, 2000.
37. Bemporad, Alberto, Morari, Manfred and Ricker, Lawrence. "*Model predictive control toolbox for use with Matlab*". s.l. : MathWorks, User's guide, Version 2, 2006.

38. De Prada, Cesar. "Instrumentacion y control de procesos: Fundamentos de control predictivo de procesos". *Los Manuales de Ingeniería Química. Universidad de Valladolid (1997)*. [Online] <http://www.alcion.es/Download/ArticulosPDF/iq/gratis/08articulo.pdf>.
39. R.R. Negenborn, B. De Schutter, J. Hellendoorn. Multi-Agent Model Predictive Control: A Survey. Technical Report: 04-010. Delft Center for Systems and Control, TU Delft, Delft, The Netherlands, December 2004.
40. Pannocchia, G and Rawlings, J B. "Disturbance Models for Offset-Free Model Predictive Control". *AIChE Journal*. Vol. 49, pp. 426-437, 2003.
41. Venkat, A, et al. "Distributed Output Feedback MPC for Power System Control". *Proceedings of the IFAC Symposium on Power Plants and Power Systems Control*. 2006.
42. Talukdar, S, Dong, J, Hines, P, and Krogh, B. "Distributed Model Predictive Control for the Mitigation of Cascading Failures". *IEEE Conference on Decision and Control, and the European Control Conference*. Sevilla, Spain, pp. 4440-4445, December 2005.
43. Hines, Paul, Jia, Dong and Talukdar, Sarosh. "Distributed Model Predictive Control for Electric Grids". *Proc. of the Carnegie Mellon Transmission Conference. (December 2004)*. [Online] [http://www.andrew.cmu.edu/user/phines/pdfs/Hines\\_2004\\_CMU.pdf](http://www.andrew.cmu.edu/user/phines/pdfs/Hines_2004_CMU.pdf).
44. Capehart, B, Turner, W and Kennedy, W. "Guide to Energy Management". 5 ed. s.l. : CRC, pp. 1-6, 2006.
45. Shen, John, et al. "Automotive Electric Power and Energy Management -- A System Approach". [Online] [http://www.touchbriefings.com/pdf/11/auto031\\_r\\_shen.pdf](http://www.touchbriefings.com/pdf/11/auto031_r_shen.pdf).
46. Winkler, G, et al. "Intelligent Energy Management of Electrical Power Systems with distributed feeding on the Basis of Forecasts of Demand and Generation". *IEE Conference Publication CIRED*. June 2001.
47. West, M.J, Bingham, C.M and Schofield, N. "Predictive Control for Energy Management in all/more Electric Vehicles with Multiple Energy Storage Units". *IEEE Electric Machines and Drives Conference*. Vol. 1, pp. 222-228, June 2003.
48. Koot, Michiel, et al. "Energy Management Strategies for vehicular Electric Power Systems". *IEEE Transactions on vehicular technology*. Vol. 54, No 3. May 2005.
49. The Mathworks. "MATLAB - Simulink Documentation". (October 2006). [Online] <http://www.mathworks.com/access/helpdesk/help/toolbox/simulink/>.

50. Ortiz-Rivera, E and Peng, F.Z. "Analytical Model for a Photovoltaic Module using the Electrical Characteristics provided by the Manufacturer Data Sheet". *IEEE 36th Power Electronics Specialists Conference*. pp. 2087-2091, 11-14 Sept 2005.
51. Knauff, M.C, et al. "Simulink Model for Hybrid Power System Test-bed". *IEEE Electric Ship Technologies Symposium (ESTS)*. Arlington VA. : s.n., pp. 421-427, May 21-23, 2007.
52. Doerry, N. USN Capt. "Zonal Ship Design". *Naval Engineering Journal*. s.l. : American Society of Naval Engineers, Vol. 118, pp. 39-53, Winter 2006.
53. Chen, Min. and Rincón-Mora, Gabriel A. "Accurate Electrical Battery Model Capable of Predicting Runtime and I-V Performance". *IEEE Transaction on Energy Conversion*. Vol. 21 No 2., pp. 504-511, June 2006.
54. Valenciaga, F., Puleston, P.F and Battaiotto, P.E. "Variable Structure System Control Design Method based on a Differential Geometric Approach: application to a Wind Energy Conversion Subsystem". *IEE Proceedings on Control Theory Applications*. Vol. 15. Nº1, pp. 6-12. January 2004.

# Appendices

## A. PV array Data Sheet

### Module Datasheet Type SLK60M6



#### Quality

Siliken photovoltaic modules are produced with components of the highest quality and in tightly controlled processes. These processes are based on successful techniques known in the production as Kaizen-technique. This allows Siliken to manufacture high quality modules for a good price because of lower rejection ratio in production. Therefore Siliken supplies its modules with a 10 years limited warranty on 90% of the power output and 25 years on 80%.

#### Manufacture Characteristics

The used solar cells are kept in place by several layers of EVA behind 3.2mm thick tempered glass. High efficiency monocrystalline 150x150 mm<sup>2</sup> cells with antireflection coating are being used. The electrical conductors are made of copper with tin and silver in order to improve conductivity. The conductors are welded by multiple points, which minimises the tension.

#### Junction box, SOLARLOK system from Tyco



Tyco junction box with anti-error + and - connector. It is possible to connect cables up to 6 mm<sup>2</sup> (AWG 8). Includes three bypass diodes, these can easily be replaced. The SOLARLOK System does not use welded junctions, to minimise possible welding errors.

#### Certifications

This module has been designed and manufactured according to IEC 61215 and safety standards of class II.

#### Models Type SLK60P6

SLK60M6-210Wp-30Vmp

# Module Datasheet Type SLK60M6



## Electrical Data

Power max. ( $\pm 5\%$ )	$P_{mpp}$	210 Wp
Voltage mpp	$V_{mpp}$	30.6 V
Current mpp	$I_{mpp}$	6.86 A
Open Circuit Voltage	$V_{oc}$	37.2 V
Short Circuit Current	$I_{sc}$	7.52 A

Data related to standard test conditions (STC): 1000W/m<sup>2</sup> radiation, spectrum AM 1.5 and cell temperature 25°C.

## Dimensions

Dimensions (tolerance $\pm 2$ mm)	955x1580 mm <sup>2</sup>
Thickness with frame, including junction box	40 mm
Approximate weight	17 kg

## Module temperature coefficients

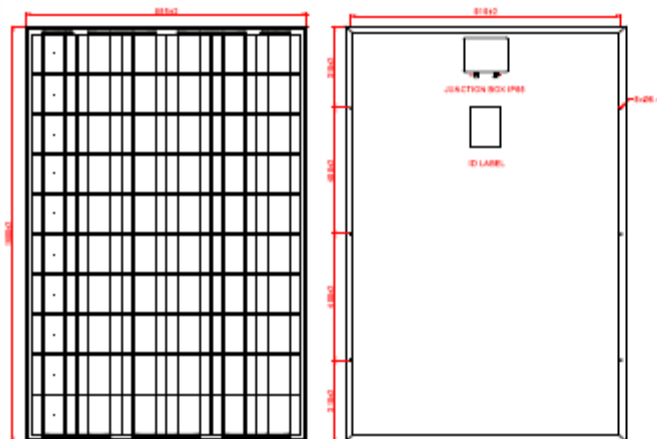
Nominal Operation Cell Temperature	NOCT	43 $\pm 2$ °C
Power coefficient	$T_k (P_n)$	-0.43%/°C
Open circuit voltage	$T_k (V_{oc})$	-127mV/°C
Short circuit current	$T_k (I_{sc})$	+2.2mA/°C

NOCT Nominal operation cell temperature: Radiation 800W/m<sup>2</sup>, ambient temperature 20°C, wind speed 1 m/s.

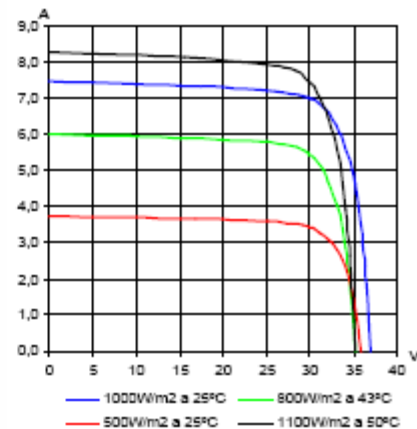
## Operation Limits

Maximum system voltage	750 $V_{oc}$
Operation temperature	-40°C a +85°C
Wind resistance	200 km/h
Hailstone max. diameter	25 mm
Hailstone speed impact	23 m/s

## Module plan



## I-V characteristics, radiation and cell temperature



Siliken S.L.  
Massamagrell, 40 - P.I. L'Horteta  
E-46138 - Rafelbunyol - Valencia - Spain  
[info@siliken.com](mailto:info@siliken.com) - [www.siliken.com](http://www.siliken.com)